Design of porous solids from 2-D and 3-D coordination frameworks utilizing imidazolylbenzoic acids and esters

by

Lisa Lee

A Thesis

Submitted to the Faculty of the

Department of Chemistry & Biochemistry

WORCESTER POLYTECHNIC INSTITUTE

Worcester, MA 01609-2280, USA

In partial fulfillment of the requirements for the

Degree of Master of Science

In Chemistry

APPROVED :

Prof. John C. MacDonald, Research Advisor

Signature: _____ Date: _____

Prof. Kristin Wobbe, Department Head

Signature: _____ Date: _____

Abstract

The investigation through design and synthesis of metal-organic frameworks was conducted in an effort to create new types of porous crystalline solids. The supramolecular chemistry and crystal structures of six novel frameworks (**1-Cd, 2Cd, 1-Cu, 2a-Cu, 2b-Cu, 3-Cu**) are reported. We are targeting porous solids composed of the transition metals Cu^{2+} and Cd^{2+} with three related families of organic molecules: Ethyl 4-(1*H*-imidazol-1-yl)benzoate, 4-(1*H*-benzo[*d*]imidazol-1-yl)benzoic acid, and Ethyl 4-(2-methyl-1*H*-imidazol-1-yl)benzoate. These molecular building blocks self assemble via metal coordination into coordination polymers that form a variety of 1-D, 2-D, and 3-D architectures. The networks are comprised of M•••O and M•••N bonds that coordinate into different geometrical arrangements dependent on steric hindrance and the metal ions that are used. The frameworks synthesized display porous behavior using weight measurements that are also seen to be reversible in some cases using atmospheric reuptake of guest molecules from growth solution. The uptake of rhodamine b was examined for the framework **3-Cu**.

Acknowledgements

I would like to thank my advisor Professor John C. MacDonald for his guidance and support during this research. I am thankful for the time I have spent doing research and the chemistry that I have learned from him. I am sure the knowledge and techniques that I have learned will greatly benefit my future endeavors.

I would like to thank Professor Thalladi for taking the time to talk to me and answer any question I had during my time here, no matter how insignificant.

I would also like to thank Ann Mondor for being a great friend to me here at WPI. My experience here would not have been as enjoyable without her presence.

During my two years at this school, three undergraduate students were a great help to my research. Tim Lawton, Marshall McGoff, and Andrew Camann all spent a large amount of time in lab contributing to my work for which I am grateful.

Lastly would also like to thank all the faculty and graduate students for helping me to acclimate to graduate life and making my time here a great learning experience.

TABLE OF CONTENTS

LIST OF FIGURES

LIST OF TABLES

1. INTRODUCTION

Throughout our lives we encounter porous materials on a daily basis. Below are two images of porous materials. On the left is a sponge which is one of the most recognized types of porous materials and is known to be macroporous due to the large pore sizes.[1] On the right side is an image of a pore cast of the microporous matrix of a rock.[2] Porous materials are useful in a variety of everyday applications such as cleaning and permeate throughout nature.

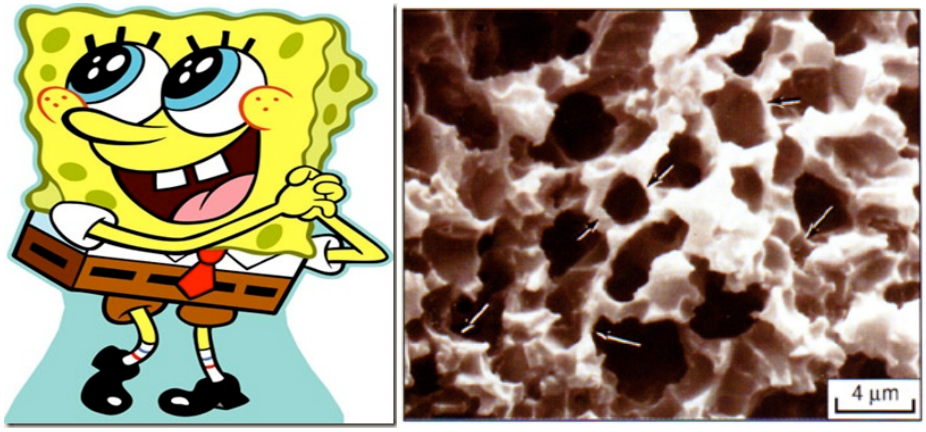

Figure 1. Cartoon SpongeBob Squarepants who is a macroporous sponge.[1] SEM view of epoxy pore cast of rock with microporous matrix with the arrows pointing out micropores.[2]

Porous crystalline solids have been of great interest in the scientific community as of late.[3-37] Most recently the focus has been devoted to development of 1-D, 2-D, and 3-D extended organic and metal-organic supramolecular frameworks.[38-53] These frameworks exhibit open pores and channels on the nanoscale, some of which display robustness upon removal of solvent or guest molecules that are included within the framework during growth. Inclusion of molecules, known as guest molecules or solvent molecules present in the growth solution, into the void space of the framework is common. The framework

is considered robust if it can maintain its structure upon removal of guest molecules through either heat or vacuum.

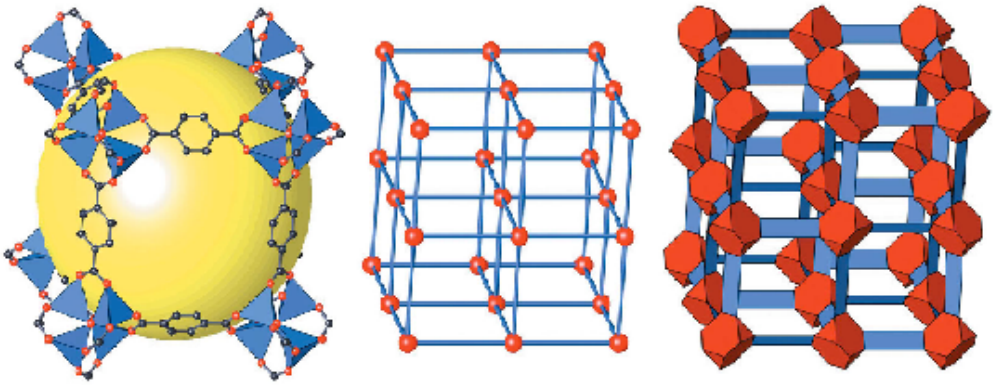

Figure 2. Image of MOF-5, a MOF designed by Yaghi that is comprised of zinc metal ions and organic linker molecules that bind together to form a framework. This gives an extended 3D cubic framework with open pores that can be occupied by guest molecules. (Yellow sphere represents the largest sphere that can occupy the pores without coming within the van der Waals size of the framework). [54]

These frameworks have the potential for a variety of commercial uses such as molecular separation, storage of reagents or gases, catalysis and synthesis in solids, design of sensors, and use as LEDs.[55] A MOF developed by Yaghi is currently being manufactured for commercial use as a gas storage material. Below is an image of **MOF-5**, which was shown above, and the gas adsorption sites at differing temperatures.[54] With the world looking towards alternative fuel sources, MOFs are of great interest as hydrogen gas storage materials.

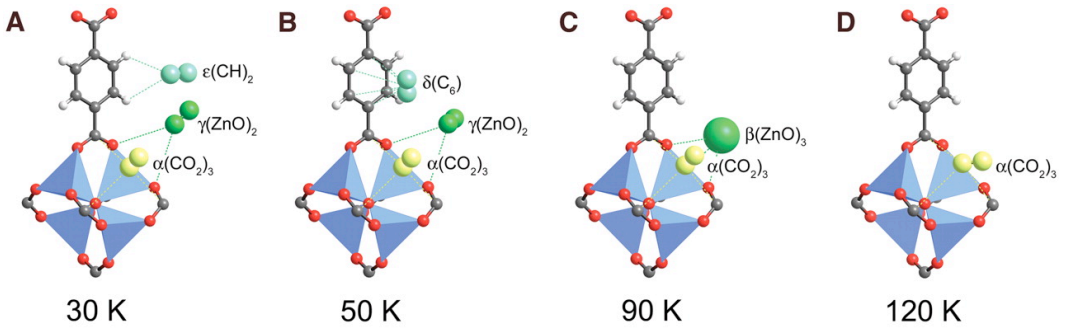

Figure 3. Partially occupied gas adsorption sites by N_2 on **MOF-5** at increasing temperatures from 30 K to 120 K.[54]

MOFs are also being examined as advanced material for violet-blue light emitting device. The ligand displays an intense violet-blue color when complexed into a framework with zinc as opposed to emission on its own.[55]

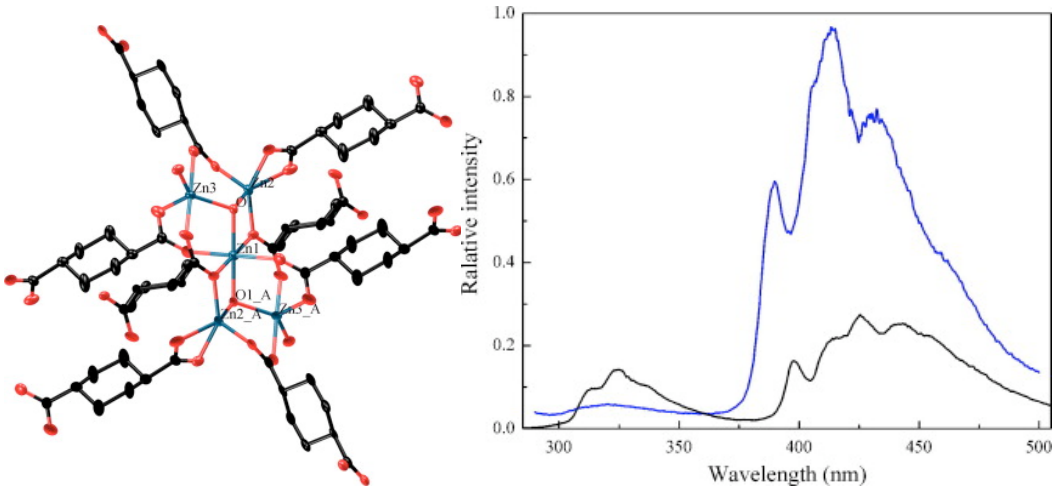

Figure 4. A photoluminescent framework with hex topology that displays a violet-blue color with significant intensity increase in framework (blue) vs. free ligand (black).[55]

With the great variety of applications that these crystalline solids are used in, it is no surprise that considerable effort has been made to develop novel strategies and methodologies to design new porous materials. Even with the significant research being conducted on these materials, a general methodology for designing, synthesizing, and

optimizing porous behavior of these crystalline materials has been developed for metal-carboxylates.[56-61] The main focus has been on controlling and modifying parameters such as the size and shape of channels and cavities, surface exposed functional groups, trapping or exchange of guest molecules, and molecular recognition and selectivity. The sheer numbers of parameters that can be altered allow the great versatility seen with supramolecular frameworks.

Hydrogen bonded frameworks are one type of supramolecular frameworks that have been examined extensively. They are similar to MOFs in that they are comprised of organic molecules and metal ions. Below a hydrogen-bonded layer of 2,6-pyridinedicarboxylate with various metal ions exhibits a porous grid network.[62-63] The use of organic molecules is ideal since they are easily modified through synthesis. They are problematic due to their low thermal and mechanical stability making them poor candidates for applications. They tend to not be robust enough to maximize favorable intermolecular contacts necessary for an ideal porous material.

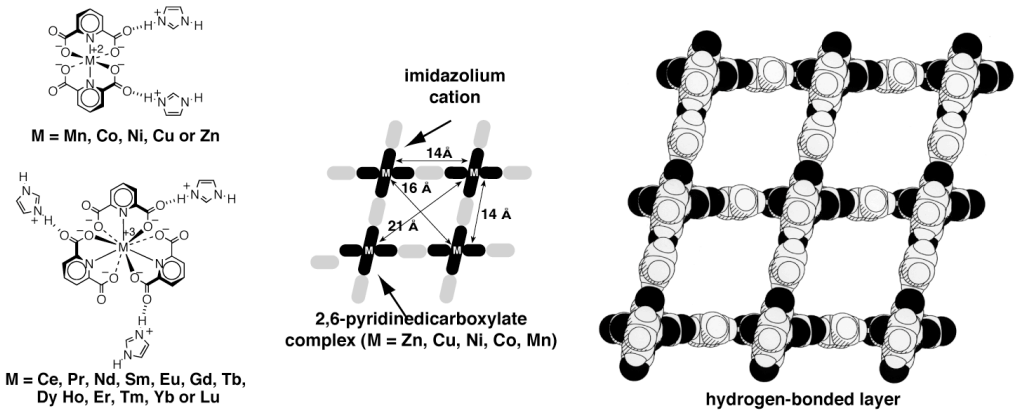

Figure 5. Organic molecules of bis- and tris(imidazolium 2,6-pyridinedicarboxylate) complexed with transition and lanthanide metals (left) form two-dimensional hydrogen-bonded frameworks with open pores (center and right).[62-63]

Zeolites are also a well known type of porous material.[64] They are hydrated, crystalline tectoaluminosilicates that are constructed from oxygen and a tetrahedral atom such as Si or Al. They are mostly known for their ability to act as a molecular sieve and are commonly used in laundry detergents and water softeners to remove unwanted ions from the water. They are highly stable and reusable but the openings of the pores are small (add in why Zeolites are bad.) The image below of a zeolite shows a large pore however the openings into the zeolite is significantly smaller than the pore volume allows.

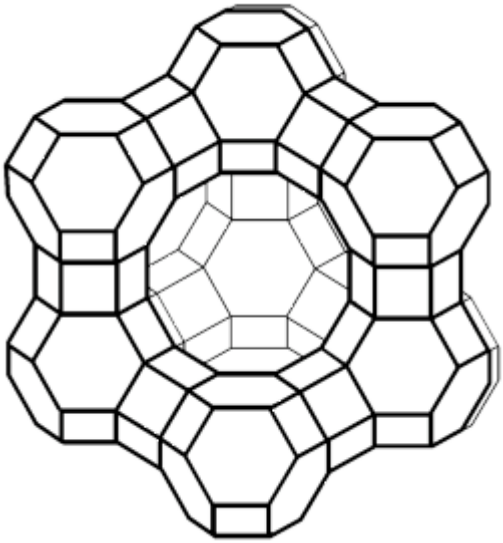

Figure 6. Zeolite that has exhibited the ability to adsorb and bind hydrofluorocarbons.[64]

When comparing MOFs to the previously mentioned porous materials they have a number of advantages over their counterparts. The variability of the organic ligands that are used, make MOFs extremely versatile and easily modified. Just by using a longer organic linker the pore size of the MOF can be expanded. The only limit of the organic linker is whether or not it can be synthesized. The metal ions that have been used to make

MOFs have ranged through from the transition metals to lanthanides. Using a different metal ion leads to both different arrangements of ligands as well as properties such as fluorescence or magnetic properties.[65] When comparing the strength of bonds that are exhibited in hydrogen bonded frameworks vs. MOFs, the metal-organic bond strength is at least one order of magnitude greater.[62-63]

Advantages aside there are many issues with assembling extended organic and metal-organic supramolecular frameworks that must be overcome. Principle's of closest packing teaches us that when molecules crystallize, they seek the most energetically favorable packing arrangement possible. Consequently molecules want to be as tightly packed as physically able since maximizing favorable intermolecular contacts provides the lowest internal energy for the system. As a result, metal-organic frameworks (MOFs) specifically designed to have large holes or channels within the crystal can be particularly troublesome to prepare. Trying to overcome this energetically driven closest packing is extremely difficult leading to all kinds of synthesis issues and problems with overall framework stability.

Solids that display a high regular repeating pattern of organization are classified as crystalline. Crystallization is the process of crystalline solids precipitating out of solution. As stated above, when crystal formation occurs, the substituents want to have the lowest internal energy possible for the system. The most common types of crystals such as salt or sugar accomplish this by packing the molecules closely to each other. In the top portion of the image below, it is seen that the molecules form aggregates that nucleate into a large crystal. In the nonporous crystal the molecules pack as efficiently as they can with hardly any spaces between the molecules. For the porous crystal, the molecules are

made up of blocks (metal ions) and rods (organic ligands) that come together as aggregates then nucleate and form a large porous crystal. It can be seen that the crystal is a 2-D grid with large pores. If considering that the crystals want to pack as efficiently as possible, then it is easy to understand why porous crystals are difficult to synthesize.

The main goal of synthesizing MOF crystals is to have a large single crystal that can be x-rayed to determine the structure. When growing crystals a common occurrence is multiple nucleation sites which lead to many small crystals that are not viable for x-ray. Dependent on the conditions that are used and how well the substituents bind to each other multiple nucleation sites are an issue.

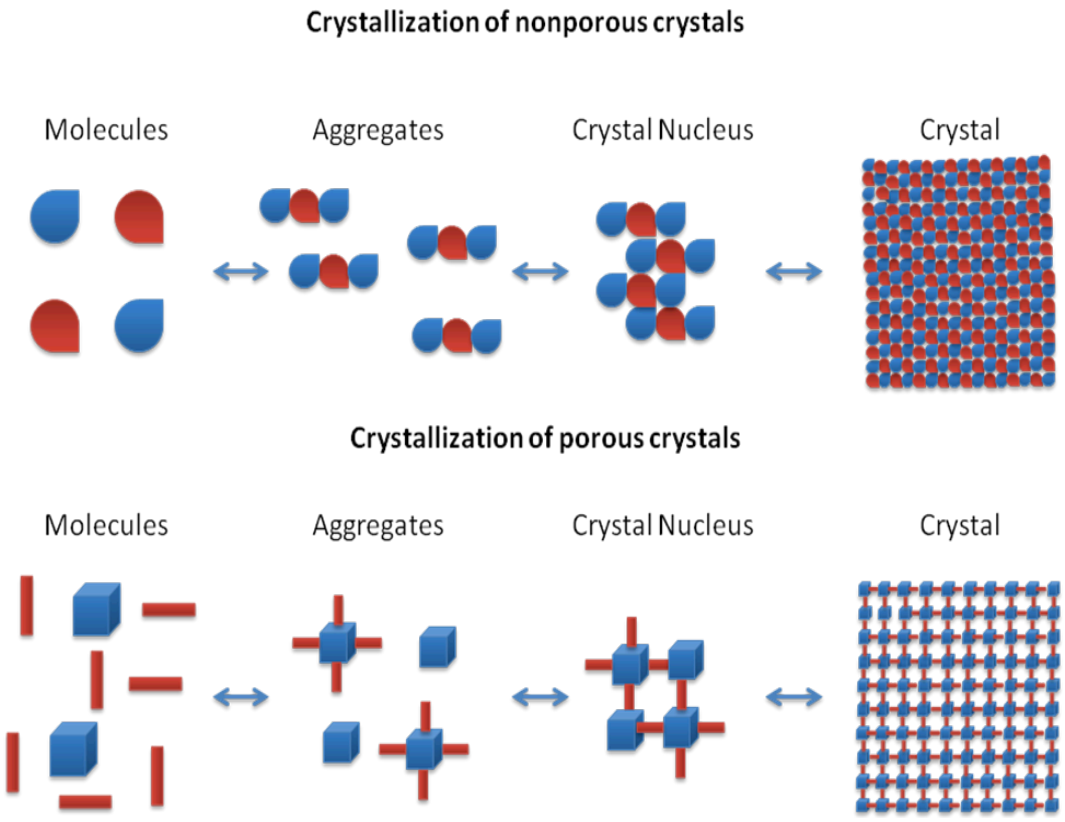

Figure 7. Cartoon of crystallization of nonporous vs. porous materials.

Multiple Nucleation Sites.

One of the advantages of MOFs is the readiness of the organic linker and the metal ion binding. The preferential need to bind is one of the main reasons why this type of system is ideal, however it contributes to synthesis issues that can and do arise. When the aggregates form, they tend to form rapidly and at multiple nucleation sites. As stated before multiple nucleation sites results in the formation of poor quality microcrystals that are exceedingly difficult to characterize using X-ray diffraction.[47]

Interpenetration.

When a framework is managed to be synthesized there are other problems that can arise. For use as host materials for molecular guests the pore sizes of the framework must be large enough to fit the guest molecule. During crystallization, favorable enthalpic interactions between molecules often leads to interpenetration. Interpenetration occurs when two or more separate frameworks grow within each other. This process results in a decrease in void volume available to guests. Interpenetration is a pervasive problem in crystals that plagues formation of porous solids from MOFs as interpenetration generally reduces the size of pores or eliminates formation of pores altogether.[47] Moreover, the incidence of interpenetration is difficult to predict, and even more difficult to control.

Framework stability.

Frameworks with pores that can comfortably fit large guest molecules often tend to be too fragile to maintain the structure of the MOF upon removal of solvent guest molecules. Many frameworks are known to trap solvent and other guest molecules during growth of crystals from the growth solution. However many known structures collapse or

undergo irreversible structural rearrangement when solvent or guest molecules are removed. This problem arises from energetic considerations whereby molecules rearrange to achieve the most closely packed arrangement possible. A framework can undergo rearrangement and still maintain porosity; in such cases the structural integrity of the overall crystal often diminishes, making it challenging to characterize the structure of the resulting solid by x-ray diffraction.

When transition metals bind to other elements there are a number of arrangements that can occur depending on the metal ion and the anion or neutral molecule bound to the metal. The image below shows the types of coordination geometries that are seen exhibited by these metals.

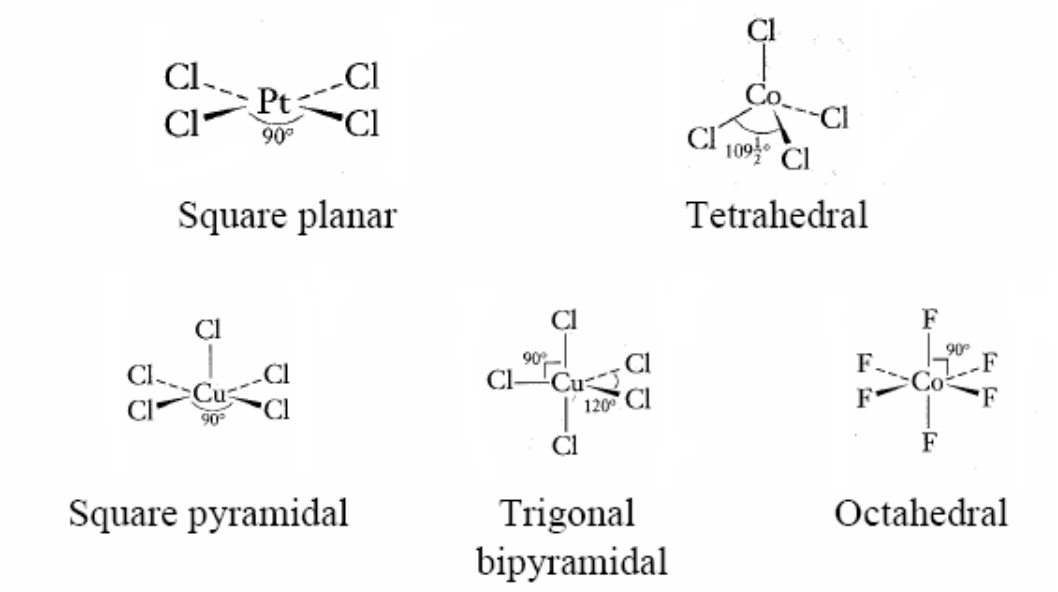

Figure 8. Modes of coordination geometries.

Both carboxylates and imidazoles bind easily to metal ions making them prime candidates for ligand complexation and have been studied extensively.[56-61] In particular

the organic compound 2,6-Pyridinedicarboxylic acid which contains both carboxylate groups and an imidazole has been seen to complex readily with transition metals by MacDonald. The figure below shows the reaction of the organic ligand with imidazole and metal ions to form a hydrogen-bonded chain.

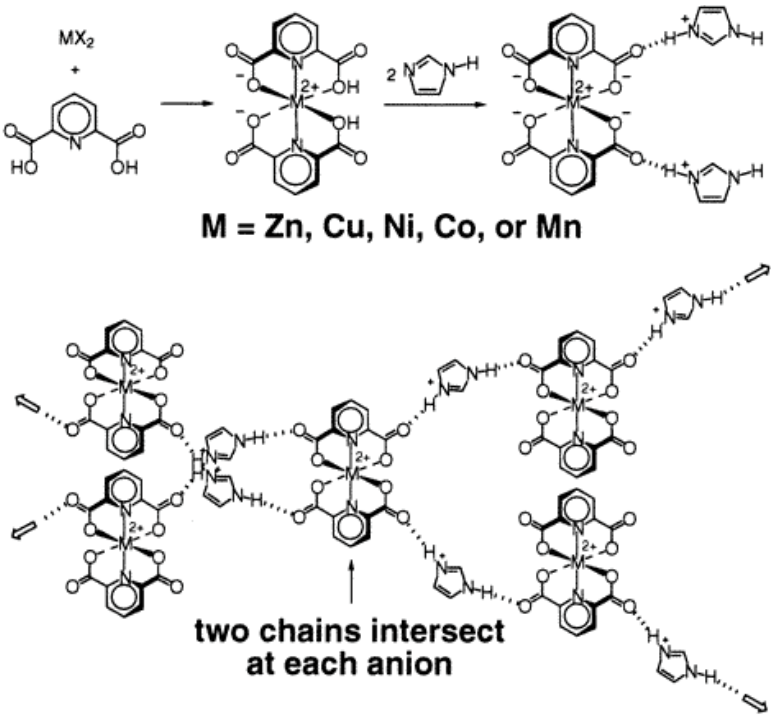

Figure 9. Reaction of transition metals with 2,6-pyridinedicarboxylic acid and imidazole.[62-63]

Because of the well established binding ability of carboxylates and imidazoles, both functional groups will be utilized as part of the organic linker.[62-63] This ensures that the ligand will bind well to the metal ion for framework synthesis.

2. CURRENT WORK

Our work is to synthesize framework materials that exhibit large pore volume, guest uptake reversibility, framework stability and little to no interpenetration. A strategy of using self coordinating rigid organic linker molecules as building blocks for molecular self assembly with metal ions was explored. Using slightly rigid bent organic linker molecules will help grow frameworks that can maintain their structural integrity throughout the synthesis process.

If a flexible organic linker is used it can lead to a less stable overall structure. The organic linkers that were chosen to be synthesized are not completely rigid and are slightly bent, leading to variability in the structures. This variability allows arrangements of the ligand to the metal that would not be possible with a rigid linker. An example would be if a person was building a framework with just sticks and blocks, there is only one way the framework will end up looking. If on the other hand you had blocks and curved rods, the final structure of the framework has a greater number of possibilities in terms of arrangement.

In literature it is well established that imidazoles and carboxylates coordinate to metal ions readily. Utilizing this occurrence we aimed to design new bi-functional organic ligands featuring imidazole and carboxylate groups that would coordinate to 1st row transition metal ions and promote growth of large stable pores. We propose that adjustment of the organic linker can modify the framework by lowering interpenetration and increasing overall pore size. The figure below shows the basic model for the organic linker and the modifications. Using this proposed strategy we expect to be able to grow large robust frameworks with porous properties with little to no interpenetration. The

frameworks are expected to be able to remain intact upon removal of guest molecules under vacuum or heating and maintain structural integrity. The effect of using different transition metals, which can coordinate differently with the rigid organic linker, is also explored using copper and cadmium.

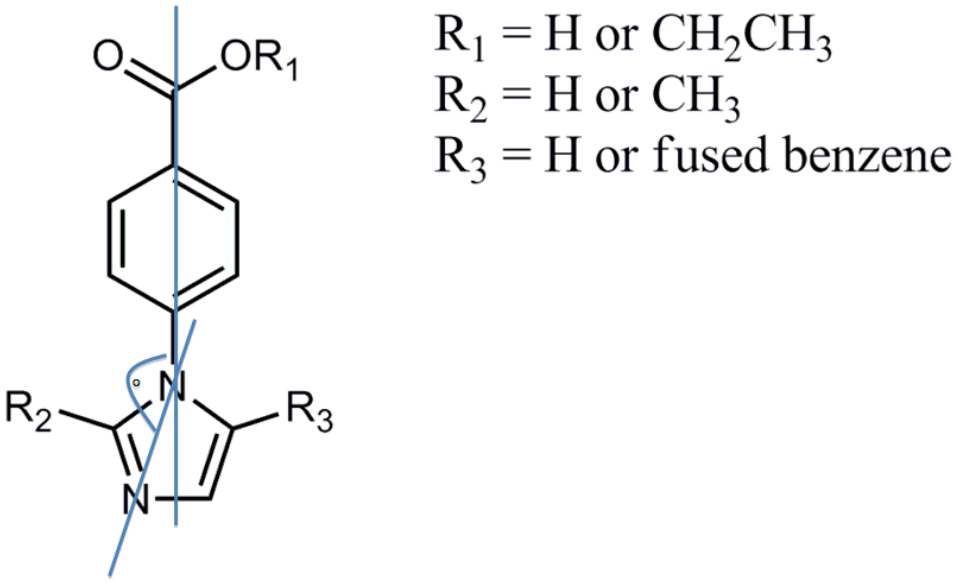

Figure 10. Image displays a general structure for the imidazolyl benzoic acid family of ligands.[66]

A class of organic linker building blocks was chosen to be synthesized with a benzoic carboxylic ester or acid functional group on one end and an imidazole ring on the opposite end as can be seen above. The ester was proposed due to its ability to protect the carboxylate during addition of the imidazole ring in the preparation of the organic linker.

There are two methods that can be used to complex the metal ions with the organic ligands. The first method is to conduct the experiments at room temperature. Since the ligand is protected by the ester a de-esterification reaction must be done on the ligand to have a free acid ready to bind with the metal ion. Once the free acid is synthesized,

suitable solvent conditions must be determined. Solubility in the growth solution is a problem when dealing with the organic ligands regardless of whether the ligand is an ester or an acid. This makes the first method more arduous and time consuming. One way to remedy the solubility issue and bypass the de-esterification reaction is to conduct these experiments at high temperatures. This is possible with hydrothermal synthesis.

Hydrothermal synthesis takes all the substituents and places them into a sealed reaction vessel as seen below in figure 11. The vial is sealed to negate solvent loss since the vials are heated to temperature that is usually higher than the boiling point of the solvents being used in the reaction. Heating the solvent mixture can also improve solubility of the organic ligand so it can react and bind to the metal.

Figure 11. Image of microwave vials with increasing volume capacity.

These vials were created to be used as microwave synthesis vials, however it was suggested that they could be used for hydrothermal oven reactions. The thick glass walls and metal cap provide a strong resistance to explosions and solvent leakage. By increasing the temperature in a sealed off reaction vessel with water present the ester groups are hydrolyzed to carboxylate groups *in situ* slowly at high temperature allowing

formation of large single crystals instead of microcrystalline powder. A typical hydrothermal synthesis is heated to 100-150 °C with crystals forming within 24-48 hours. Utilizing hydrothermal synthesis during synthesis of the MOFs it is possible to slow the binding rate of the organic linkers to the metal, allowing slow growth of large single crystals as opposed to micro-crystalline solids.

The three synthesized ligands differ in that the imidazole ring has added substituents that can affect assembly of the linker molecules with the metal ion due to steric interaction and steric hindrance. By adjusting this building block it is possible to see how manipulating the imidazole substituent can affect interpenetration, pore size, framework stability, and the overall dimensional structure. Due to the bi-dentate nature of the carboxylate, one or both of the oxygen's can bind to the metal ion. Stoichiometry plays a role in overall binding ratios of the ligand to metal ion. Altering ratios of ligand or metal present in the growth solution the binding ratio of ligand to metal can be affected.

It is expected that the building blocks can assemble into a 1-D, 2-D, or 3-D structure depending on how the binding of the oxygen and nitrogen functional groups occur and what mode of binding the metal ion will allow.

With the above goals in mind, a new class of rigid organic linker molecules (**1-3**) was synthesized and complexed with copper and cadmium metal ions. With the binding nature of the nitrogen and oxygen substituents on the organic linker we expected them to complex with the metal ions and form complexes fairly readily.

Dependent on the metal binding geometries there are a number of different ways the ligands can orient themselves around the metal site as seen in figure 12 of the introduction. In the figure below a schematic of a few possible binding patterns is shown. The three different dimensional bindings that can occur are shown as well. The most desirable binding dimension is a 3-D framework since these are the frameworks that display the largest pore and channel volumes compared to the 1- or 2-D frameworks.

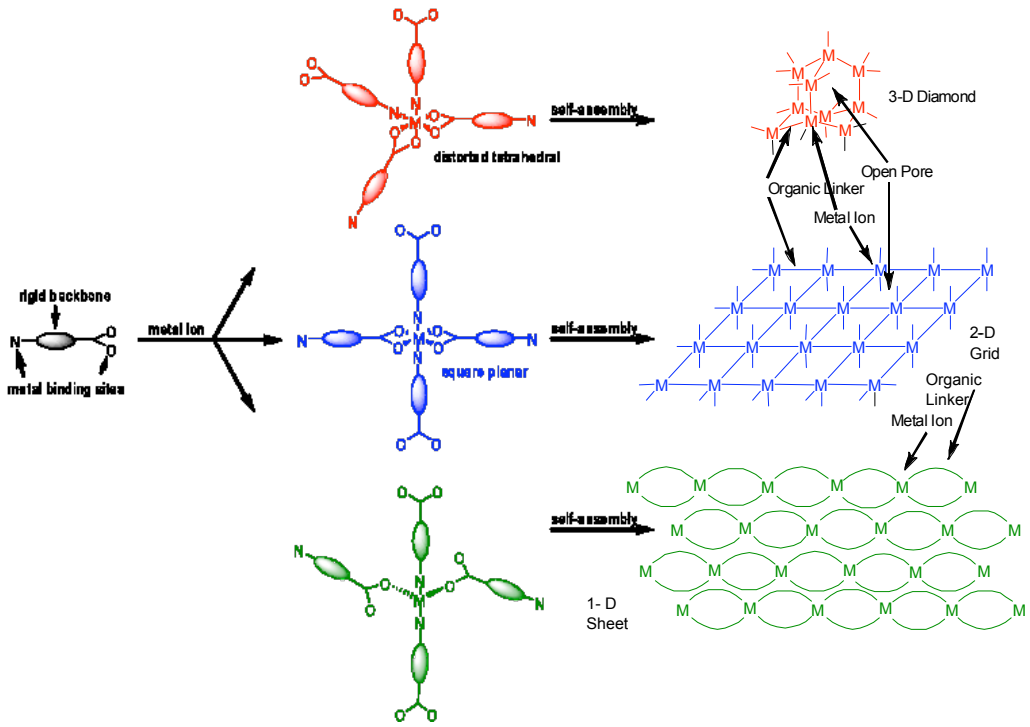

Figure 12. Diagram of ligand metal strategy for self assembly into the frameworks.

We expected that any framework that was synthesized would form with guest solvent molecules within the pores or channels as well as possible interpenetration of one or more frameworks. Based upon the possible binding patterns for a 3-D framework the predicted pores and channels would be large enough for solvent molecules to be included within the void spaces of the framework. Also if there are exposed metal binding sites that have

not been occupied by binding of the organic linker building block then solvent molecules can bind onto these exposed metal sites. During the growth of the crystal, interpenetration can occur, drastically reducing the size of the void spaces of the framework. Interpenetration can also completely diminish porous behavior of the framework by blocking the pores and channels that would otherwise be available for guest molecules. With the reduction in void space, solvent molecules, can become trapped within the framework and thus are not allowed to move easily through the channels. With the different organic linker molecules we hope to be able to control interpenetration by introducing substituents that would hinder interpenetration and favor a less interpenetrated framework or a completely non-interpenetrated framework. In order to determine if the framework retains the overall structure it can be monitored using X-ray powder diffraction. If the framework manages to retain its structure then the powder diffraction patterns will be identical or similar before and after removal of guest molecules.

Incorporation of guest molecules can occur in two ways for MOFs. During synthesis of the MOFs, targeted guest molecules can be present within the growth solution and the framework can grow around these molecules. The other method of incorporation is when the targeted molecules are exchanged with the guest molecules after the MOFs have already been synthesized. This incorporation can occur via a solvent exchange either atmospherically, under pressure, or directly in the guest solvent itself. There are different methods that can be utilized in order to determine whether or not this exchange has actually occurred. The best method would be to use single x-ray diffraction in order to see the guest molecules within the framework. However most of the frameworks have

such large pores and channels that the guest molecules tend to be disordered within the structure and exceedingly difficult to see with single x-ray diffraction. Instead FT-IR, TGA, DSC and GC-mass spectrometry must be used to determine if the targeted guest molecule has in actuality been taken up by the framework. In order to determine how large of a guest molecule can be taken into the framework an array of guest molecules with differing size and orientations can be introduced into the framework and analyzed to see if the guest molecules was indeed taken into the framework. A good array of guest molecules to use would be a series of dye molecules which can readily be seen entering the framework by overall color change of the crystal. By using dye molecules of increasing size, the largest molecule that can fit within the pores or channels can be found. If the crystal is then decomposed in a solution, UV-Vis spectroscopy can be used to determine the amount of dye molecules present in the overall crystal.

Evacuation of the crystal frameworks by either heating or vacuum can show whether a framework is robust or weak. In terms of a robust framework, removal of guest solvent molecules, will not affect the framework and will result in a porous structure with open channels and pores. If the framework is not robust then the porous structure undergoes a structural rearrangement to a non-porous arrangement. In order to determine if the framework contains guest solvent molecules thermogravimetric analysis (TGA) can be utilized to measure loss of mass as a function of temperature. Using the data from TGA it is possible to calculate the integral molar amount and possible ratios of guest solvent molecules that were contained within the framework. To determine if porous behavior of the framework is still being exhibited exposure of the evacuated crystals to various

solvents can be done followed by TGA to determine if any solvent has been absorbed back into the framework. Another method of determining if the crystals have retained their structure is to analyze them by powder X-ray, which generates a powder pattern from the scattered X-rays that are passed through a sample of randomly oriented crystals. By comparing the powder pattern of crystals before and after evacuation of the frameworks, structural integrity can be determined. Using differential scanning calorimetry (DSC) the thermal behavior of the framework crystals can be examined. DSC measures endo- and exothermic changes such as heat of fusion (melting point) and phase transitions that occur as the sample is being heated. The DSC data correlates to the TGA data in that you can measure absorption or release of heat associated with loss of solvent molecules as well as possible phase transitions and decomposition of the overall crystal lattice.

If the pores and channels of the 3-D framework material are of a large enough size then it is conceivable to place large entities into the pores and channels once they have been evacuated. If the guest molecule has a higher affinity for the pores or channel than a solvent exchange can be done instead of exposing the guest molecules once the pores have been evacuated. Nitrated compounds, such as TNT, could be placed in the framework either by having them present in the growth solution or exposing frameworks to the nitrated compounds after they have been evacuated or via a solvent exchange. Certain frameworks can be geared to certain types of guest molecules. If the ligand used tends to be hydrophobic or hydrophilic then it is conceivable that the pores will exhibit similar properties. If there are exposed metal binding sites on the MOF, this leaves open

sites for binding of guest molecules, which could be selective for certain types of guest molecules.

3. OBJECTIVES

The objectives of the experiments are as followed;

- Design a new family of bi-functional organic ligands featuring imidazole and carboxylate functional groups as new building blocks to form porous MOFs.
- Prepare MOFs by reacting new ligands with 1st row transition metals via hydrothermal and room temperature solution based syntheses.
- Grow single crystals of MOFs to characterize the structures of resulting MOFs via x-ray diffraction to establish whether MOFs form open, porous structures, whether interpenetration occurs, and whether guests are included in pores/channels.
- Characterize the porous behavior of the resulting MOFs including
    - stability of host MOF upon loss of guests
    - stability of guests in MOF
    - exchange/re-uptake of guests
    - ability of a given MOF to accommodate different guests
- Examine how structural perturbations on the organic ligand (i.e. introduction of substituents) affect the mode of coordination, structure of MOFs and porous behavior for a given metal ion.
- Examine how different 1st order transition metal ions affect the mode of coordination, structure of MOFs and porous behavior for a given ligand.

4. EXPERIMENTAL

4.1 Materials and Methods

General Techniques. Copper (II) nitrate, cobalt (II) nitrate, europium (III) acetate, imidazole, 2-methyl imidazole, benzimidazole, ethyl 4-fluorobenzoate, and potassium carbonate were purchased from Acros, Aldrich, Alfa Aesar, TCI, and Strem. All chemicals were used as received without further purification. IR samples were prepared as powders. IR spectra were obtained in a Nexus 670 FT-IR instrument. Melting point data were collected with a Meltemp instrument and are uncorrected. Differential Scanning Calorimetry data were collected using a TA instruments, DSC 2920 Modulated DSC, at a heating rate of 10 °C/min. Thermo Gravimetric Analysis data were collected using a TA instrument, Hi-Res TGA 2950 Thermo Gravimetric Analyzer at a heating rate of 10 °C/min. Hydrothermal synthesis was conducted using a Yamato DKN 400 Mechanical convection oven. Single crystal X-ray analysis was done using a Bruker Kappa Apex II instrument and a Bruker D8 Focus instrument was used to collect powder x-ray data. Mass spectrometry data was collected using an Agilent 1200 Series 6130 Quadropole LC/MS using analytical grade ethyl acetate for the sample. A short column with a fast gradient was used with a 1 μL injection sample volume. ^{1}H and ^{13}C NMR data was collected using a Bruker Avance 400 MHz spectrometer.

Thermal Behavior. Crystals were heated in a Fisher-Johns melting point apparatus up to 300 °C. The crystals were placed between two micro cover glass slides and examined using a small magnifier for color change or structural changes and possible melting.

4.2 Synthesis of ligands

The synthesis of the series of organic compounds that contain both an imidazole ring and an ester functional group was undergone using a synthetic scheme from the *J. Med. Chem.* **1990**, *33*, 1091-1097. Ethyl 4-fluorobenzoate is reacted with the appropriate imidazole in dimethyl sulfoxide using potassium carbonate as a base to give the appropriate compound. In the article the two imidazoles used were imidazole and 2-methyl imidazole. This resulted in the synthesis of ethyl 4-(1*H*-imidazol-1-yl)benzoate and ethyl 4-(2-methyl-1*H*-imidazol-1-yl)benzoate.

Using the synthesis conditions from the journal article it was possible to substitute the 2-methyl imidazole and imidazole that was used in the reaction with benzimidazole to synthesize a new organic compound yielding ethyl 4-(1*H*-benzo[*d*]imidazol-1-yl)benzoate. Since only hydrothermal synthesis could be used for the ester protected carboxylate ligands a de-esterfication reaction was performed on the ethyl 4-(1*H*-benzo[*d*]imidazol-1-yl)benzoate compound in order to allow for room temperature synthesis conditions to be carried out. Preparation of these ligands was characterized by NMR and mass spectroscopy to determine that the compound was indeed synthesized.

Synthesis of Ethyl 4-(1*H*-imidazol-1-yl)benzoate (1). Imidazole (4.1 g, 0.06 mol), 4-fluorobenzoic acid ethyl ester (10.0 g, 0.06 mol) and potassium carbonate (16.6 g, 0.12 mol) were combined with dimethyl sulfoxide (20 mL). The reaction was heated at 120°C for 12 hours under a N_2 atmosphere. The mixture was then poured into 200 mL of cold water. The white precipitate was then filtered resulting in a yield of 8.42 g (65% yield). ^{1}H NMR ($CDCl_3$) δ (ppm) 8.2 (d, 2 H), 7.97 (m, 1H), 7.50 (d, 2H), 7.37 (m, 1H), 7.28 (m, 1H), 3,97 (s, 3H). IR(cm^{-1}): 3100, 1700, 1600, 1270, 1080. Mass Spectrometry mass 216.1.

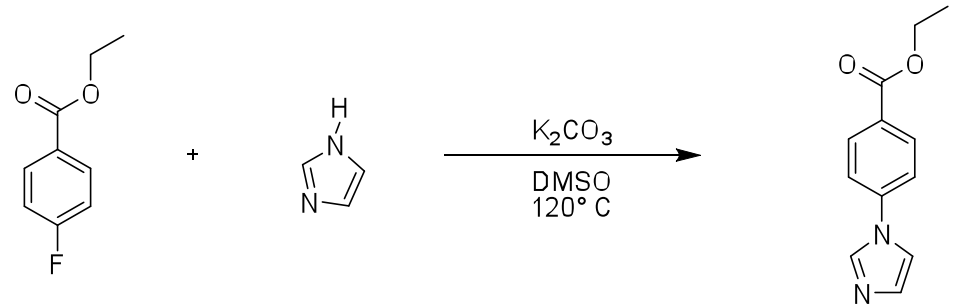

Figure 13. Synthetic scheme for Ethyl 4-(1*H*-imidazol-1-yl)benzoate (**1**).

Synthesis of Ethyl 4-(1*H*-benzo[*d*]imidazol-1-yl)benzoate (2x). Benzimidazole (7.1 g, 0.06 mol), 4-fluorobenzoic acid ethyl ester (10.0 g, 0.06 mol) and potassium carbonate (16.6 g, 0.12 mol) were combined with dimethyl sulfoxide (20 mL). The reaction was heated at 120°C for 12 hours under a N_2 atmosphere. The mixture was then poured into 200 mL of cold water. The white precipitate was then filtered resulting in a yield of 14.0 g (87% yield). ^{1}H NMR ($CDCl_3$) δ (ppm) 8.27 (d, 2H), 8.18 (s, 1H), 7.90 (m, 1H), 7.62 (d, 2H), 7.60 (m, 1H), 7.38 (m, 2H), 4.44 (t, 2H), 1.44 (q, 3H). IR(cm^{-1}): 3110, 1750, 1600, 1545, 1245, 1220, 1680, 1090. Mass Spectrometry mass 266.2.

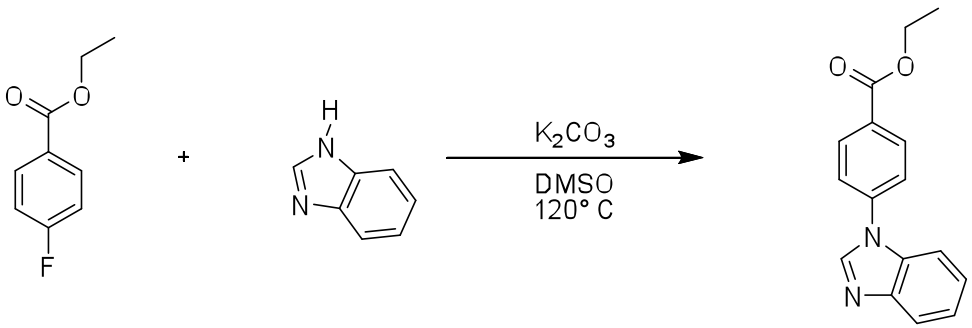

Figure 14. Synthetic scheme for Ethyl 4-(1*H*-benzo[*d*]imidazol-1-yl)benzoate (**2x**).

Synthesis of Ethyl 4-(2-methyl-1*H*-imidazol-1-yl)benzoate (3). 2-Methylimidazole (7.32 g, 0.089 mol), 4-fluorobenzoic acid ethyl ester (10.0 g, 0.059 mol) and potassium carbonate (16.6 g, 0.12 mol) were combined with dimethyl sulfoxide (20 mL). The reaction was heated at 120°C for 12 hours under a N_2 atmosphere. The mixture was then poured into 200 mL of cold water. The resultant whitish-yellow precipitate was then

filtered resulting in a yield of 6.11 g (45 % yield). ^{1}H NMR ($CDCl_3$) δ (ppm) 8.18 (d, 2H), 7.39 (d, 2H), 7.05 (m, 2H), 4.42 (q, 2H), 2.41 (s, 3H), 1.43 (t, 3H). IR(cm^{-1}): 1700, 1600, 1390, 1245. Mass Spectrometry mass 230.1.

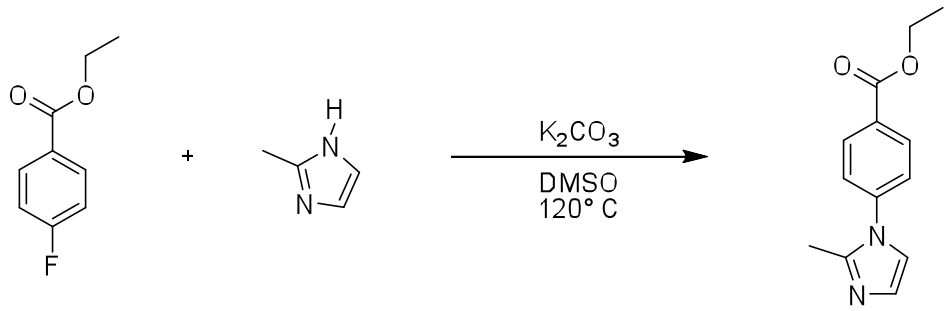

Figure 15. Synthetic scheme for Ethyl 4-(2-methyl-1*H*-imidazol-1-yl)benzoate (**3**).

Synthesis of 4-(1*H*-benzo[*d*]imidazol-1-yl)benzoic acid (2). Sodium hydroxide (0.96 g, 0.024 mol) and **2a** (3.2 g, 0.012 mol) were combined with 95% ethanol (100 mL). The reaction was refluxed for 2 hours. The mixture was then neutralized to pH 7.0 with HCl. The resultant white precipitate was then filtered and collected resulting in a yield of 2.3 g (81% yield). ^{1}H NMR (DMSO) δ (ppm) 8.69 (s, 2H), 8.18 (d, 1H), 7.90 (d, 1H), 7.70 (d, 2H), 7.20 (m, 1H), 3.4 (s, 2H), 2.1 (s, 2H). IR(cm^{-1}): 3190, 1690, 1600, 1570, 1220, 780, 690. Mass Spectrometry mass 237.1.

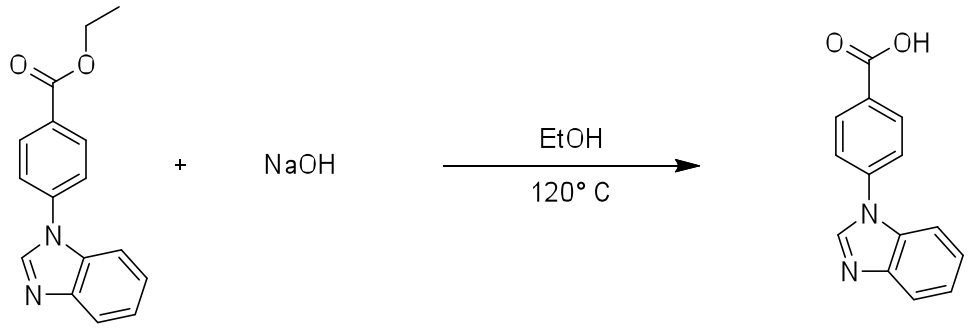

Figure 16. Synthetic scheme for 4-(1*H*-benzo[*d*]imidazol-1-yl)benzoic acid (**2**).

4.3 Preparation of MOFs

MOFs were prepared using two different methods, the first being hydrothermal synthesis and the second being room temperature synthesis. Hydrothermal synthesis was conducted on a Yamato DKN 400 programmable mechanical convection oven. Room temperature synthesis reactions were conducted on a standard hotplate. Both reaction conditions were utilized due to solubility issues of the esters versus the acids. 4-(1*H*-benzo[*d*]imidazol-1-yl)benzoic acid is soluble in a mixture of ethanol and water below the boiling point of the solvent mixture. The ester protected ligands needed to be in solution as well as have a de-protected carboxylate.

Hydrothermal synthesis of [(4-(1*H*-imidazol-1-yl)benzoate)cadmium(II)] (1-Cd). (*i*) A solution containing **1** (108 mg, 0.5 mmol) and $Cd(NO_3)_2$•6 H_2O (154 mg, 0.5 mmol) in 5 mL of 4:4:2:1 EtOH:DMF:glycol:H_2O was placed in a 10mL microwave glass vial and sealed. The vial was heated for 6 hours to 120 °C and kept at that temperature for 48 hours then cooled to 25 °C for 12 hours, yielding clear flat rectangular crystals of **1-Cd**. Crystals of **1-Cd** were present in the vial upon removal from the oven. MP; Turns opaque at room temperature.

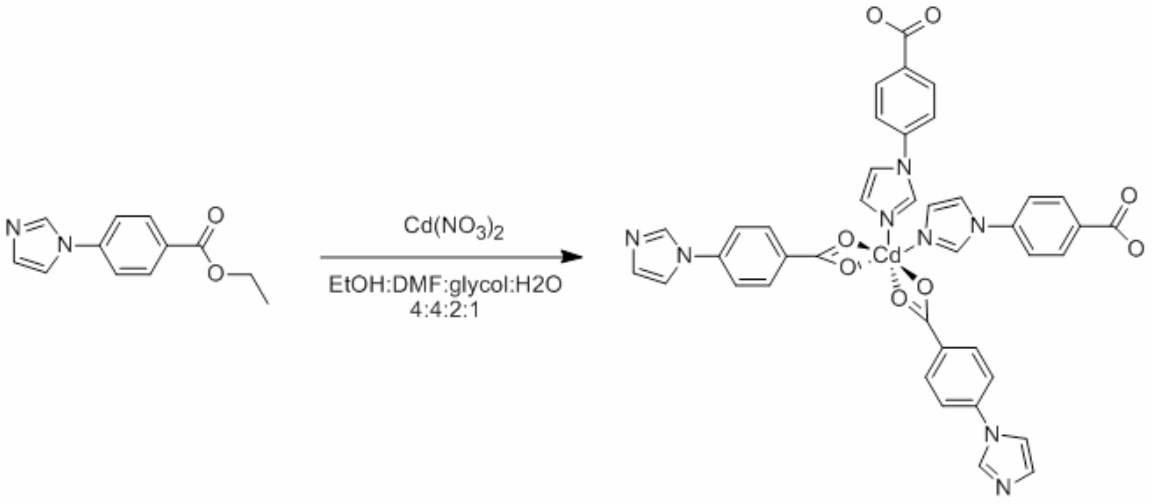

Figure 17. Hydrothermal synthesis of [(4-(1*H*-imidazol-1-yl)benzoate)cadmium(II)] (**1-Cd**).

Hydrothermal synthesis of [(4-(1*H*-imidazol-1-yl)benzoate)copper(II)] (1-Cu). (*ii*) A solution containing 1 (10.7 mg, 0.05 mmol) and $Cu(NO_3)_2$•3 H_2O (6 mg, 0.025 mmol) in 5 mL of 1:1 EtOH:H_2O and placed in a 10 mL microwave glass vial and sealed. The solution was sonicated until all solids had dissolved and the vial was heated for 6 hours to 120 °C and kept at that temperature for 48 hours then cooled to 25 °C for 12 hours, yielding dark blue rectangular block-like crystals of **1-Cu**. Crystals of **1-Cu** were present upon removal from the oven. MP; 249-251 °C.

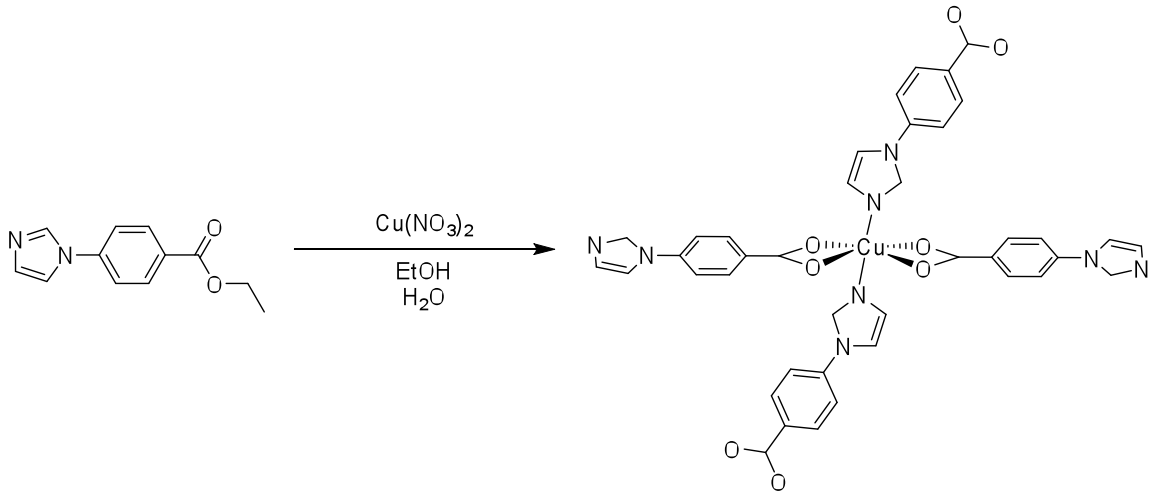

Figure 18. Hydrothermal synthesis of [(4-(1*H*-imidazol-1-yl)benzoate)copper(II)] (**1-Cu**).

Room temperature synthesis of [(4-(1*H*-benzo[*d*]imidazol-1-yl)benzoate)copper(II)] (2a-Cu). (*iii*) A solution containing **2b** (10 mg, 0.04 mmol) was combined with 10 mL of 1:2 EtOH:H_2O and placed in a beaker and heated until dissolvation. Upon removal from heat $Cu(NO_3)_2$•3 H_2O (16 mg, 0.07 mmol) was added and the solution was allowed to evaporate under normal conditions for four days, yielding blue cubic type crystals of **2a-Cu**. MP; Turns light blue at 180°C.

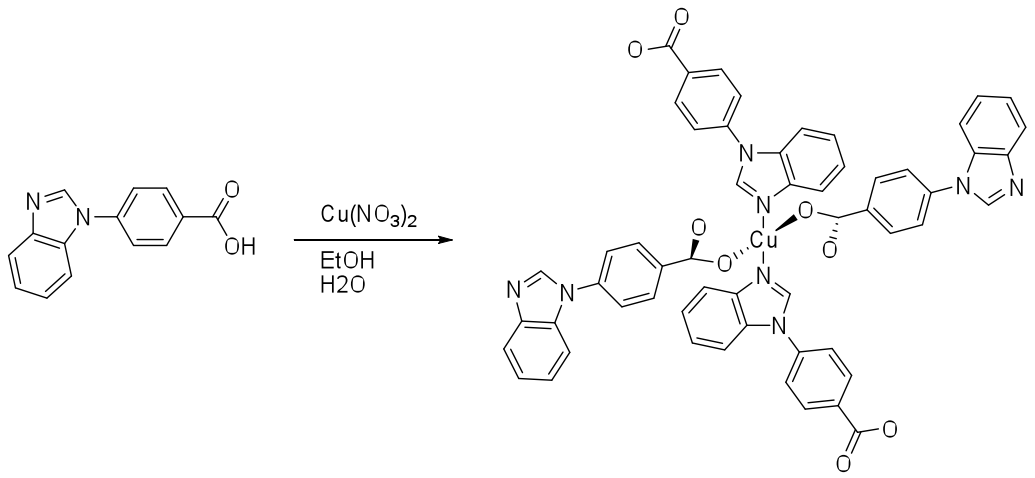

Figure 19. Room temperature synthesis of [(4-(1*H*-benzo[*d*]imidazol-1-yl) benzoate) copper(II)] (**2a-Cu**).

Room temperature synthesis of [(4-(1*H*-benzo[*d*]imidazol-1-yl)benzoate)copper(II)] (2b-Cu). (*iv*) A solution containing **2b** (10 mg, 0.04 mmol) was combined with 10 mL of 2:1 EtOH:H_2O and placed in a beaker and heated until dissolvation. Upon removal from heat $Cu(NO_3)_2$•3 H_2O (7.87 mg, 0.03 mmol) was added and the solution was allowed to evaporate under normal conditions for four days, yielding purple parallelogram type crystals of **2b-Cu**. MP; Turns opaque at room temperature.

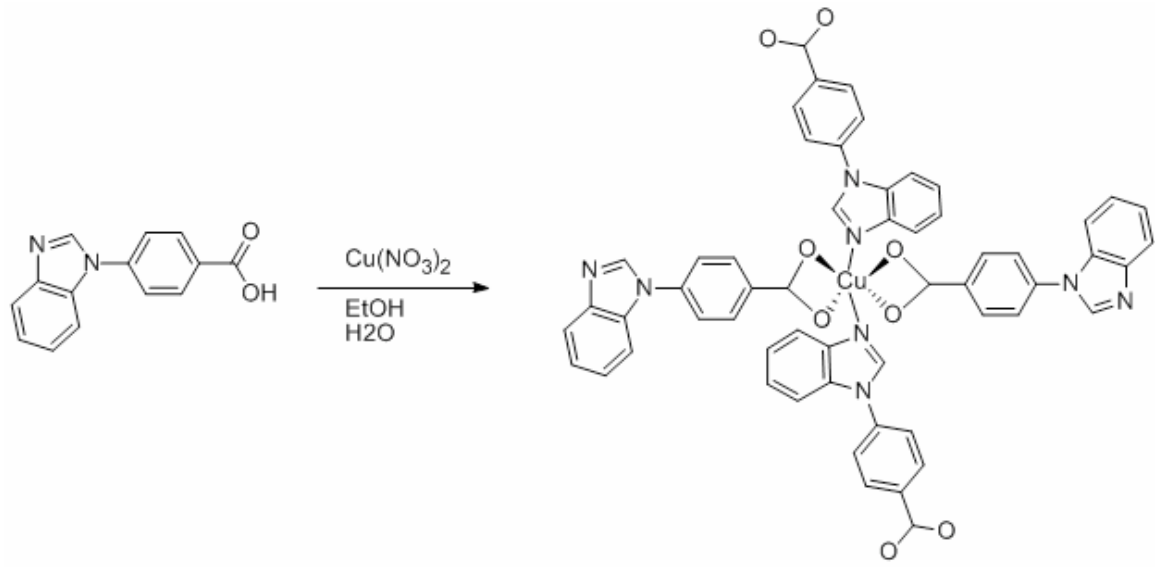

Figure 20. Room temperature synthesis of [(4-(1*H*-benzo[*d*]imidazol-1-yl) benzoate) copper(II)] (**2b-Cu**).

Hydrothermal synthesis of [(4-(2-methyl-1*H*-imidazol-1-yl)benzoate)cadmium(II)] (2-Cd). (*v*) A solution containing **3** (10 mg, 0.04 mmol) and $Cd(NO_3)_2$•6 H_2O (5 mg, 0.02 mmol) was combined with 6 mL of 2:1 EtOH:H_2O and placed in a 10 mL microwave glass vial and sealed. The vial was heated for 6 hours to 120 °C and kept at that temperature for 48 hours then cooled to 25 °C for 12 hours, yielding clear long rectangular prism crystals of **2-Cd**. Crystals of **2-Cd** were present when the vial was removed from the oven. MP; Turns opaque at room temperature.

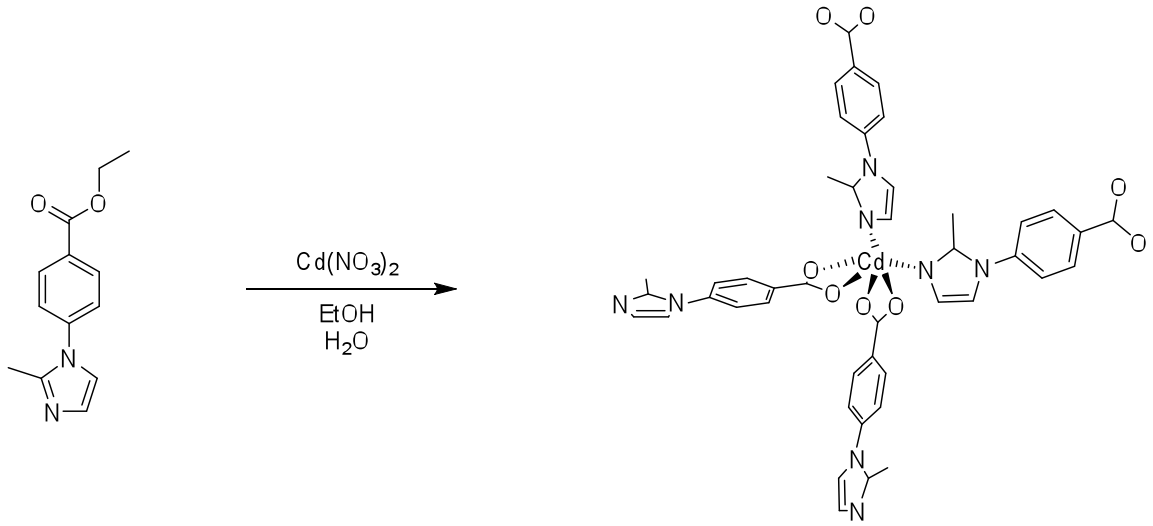

Figure 21. Hydrothermal synthesis of [(4-(2-methyl-1*H*-imidazol-1-yl)benzoate) cadmium(II)] (**2-Cd**).

Hydrothermal synthesis of [(4-(2-methyl-1*H*-imidazol-1-yl)benzoate)copper(II)] (3-Cu). (*vi*) A solution containing **3** (10 mg, 0.04 mmol) and $Cu(NO_3)_2$•3 H_2O (6.7 mg, 0.02 mmol) was combined with 6 mL of 2:1 EtOH:H_2O and placed in a 10 mL microwave glass vial and sealed. The vial was heated for 6 hours to 120 °C and kept at that temperature for 48 hours then cooled to 25 °C for 12 hours, yielding clear long rectangular prism crystals of **3-Cu**. Crystals of **3-Cu** were present when the vial was removed from the oven but more appeared after the vial was allowed to sit for 24 hours. MP; Turns green at 246-250°C.

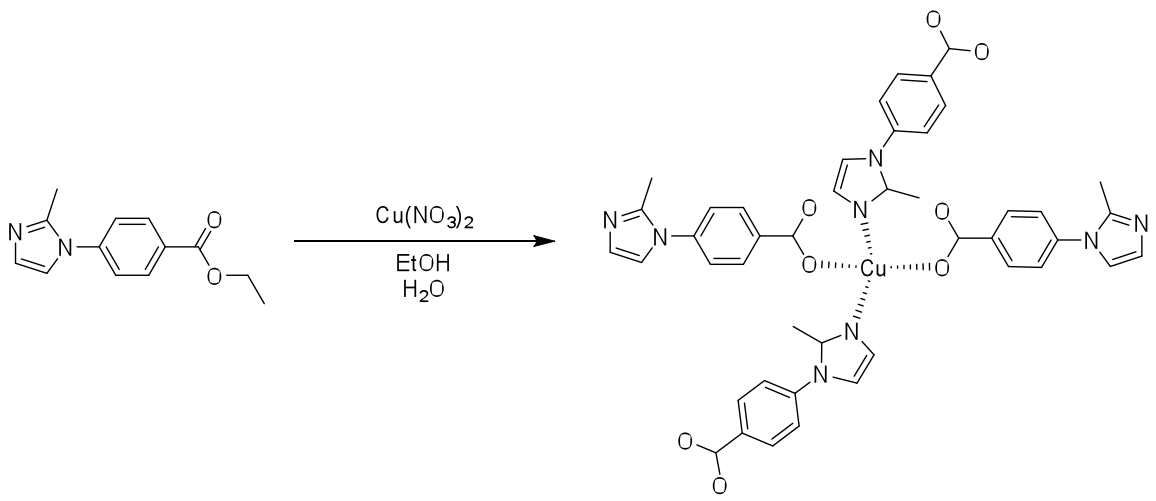

Figure 22. Hydrothermal synthesis of [(4-(2-methyl-1*H*-imidazol-1-yl)benzoate) copper(II)] (**3-Cu**).

4.4 Characterization of MOFs

Determination of X-ray crystal structures. Single-crystal X-ray diffraction data were collected on a Bruker AXS Kappa Apex II diffractometer with graphite monochromated Mo Kα radiation and equipped with an Oxford cryosystems cryostream device for all the MOFs (**1-Cd, 2-Cd, 1-Cu, 2a-Cu, 2b-Cu, 3-Cu**). Mounted crystals displayed no imperfections and were examined to ensure that it was a single crystal. Diffracted data were corrected for absorption using the APEX 2 v2.2-1 program. X-Shell 6.3.1 software was used to solve and refine structures. Refinement was based on F^2. All non-hydrogen atoms were refined anisotropically. Hydrogen atoms on heteroatoms were located and refined with isotropic thermal parameters. The remaining hydrogen atoms were fixed in calculated positions and refined isotropically with thermal parameters based upon the corresponding attached carbon atoms. Mercury 1.4.2 software was used to examine solved X-ray crystal structures. All crystal single X-ray data was collected at 100 K to

minimize thermal movement of the framework as well as minimize loss of guest solvent molecules from the pores. The crystals were removed from solution and placed directly into paratone oil and mounted onto a MiTeGen polymer mount. Excess oil was tapped off and the mount was placed into the Bruker instrument directly under the nitrogen cryostream. Unit cell data was collected then a data collection strategy was generated. Data was collected and solved.

X-ray powder diffraction data.

Differential scanning calorimetry and Thermogravimetric analysis. The TGA method was used to determine how much guest molecules were lost upon heating of the crystal as well as the amount of guest molecules that were lost when kept at room temperature. DSC was used to determine any exotherms or endotherms the sample underwent upon heating. Both instrument samples were removed from the growth solution and placed onto a filter paper to remove surface adsorbed solvent. The crystals were then placed onto a tared platinum TGA pan or into a DSC aluminum pan and placed onto the respective instrument and heated at a rate of 10°C/min. When examining loss of guest molecules as a function of time, the sample was kept at 25°C for two hours.

Exchange/Removal of guest molecules. TGA was used to monitor reuptake of guest molecules into the crystal. Crystals were removed from solution and dried on a filter paper and placed into a dessicator hooked up to a high power vacuum pump for at least twenty-four hours to remove guest molecules from within the framework. The crystals were then removed from the dessicator and placed into a container with the bottom filled with guest solvent. The container was sealed off by applying a low house vacuum through an open vent for twenty minutes and then the vent was closed. The container was

left undisturbed for two days and the crystals were removed and placed onto a TGA pan and weighed.

Uptake/exchange of rhodamine B. Rhodamine B was introduced into crystal **3-Cu** using two different types of sample crystals. The first sample set contained crystals removed straight from solution that was dried on filter paper. The second sample set contained crystals that were evacuated using high vacuum. Both crystal sample sets were placed into a saturated rhodamine b dichloromethane solution. The crystals were allowed to sit in the capped off solution for twenty-four hours then were removed from solution and placed onto fluted filter paper. The crystals were rinsed repeatedly until no more rhodamine b was seen coming out of the crystals. The crystals were then covered with a 5% NaOH methanolic solution and allowed to sit for 10 minutes. The solvent was filled to two mL with methanol and examined using UV-spectroscopy. A standard series was made to determine the amount of rhodamine b that was present within the crystals.

Growth of MOFs in the presence of nitrophenol. Growth conditions of **3-Cu** were slightly modified to determine if guest molecules could be grown within the framework during crystal synthesis. The only modification to the synthesis conditions was the addition of 20 mg of 3-nitrophenol to the growth solution.

5. RESULTS and DISCUSSION

5.1 Synthesis of ligands

As mentioned in the experimental the following ligands were successfully synthesized using the same conditions from *J. Med. Chem.* **1990**, *33*, 1091-1097. The only modification that was done was to substitute the different imidazoles for the different reactions. The resulting yield for the reaction of the imidazole was comparable to the yield seen in the literature. The reaction used to convert the ester of 4-(1*H*-benzo[*d*]imidazol-1-yl)benzoate to a free acid was done simply by reacting the ester with sodium hydroxide and allowing the reaction mixture to reflux overnight.

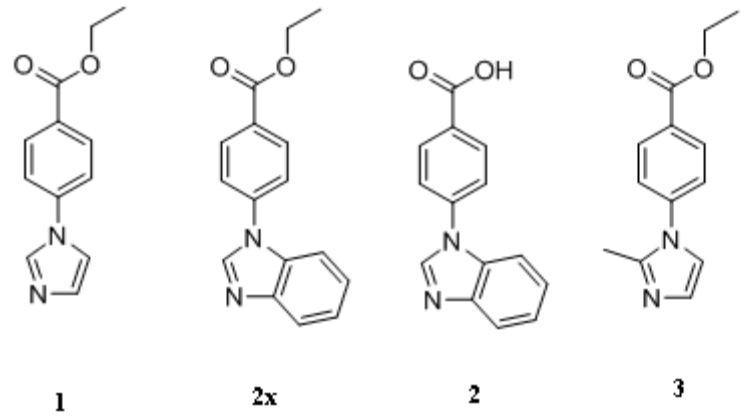

Figure 23. Synthesized organic ligands.

5.2 Synthesis of MOFs and crystalline products

During synthesis of the framework, there are many different factors that must be taken into account for a successful synthesis. If the carboxylate is protected by an ester, the reaction must be heated to a high enough temperature to allow water to react with the

ester leaving a free carboxylate ready to bind to metal ions. The rate of cooling is also a significant factor in order to synthesize single x-ray quality crystals. As an undergraduate we were told that during recrystallization we need to allow the mother liquor of the solution to cool slowly and without any disturbances in order to get large good quality crystals. The same lesson must be applied to the synthesis of MOFs. Using a programmable oven it was possible to set up a temperature program that would be digitally controlled and allow stabilization of a high temperature and a slow rate of cooling.

The next factor that must be considered is the growth solution that the reaction should be carried out in. A solution which is able to dissolve the ligand and metal at room temperature is preferable. However due to the fact that the solutions will be heated to a high temperature the ligand and metal don't necessarily need to be able to dissolve at room temperature as long as dissolvation occurs at high temperature. Once the substituents are in solution they are able to react with one another and form metal complexes. When the metal complexes become large enough they come out of solution and form crystals. If this process is too rapid then what comes out of solution is a microcrystalline powder that is not good for single x-ray data collection. A solvent system that seemed to work well for the imidazole benzoate ligands was a combination of ethanol and water. All the frameworks that were synthesized were done so with an only ethanol and water solvent system except for one. The one exception was synthesized using a mixture of ethanol, dimethyl formamide, glycol (DMF), and water.

Once a proper solvent system was developed the solutions with the organic ligand and metal ion were placed into the oven. The programmable oven was necessary because it

allowed controllable rates of heating and cooling which made results easily reproducible as well as ensuring that the reaction solutions were not disturbed in any way. The temperature that was chosen was 120 °C for hydrothermal synthesis. The reason for this temperature choice is that it is high enough for the de-esterification reaction to occur. For all of the hydrothermal MOFs, except for **3-Cu**, crystals formed before the cooling of the reaction to room temperature. In the case of **1-Cu** there were two different product formations that occurred. One was a crystal that did not diffract very well and the other being **1-Cu**.

The image below displays all the molecular structures of the MOFs.

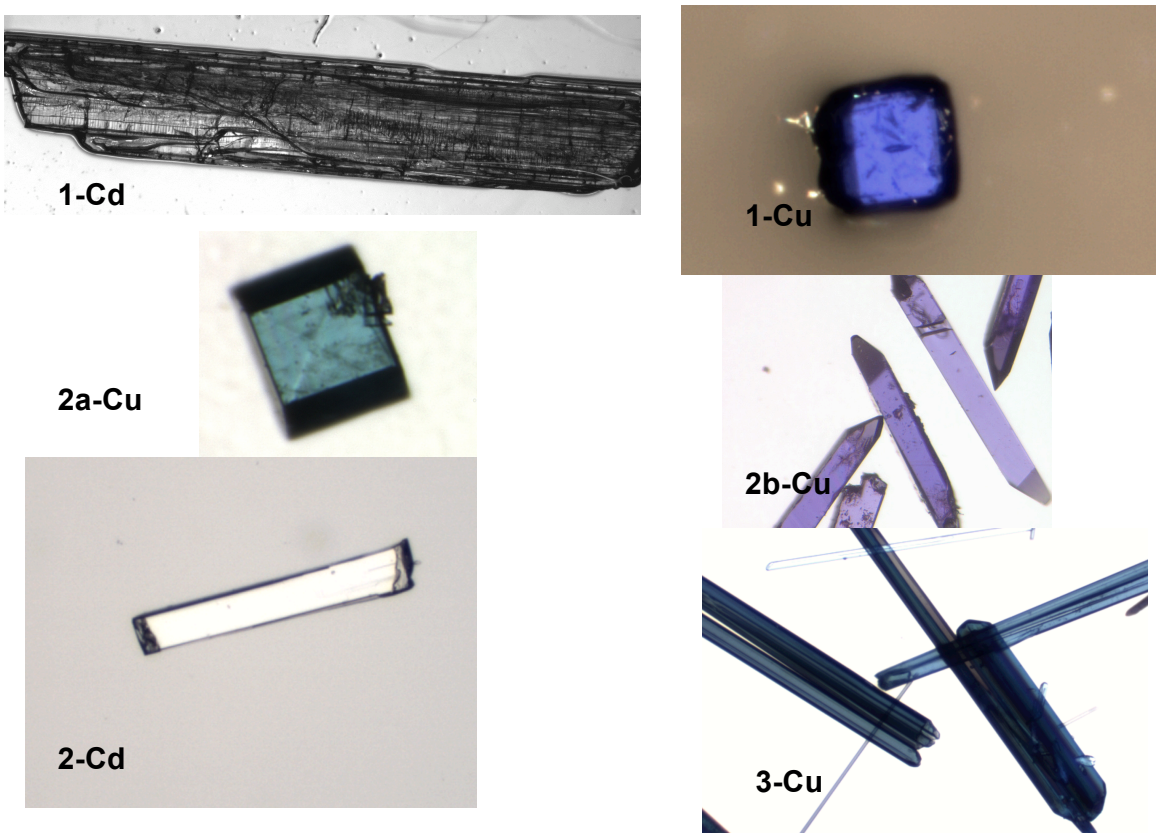

Figure 24. Collage of all the metal organic frameworks crystals images.

5.3 Molecular structures of metal complexes

The molecular structures of the different MOFs can be seen in the figure below. All the molecular structures display a tetrahedral or distorted tetrahedral type of binding arrangement. The MOFs **2a-Cu** and **3-Cu** display a monodentate binding of the carboxylate with the remaining MOFs displaying a bidentate binding of the carboxylate. Although bidentate binding was expected over monodentate binding due to the binding nature of the carboxylates, it is not surprising to see monodentate binding that arises due to steric hindrance from the imidazole substituent. There are not any monodentate binding seen for the regular imidazole ligand metal complexes. The only monodentate binding that is seen is for the benzimidazole and 2-methyl imidazole substituted ligand metal complexes. The modes of binding are also to be expected for the metal ligand binding of transition metals. Due to the binding patterns seen for the imidazole carboxylate binding, it is possible to predict that the binding for future imidazole benzoate ligands would also be tetrahedral. Whether or not there is monodentate binding or bidentate binding would depend on the steric hindrance of the imidazole substituent.

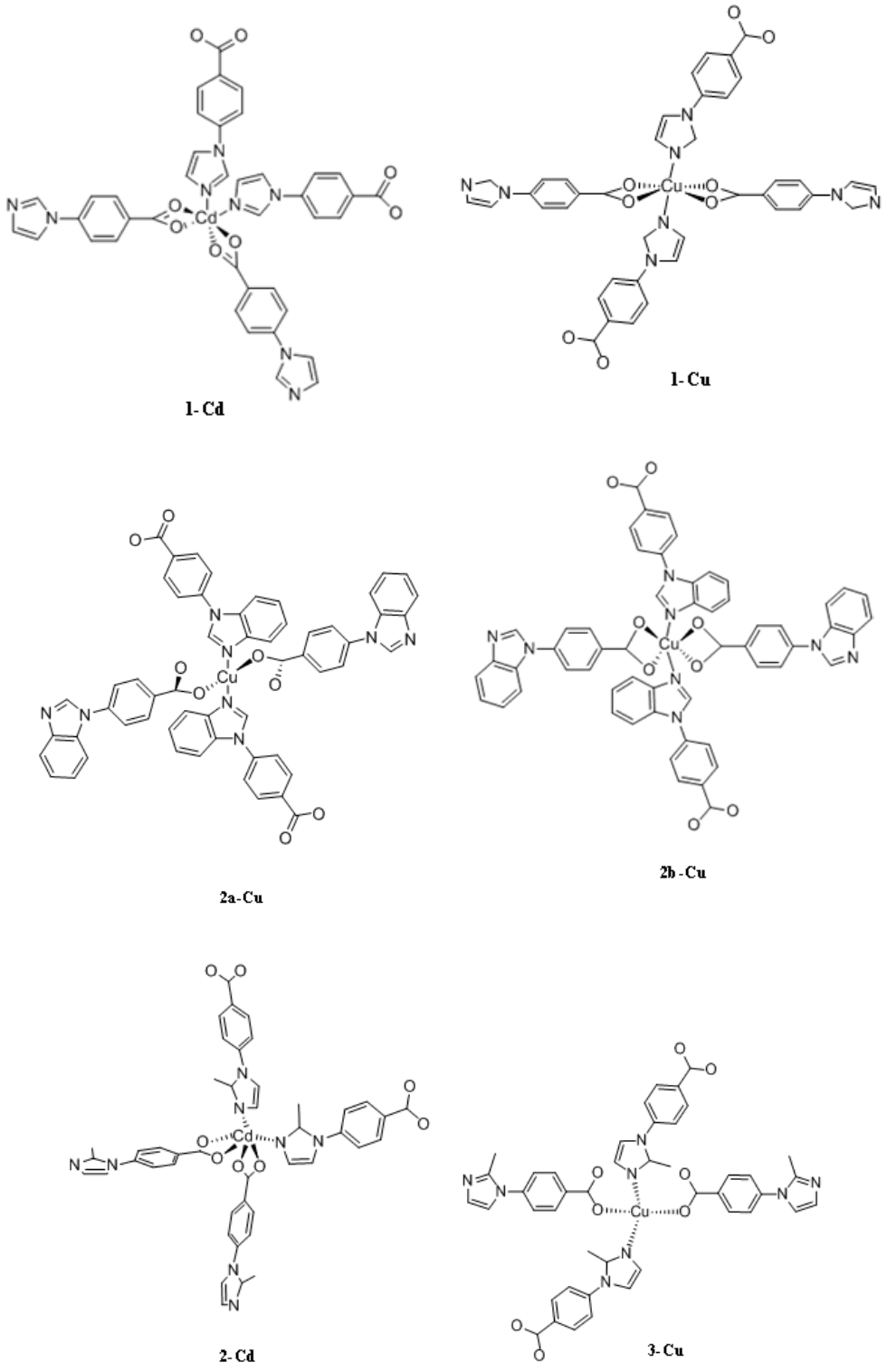

Figure 25. All the metal organic framework molecular structures.

By altering the ratio of the ligand to metal from 1:1 ligand to metal to 1:2 ligand to metal, control of **1-Cu** was accomplished. Seen below is a table that displays the ratios of ligand to metal used and the ratio of ligand to metal seen in the framework itself.

Table 1. Framework ligand to metal ratios

Framework	Ligand Used	Metal used	Ligand:Metal synthesis ratio	Ligand:Metal actual ratio
1-Cd	Ethyl 4-(1*H*-imidazol-1-yl)benzoate	Cadmium	1:1	2:1
1-Cu	Ethyl 4-(1*H*-imidazol-1-yl)benzoate	Copper	1:2	2:1
2a-Cu	4-(1*H*-benzo[*d*]imidazol-1-yl)benzoic acid	Copper	4:7	2:1
2b-Cu	4-(1*H*-benzo[*d*]imidazol-1-yl)benzoic acid	Copper	4:3	2:1
2-Cd	4-(2-methyl-1*H*-imidazol-1-yl)benzoate	Cadmium	2:1	2:1
3-Cu	4-(2-methyl-1*H*-imidazol-1-yl)benzoate	Copper	2:1	2:1

The ligand to metal ratio seen above for the synthesis are the ratios that were optimized for the highest yield of crystals. Although the optimum ligand to metal synthesis conditions vary, the actual ratio of ligand to metal seen in the framework is always 2:1. When examining the structure of the MOFs themselves it is easy to see why the ratio is 2:1, however the fact that the optimal synthesis conditions do not reflect this.

5.4 Structures of MOFs and crystals

The structures for all the MOFs were collected and solved using single x-ray diffraction. All of the MOFs display a 3-D framework arrangement except for **2a-Cu** and **2b-Cu**

which displayed a 1-D and 2-D arrangement respectively. The crystal data and refinement information for the MOFs can be seen below in Table 1.

Table 2. Crystallographic Data and Refinement Information for Metal frameworks

Complex	**1-Cd**	**1-Cu**	**2a-Cu**	**2b-Cu**	**2-Cd**	**3-Cu**
Formula	$C_{24}H_{14}CdN_4O_7$	$C_{10}H_7Cu_{0.5}N_2O_2$	$C_{20}H_{16}CuN_4O_4$	$C_{28}H_{18}CuN_4O_9$	$C_{19}H_{14}CdN_3O_5$	$C_{22}H_{18}CuN_4O_4$
Formula weight	582.79	158.84	439.91	618.00	485.54	465.94
crystal system	orthorhombic	tetragonal	orthorhombic	monoclinic	orthorhombic	hexagonal
space group	Pbca	I4(1)/a	Pca2(1)	*C2/c*	P222(1)	P6(1)
crystal color	colorless	Blue	blue	purple	colorless	blue
a(Å)	16.8924(17)	19.9773(3)	22.106(2)	13.506(4)	7.7078(3)	16.0842(3)
b(Å)	17.1946(18)	19.9773(3)	5.7751(6)	11.069(3)	14.0089(5)	16.0842(3)
c(Å)	18.3036(19)	12.8187(4)	18.2165(17)	20.238(6)	27.2929(10)	25.8851(9)
β(deg)	90	90	90	105.140(5)	90	90
V(Å^3)	5316.4(9)	5115.85(19)	2325.6	2920.7(15)	2947.03(19)	5799.3(3)
Z	8	20		4	5	11
D_{calc}(g/cm^3)	1.456	1.551		1.405	1.368	1.468
No. reflns	6125	3280		3476	6963	7540
R	0.1080	0.0267		0.1166	0.0659	0.0409
wR^2	0.2093	0.2869		0.1973	0.1586	0.3654

[a] $R = \Sigma(||F_o|-|F_c||)/\Sigma|F_o|$; $wR^2 = [\Sigma w(|F_o|-|F_c|)^2/\Sigma w(F_o)^2]^{1/2}$

As you can see from the synthetic scheme in figure 17, the ester protected ligand was placed into a solution of cadmium nitrate and EtOH:DMF:glycol:H_2O. This solution was placed into the Biotage vial and heated in the oven. When the cap was removed from the vial a strong unpleasant odor emanated from the vial, which was not present in the starting solution. It was hypothesized that the DMF somehow reacted or decomposed

during the reaction causing the smell. The clear flat rectangular crystals were removed from solution and placed in oil and single x-ray data was collected. Since these materials are proposed to be porous, placing them in oil during x-ray data collection diminished the amount of guest molecules that could be lost due to room temperature evaporation. The data was also collected at 100 °K in order to prevent guest molecule loss. An image of the molecular structure of the ligand-metal complex is shown below in figure 26. This image is the molecular structure solved from the data collected from the single x-ray instrument.

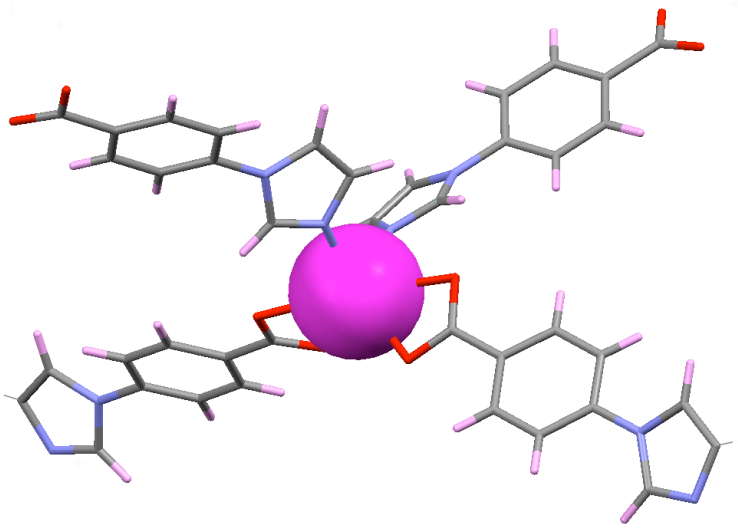

Figure 26. Molecular structure of **1-Cd** structure given from single x-ray data.

It can be noted from the molecular structure of **1-Cd** that the hydrothermal synthesis conditions were indeed successful in de-protecting the ester. The cadmium metal has 4 ligands attached to it, two carboxylate ligands and two nitrogens from the imidazole ring.

The binding occurs in a distorted tetrahedral type binding with an overall ligand to metal ratio of 2:1.

The second framework synthesized was **1-Cu**, which was made from Ethyl 4-(1*H*-imidazol-1-yl)benzoate and copper nitrate. The growth solution was a 1:1 mixture of EtOH and H_2O and resulted in large block crystals that were a deep purple color.

It can be seen from the molecular structure of **1-Cu** in figure 18, that the overall structure is similar to the binding pattern as **1-Cd**. The copper metal has 4 ligands attached, however the difference from the **1-Cd** structure is the non-distorted tetrahedral type binding with an overall ligand to metal ratio of 2:1.

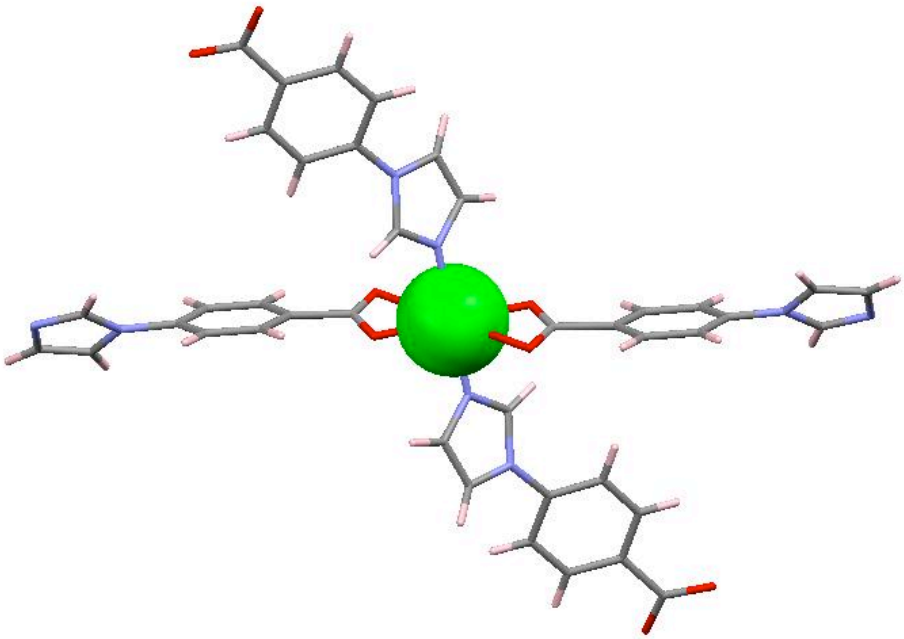

Figure 27. Molecular structure of **1-Cu** structure given from single x-ray data.

The next framework that was synthesized was from the ligand Ethyl 4-(1*H*-benzo[*d*]imidazol-1-yl)benzoate which was de-esterified to give the ligand 4-(1*H*-

benzo[*d*]imidazol-1-yl)benzoic acid. Since the ligand was the free acid and not the ester, room temperature reactions could be carried out. The free acid has a higher probability of not being soluble, however it was found that with minimal heating a mixture of ethanol and water was sufficient to dissolve the ligand into solution. With copper nitrate and differing ratios of ethanol and water two different frameworks were synthesized. The first synthetic scheme is seen in Figure 19.

The ratio of ethanol to water was 1:2 for this structure and resulted in blue block crystals of **2a-Cu**. The molecular structure as solved by single x-ray can be seen below in figure 28. It can be seen that the structure has only one of the oxygen's from each carboxylate binding to the metal in a tetrahedral type binding array.

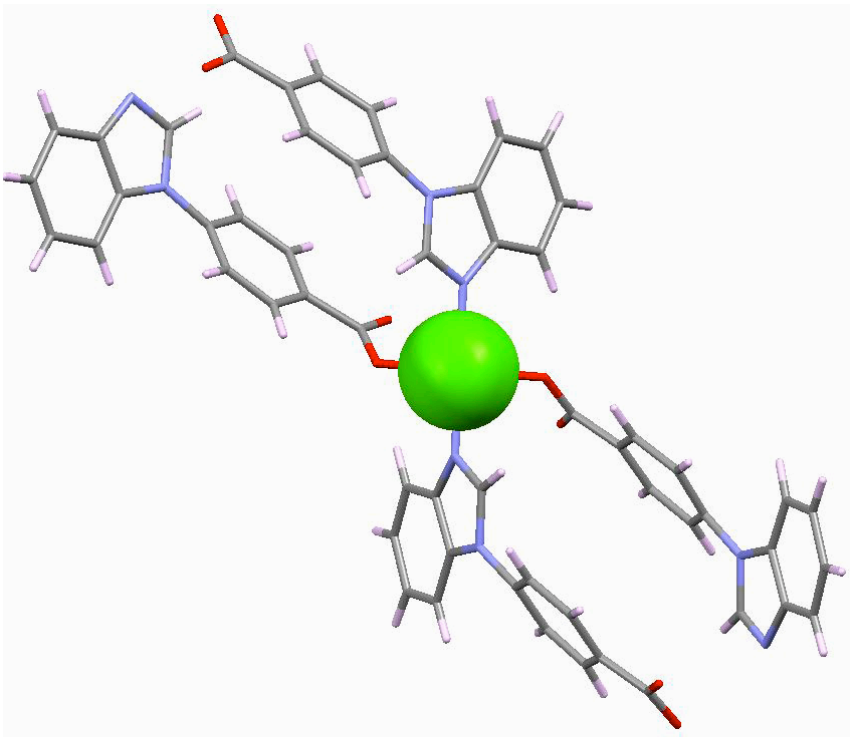

Figure 28. Molecular structure of **2a-Cu** structure given from single x-ray data.

The next framework that was synthesized using 4-(1*H*-benzo[*d*]imidazol-1-yl)benzoic acid also used copper nitrate as the metal ion, however the only difference in synthesis conditions was to change the ratio of ethanol to water to 2:1 from the 1:2 that was used for **2a-Cu**. The synthetic scheme can be seen in Figure 20.

Using the same synthesis conditions as **2a-Cu**, except for the solvent system ratio, the framework **2b-Cu** was synthesized as purple parallelogram shaped crystals. The molecular structure as solved from single x-ray data is seen below in Figure X. It can be seen that the ligand in this case has both carboxylate oxygen's bound to the metal ion. The binding pattern is similar to that of **2b-Cu** however due to the fact that both carboxylate oxygen's are bound to the metal the ligand is seen to lie in a straight line in respect to each other. The overall ligand to metal ratio was found to be 2:1.

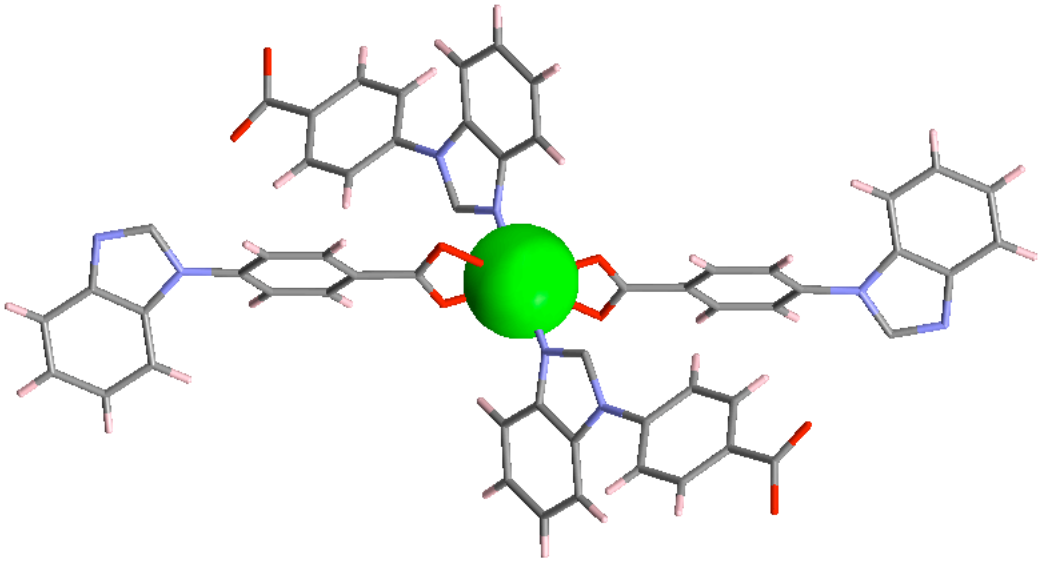

Figure 29. Molecular structure of **2b-Cu** structure given from single x-ray data.

The last two frameworks that were synthesized were done so using the ligand Ethyl 4-(2-methyl-1*H*-imidazol-1-yl)benzoate. Using cadmium nitrate and an ethanol water solution at a ratio of 2:1, a reaction mixture of all the components was prepared and placed into a Biotage vial and into the oven. The reaction vessel was heated to 120 °C for two days and cooled back to room temperature. The reaction scheme can be seen in figure 21. The vial was removed from the oven and allowed to sit for 3 days. Long clear rectangular rod shaped crystals formed and were removed and data was collected on the single x-ray instrument.

The molecular structure of **2-Cd** solved using the single x-ray instrument can be seen below in figure 30. Both carboxylates are attached fully to the cadmium metal ion and the structure looks relatively similar to that of **1-Cd**. It is also a distorted tetrahedral type binding with an overall ligand to metal ratio of 2:1.

Figure 30. Molecular structure of **2-Cd** structure given from single x-ray data.

The second framework that was synthesized with the ligand Ethyl 4-(2-methyl-1*H*-imidazol-1-yl)benzoate was done so with copper nitrate in a ethanol water solution at a ratio of 2:1. The same hydrothermal conditions were used as with **2-Cd** and the synthesis scheme can be seen in figure 22. Long rod-shaped blue single crystals of **3-Cu** formed three days after removal from the oven.

A good quality single crystal of **3-Cu** was taken and data was collected on it using the single x-ray instrument resulting in the molecular structure seen below in figure 31. Only one of the oxygen's of each carboxylate is bound to the copper metal ion, reminiscent of

the **2a-Cu** structure seen previously. The mode of binding appears to be tetrahedral with an overall ligand to metal ratio of 2:1.

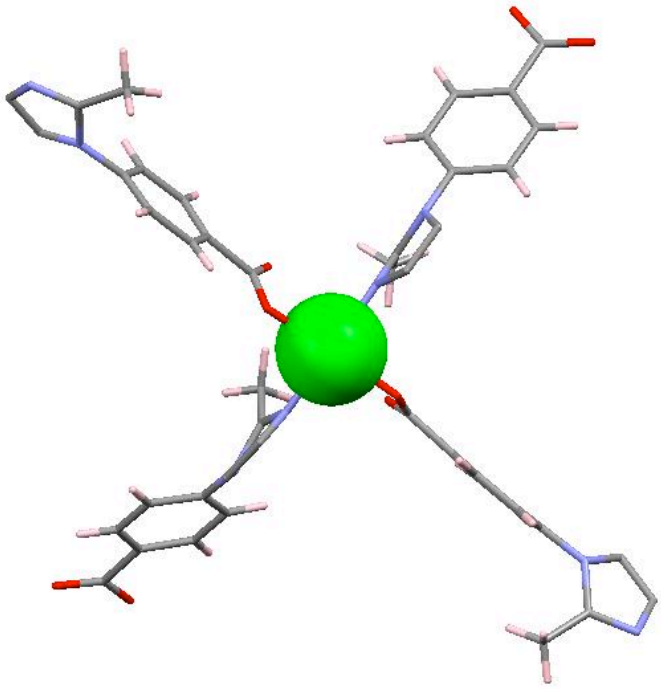

Figure 31. Molecular structure of **3-Cu** structure given from single x-ray data.

The first crystal **1-Cd** displays a diamond framework with a 4-fold interpenetration. An image of the 4-fold interpenetrated framework can be seen in figure 32 below. Each framework is highlighted in a different color to clearly show interpentration that occurs. With the 4-fold interpentration that occurs the pore sizes that would normally be available in a crystal that is not interpenetrated are significantly smaller. The crystal is still porous despite the interpenetration with pores large enough for small guests such as water and ethanol to fit comfortably. This crystal is the only crystal do display interpenetration.

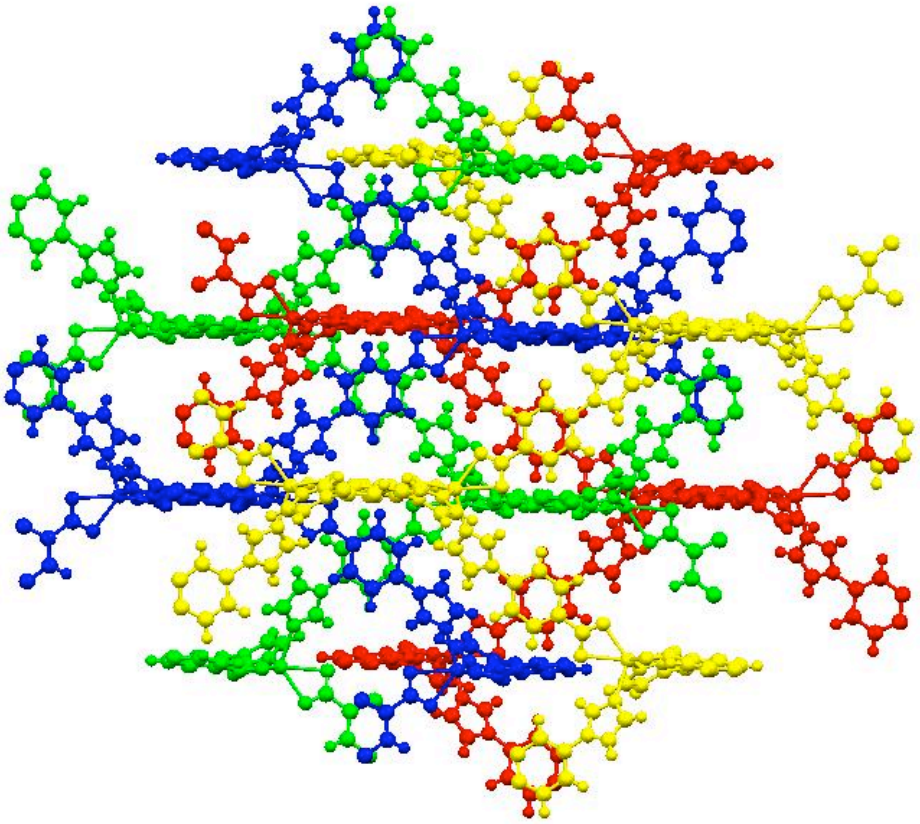

Figure 32. View along the C axis of the **1-Cd** framework. Displays a 4-fold interpenetration, with each color corresponding to a framework.

Disordered solvent can be seen in the open pores of the framework below in Figure 33 and appears to be a combination of ethanol and another solvent. Using spacefill style modeling on the disordered solvent it is possible to see that the solvent appears to fill the pores of the framework and that it is not feasible for a larger molecule to fit within the open spaces. When measured through Mercury 1.4.2 the pore size appears to be about 8.7 Å in both width and height with an infinite length. It is seen that although the ligand used for **1-Cu** is the same as for **1-Cd**, there is not intepenetration seen for **1-Cu**.

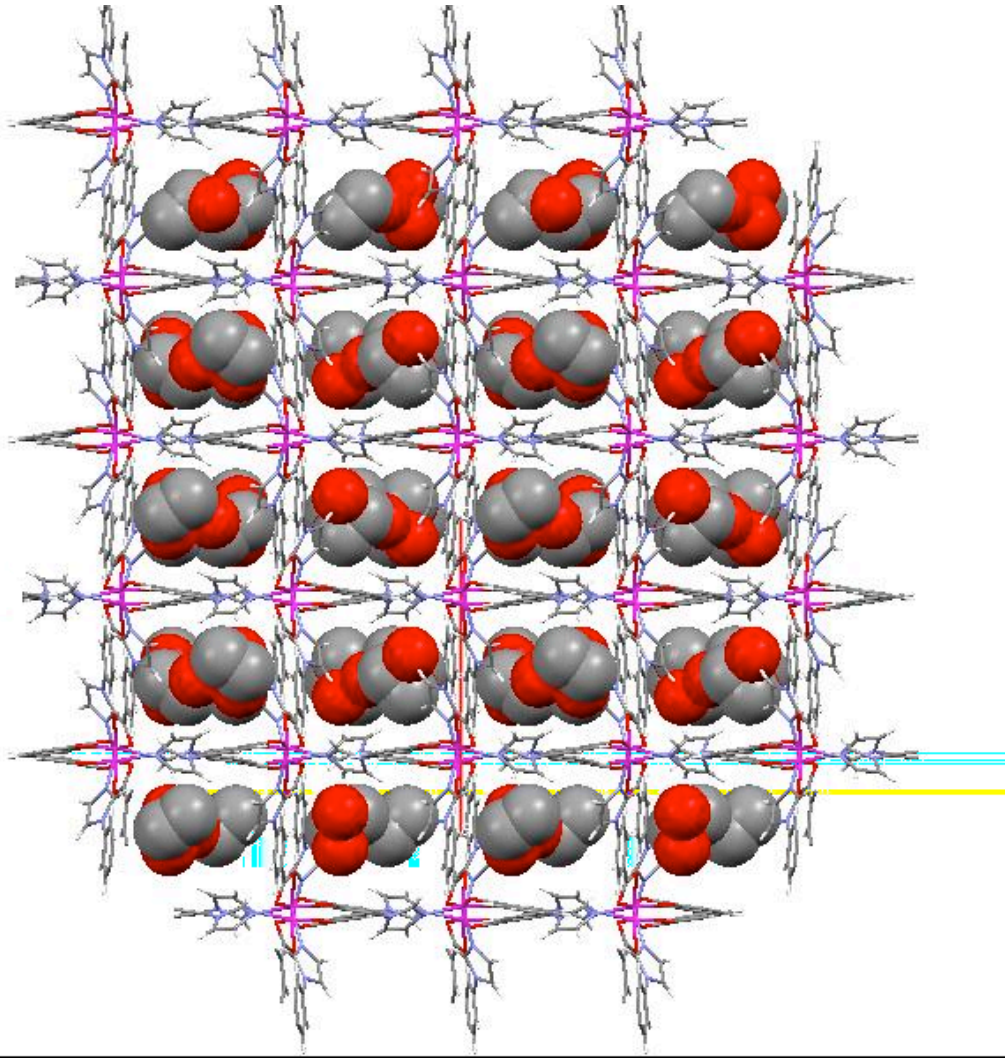

Figure 33. Image of the disordered solvent within the channels of the **1-Cd** framework. Disordered solvent molecules are shown in spacefillstyle. View is shown along the b axis.

The framework **1-Cu** framework is seen below in figure 34 with unresolved solvent molecules shown in spacefill style. When the copper ion distance is measured against the copper ion across from it along the c axis the distance appears to be about 9.9 Å. The hydrogen molecules measure about 5.8 Å across from each other. The pore size that is apparent for **1-Cu** appears a slight bit smaller than that of **1-Cd**. However the structure

still displays disordered solvent molecules in the framework, showing that the crystal is indeed porous.

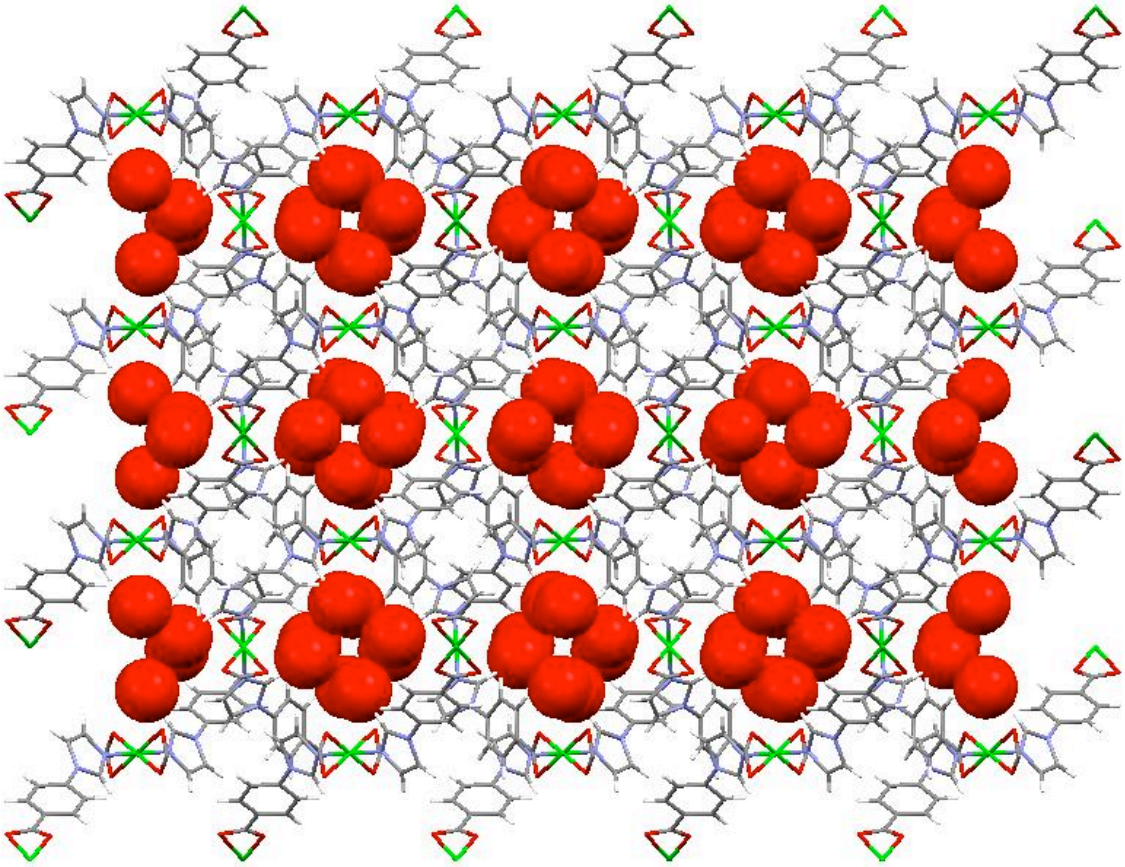

Figure 34. Disordered solvents seen in pores of **1-Cu** framework along the c axis.

The framework of **2a-Cu** appears to be a 1-D sheet that extends along the b axis. This framework is the first of the synthesized frameworks not to display a 3-D array. It appears that by using a ligand without the ester protecting group attached, the ligand has no issues binding to the metal ion without additional heat being necessary as evidenced by the 1-D sheet. It is also seen from the crystal structure that the carboxylate only has one oxygen binding to the metal in a monodentate fashion. There are no apparent pores in this crystal that guest solvent can be present in. It appears from the crystal structure that

the framework is not porous. TGA studies must be done to determine if this is indeed true or not.

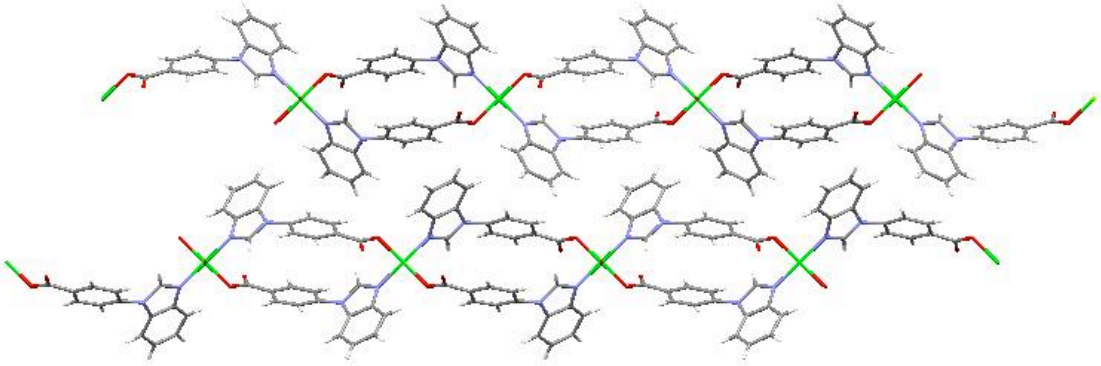

Figure 35. Packing layers of **2a-Cu** along the b axis.

Below an image of **2b-Cu** is shown with disordered solvent visible in the pores. This framework displays a 2-D pattern that has not been seen with the ligands that were used previously. There is evidence of a solvent molecule attached directly to the metal ion. It is possible to hypothesize that the guest molecule is water however TGA must be done to confirm this. The pores do not appear large enough to allow solvent out of the framework without severe changes to the framework itself. The size discrepancy between the pore size and the solvent molecules leads to the supposition that the framework will collapse upon removal of guest molecule solvent from the structure.

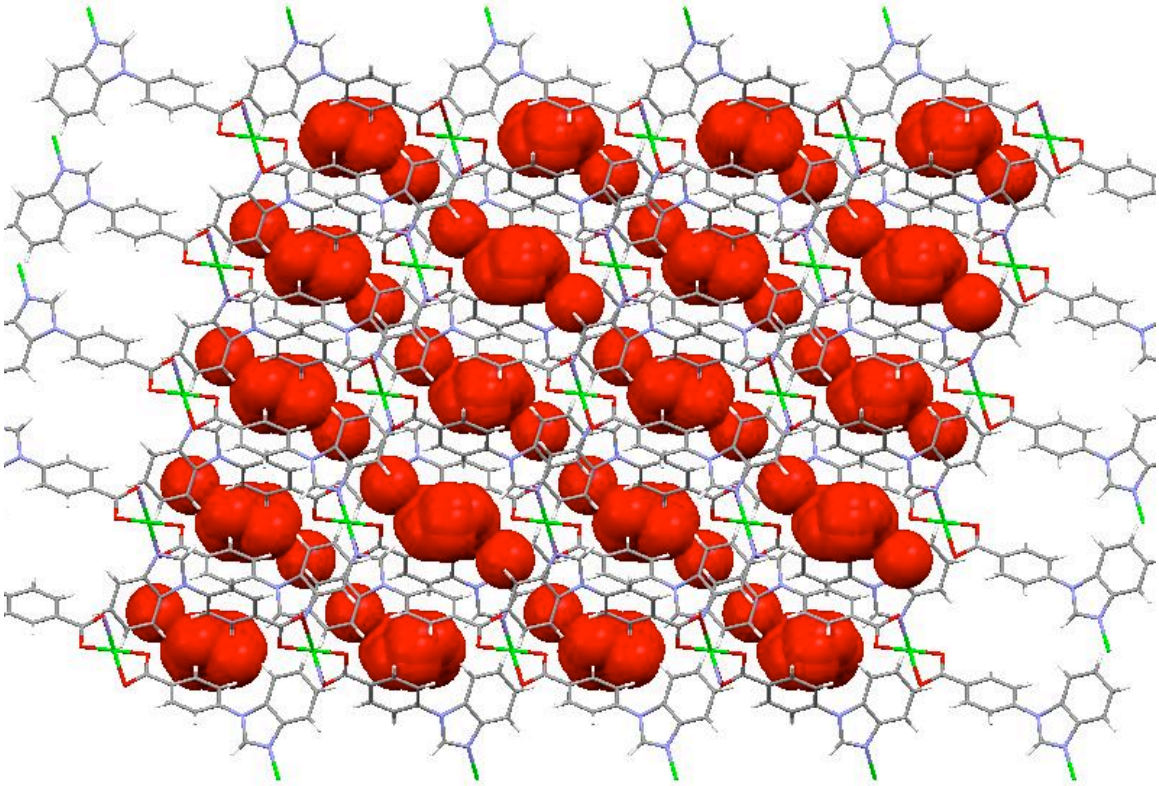

Figure 36. Pores of **2b-Cu** view along the b axis. Disordered solvent can be seen within the pore cavities.

The crystal structure shown below of **2b-Cd** is shown along the a axis with disordered solvent and ethanol in the open pores. It can be seen from the crystal structure that it displays a 3-D framework and that there is definitely ethanol and some other solvent, most likely water. The pores appear large enough that removal of guest molecules from the framework will not result in collapse of the framework due to the guest molecule leaving the framework.

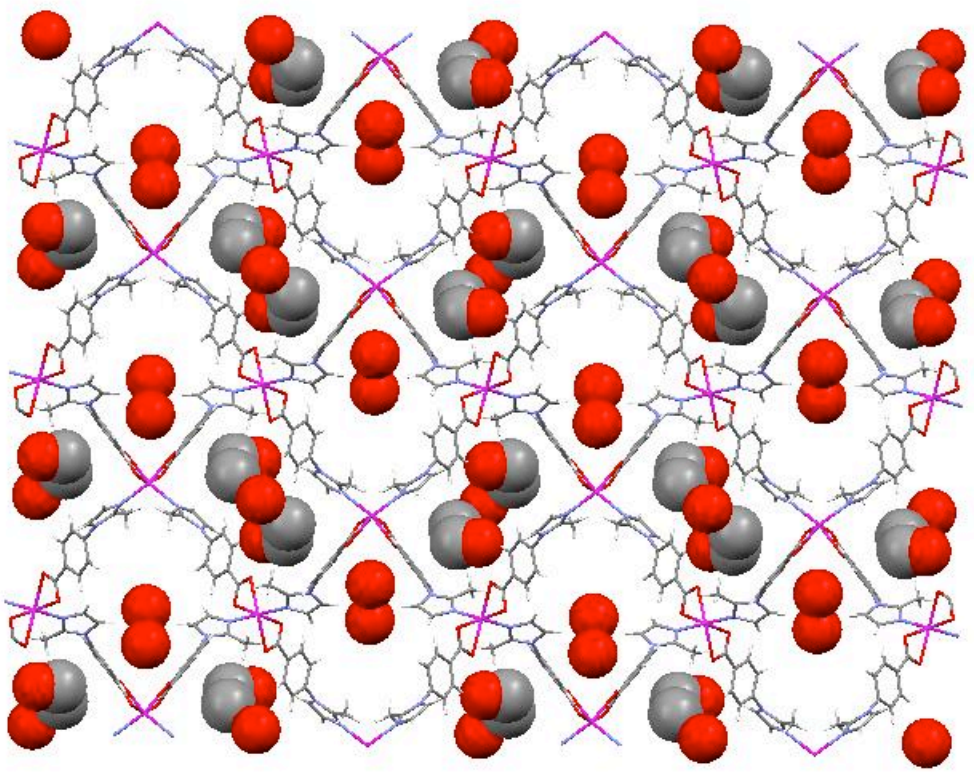

Figure 37. Image of pores of **2-Cd** framework with disordered solvent guest molecules, view along the a-axis.

The last crystal structure of the 3-D arrangement of **3-Cu** is seen below with the view along the c-axis. It can be seen from the image that the solvent molecules appear to be clustered along the sides of the open pore. The pore size is the largest seen for all of the frameworks synthesized, at about 9 angstroms height and width wise. The pores are composed of the repeating framework in a corkscrew pattern. Solvent molecules along the walls of the pore are shown in spacefill to display that even with the guest molecules that line the wall there is still room within the pores for other guest molecules. The reason why the guest molecules that are suspected to be in the pores are not shown in the image below is that the residual electron density could not be solved. Due to the fact that the

solvent molecules are not bound to anything, they experience a stronger vibrational movement in the pores, making the resolution of the molecules extremely difficult.

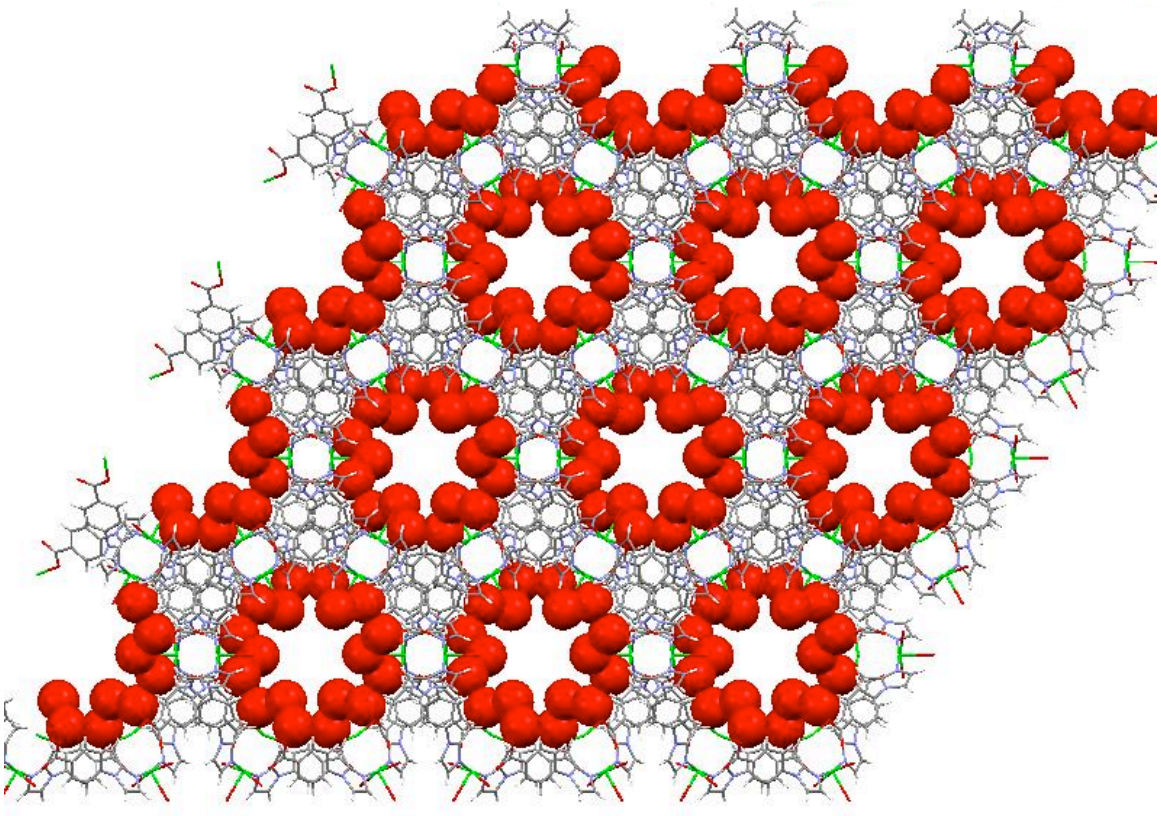

Figure 38. Image of **3-Cu** along the c-axis. Disordered solvent lining the walls of the channels are seen in red spacefill mode.

The image below shows **3-Cu** along the c-axis with the solvent molecules removed to see the copper ion. The copper molecule, seen in green, has been expanded to spacefill view. The red line sticking out of the copper molecules corresponds to the solvent molecule attached to the metal ion. Upon applying a high vaccum, the solvent molecule can be removed from the metal ion, exposing a open faced metal binding site that can by utilized for selective binding of different molecules.

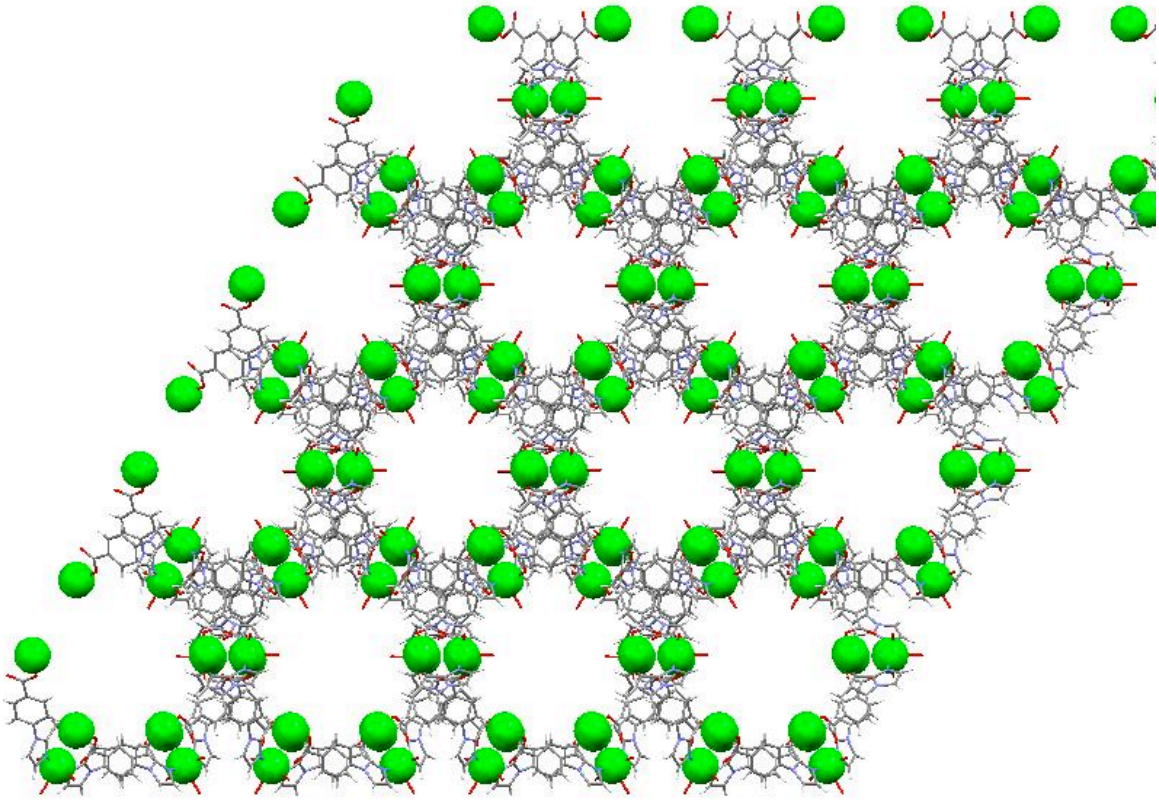

Figure 39. Exposed metal sites of the **3-Cu** framework viewed along the c-axis after removal of guest molecules within the channels. The metal site that faces the open channel shows an attached oxygen which correlates to a guest molecule.

The image of **3-Cu** seen below is displayed with a highlighted yellow area. The highlighted area is the solven accessible surface of a 1.4 angstrom molecule. This means that the Mercury program took a theoretical molecule that measures 1.4 angstroms across and rolled it along the surface of the framework shown below. Any area highlighted in area are places where the theoretical molecules can be present. This shows us how much room can be taken up by a guest molecule of a specific size. In this case 1.4 angrstroms was chosen because it is the length of a methane molecule which is a molecule of interest for gas storage.

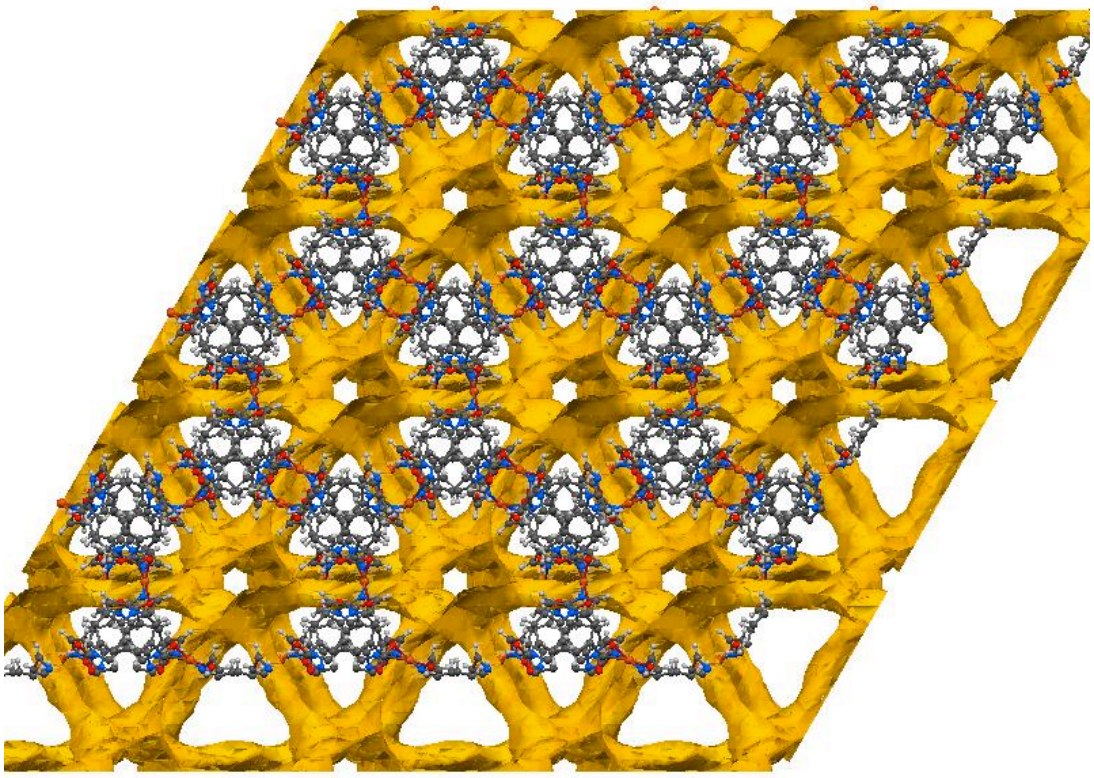

Figure 40. **3-Cu** framework along the c-axis shown with yellow highlighted area, referring to solvent accessible surface.

5.5 Porous behavior of MOFs

Resolving guest molecules structures through single x-ray data is difficult because the molecules are constantly moving around, making it difficult to get clear resolution on the disordered molecules. The only molecules that can be present within the structure are the substituents that were placed within the reaction solution allowing the use of thermogravimetric analysis (TGA) to deduce the identity of the guest molecules. The porous behavior of these frameworks can be examined using TGA to measure the weight loss as a function of both time and temperature. The sample is dried enough to remove any surface adsorbents and placed onto a tared platinum pan and weight constantly throughout the experiment. From the point where the crystals are taken out of solution,

most of the crystals tend to lose guest molecules from within their pores, so care must be taken to ensure that the least amount of time passes from removal of solvent to being placed into the instrument. Even with the care taken, at minimum, there is about a three minute delay that must be taken into account. This can lead to large discrepancies in the overall weight loss exhibited by the framework since the weight loss occurs upon removal from the growth solution. When analyzing the amount of guest solvent release another factor that must be taken into account is the fact that guest loss can be connected to decomposition of the crystal. Any calculations to determine the guest loss from the crystal is not definite due to the high number of variables that can affect the overall amount of weight loss that is truly lost versus what is seen to be lost. The one thing that is definite is that the only guest molecules that can be present in the crystal are the components present in the growth solution.

Besides heating, there is another way to remove guest solvent molecules from the framework. Placing the crystals under a high vaccum pump can allow removal of guest molecules from frameworks that are not as thermally stable as is necessary for removal by heat. Unlike TGA that records the weight loss as a function of temperature, there is no way to determine how much weight loss the crystal undergoes as a function of the amount of time spent in the high vaccum chamber. The best method available is to use the TGA to measure any weight loss displayed by the crystal after the crystal has been under vaccum for a certain amount of time.

When evacuating the crystals by heating, decomposition of the framework can occur due to thermal instability that would otherwise not occur when evacuating using vacuum. When trying to resolvate the evacuated frameworks, vaccum evacauted frameworks were

used instead of heating due to the greater likelihood of framework instability with heating than with applied vaccum. Resolvation was done under house vaccum in a sealed chamber with ethanol and water present. A low vaccum was applied to seal off the environment and allow the crystals to reabsorb solvent molecules in a somewhat saturated environment. On average the crystals were left in the chamber for 2-3 days before being examined using TGA. Loss of guest molecules from the framework is likely to have occurred from the point they are removed from the saturated environment to when they are placed into the TGA. This is further evidenced by the TGAs of the crystals that are taken sitting at room tempertuare over a length of time. This means that the weight loss percents that are shown are always lower than what the overall weight loss of the framework is in actuality. Most of the frameworks were grown from both ethanol and water with only **1-Cd** being grown from different growth conditions.

Seen below, the TGA of **1-Cd** is shown in a graph with weight loss in percent and temperature in degrees Celcius. The crystal was heated from room temperature to 400 °C at a rate of 10 °C per minute. There appears to be an immediate weight loss that begins right after heating, resulting in a 13% weight loss from the original mass. The rapid weight loss can be atrributed to guest solvent molecules that are not bound or not tightly bound within the framework. At about 70 °C there appears to be another loss of weight that plateaus around 300 °C and a rapid weight loss at around 400 °C which appears to be from decomposition of the framework. The slow weight loss that is seen after the initial weight loss stretches from 70°C to 300°C. This weight loss can be linked to a solvent that is bound or tightly bound to the framework which would result in a broader length of time for solvent loss.

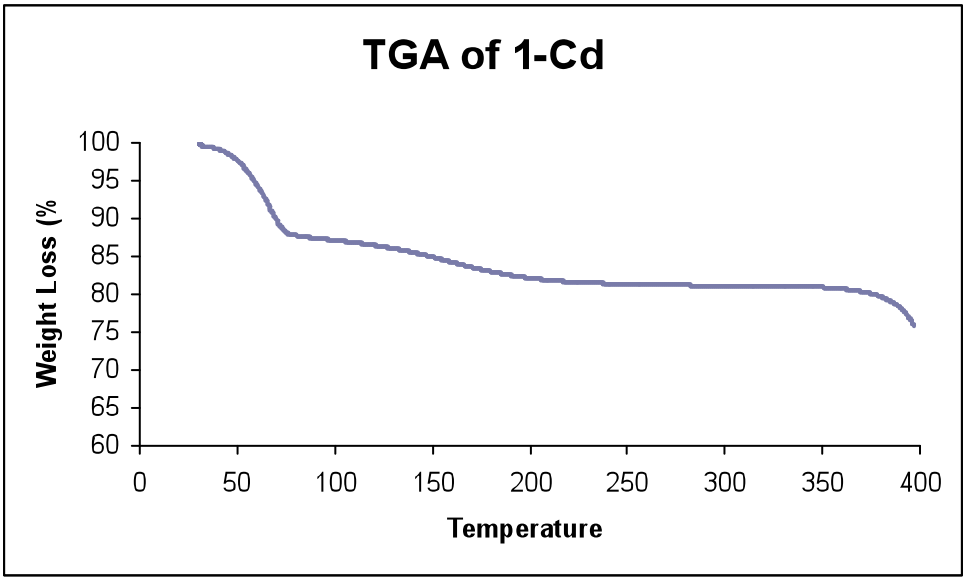

Figure 41. TGA plot of **1-Cd** crystal. The crystals were heated from room temperature to 400 °C.

The DSC of the **1-Cd** crystal shows a broad endotherm that begins at room temperature and ends at 110 °C. The endotherm can be attributed to guest solvent molecule loss.

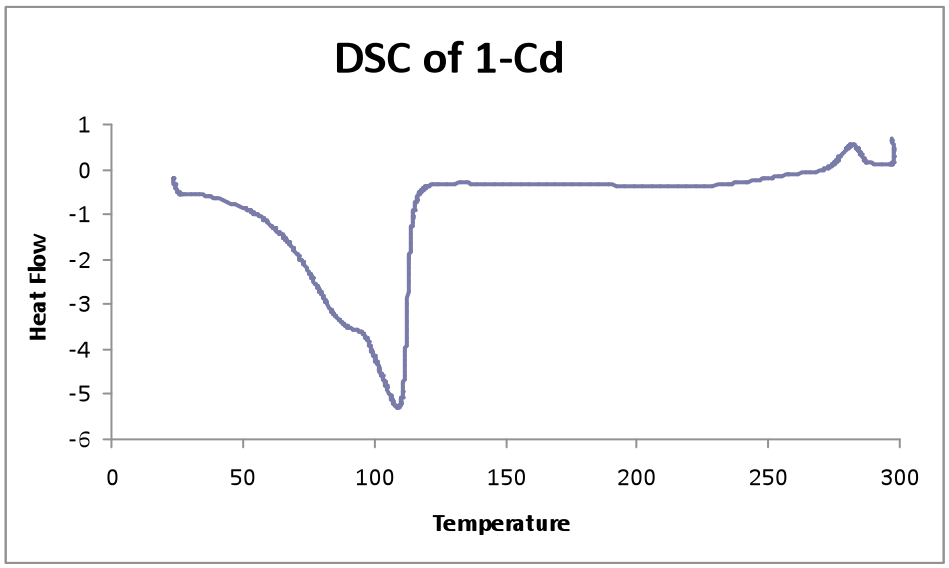

Figure 42. DSC plot of **1-Cd** crystal. Heated from room temperature to 300 °C.

The **1-Cu** crystal displays a weight loss of 20% that begins at room temperature and continues out until a little over 100 °C. The weight loss is not a very steep slope which indicates that the guest molecules inside of the crystal are somewhat bound within the crystal. The crystals plateau steadily until 270 °C where the crystal rapidly decomposes.

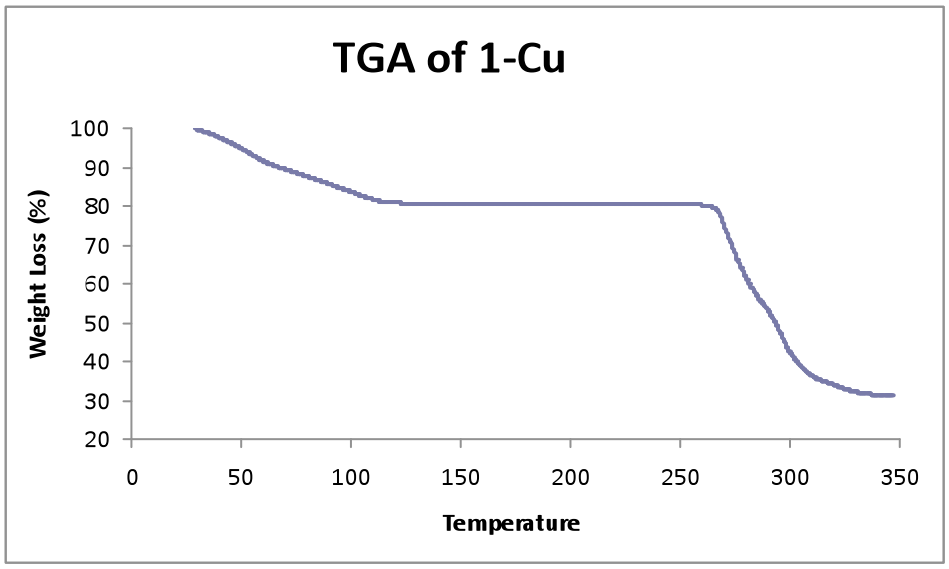

Figure 43. TGA plot of **1-Cu** crystal. Heated from room temperature to 350 °C.

The DSC of **1-Cu** shown below shows a broad endotherm that begins at room temperature and runs to 220 °C. This endotherm correlates to the guest molecules lost from the framework. Following the endotherm is a small endotherm with a exotherm. This is most likely attributed to decomposition of the framework. The rapid weight loss seen from the TGA at around the same temperature further supports this supposition.

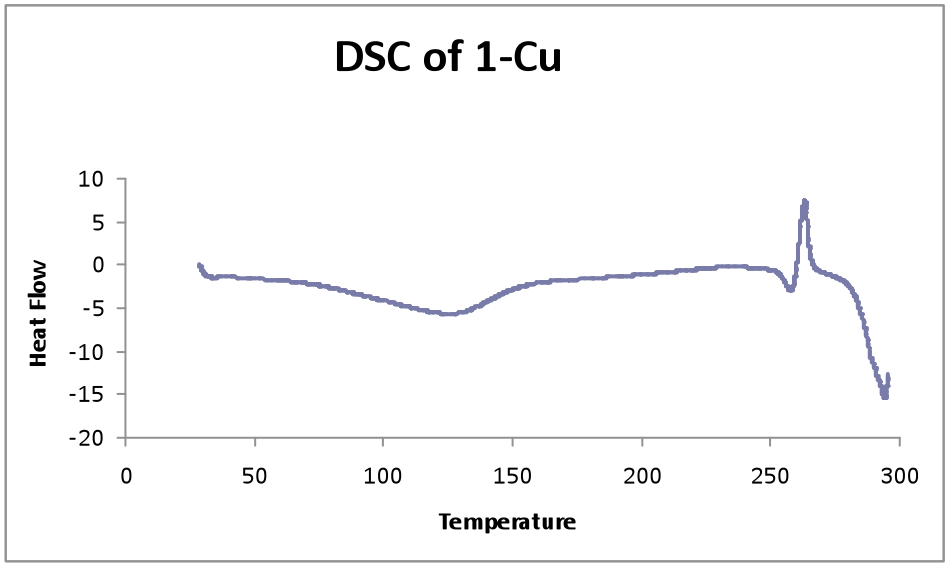

Figure 44. DSC plot of **1-Cu** crystal. The crystals were heated from room temperature to 300 °C.

From the benzimidazole benzoic acid ligand two types of frameworks were synthesized. The first framework is a 1-D framework that according to the TGA and DSC data shown below exhibits high temperature stability. Examination of crystals heated to 250 °C under the microscope showed that the crystal appeared the same as when placed into the TGA with the one exception that the color changed from blue to purple. The TGA of crystals removed straight from solution shows a weight loss of about 2-3%. This weight loss can be attributed to water loss from the framework. The next weight loss occurs at around 300 °C which can be atrributed to decomposition of the framework.

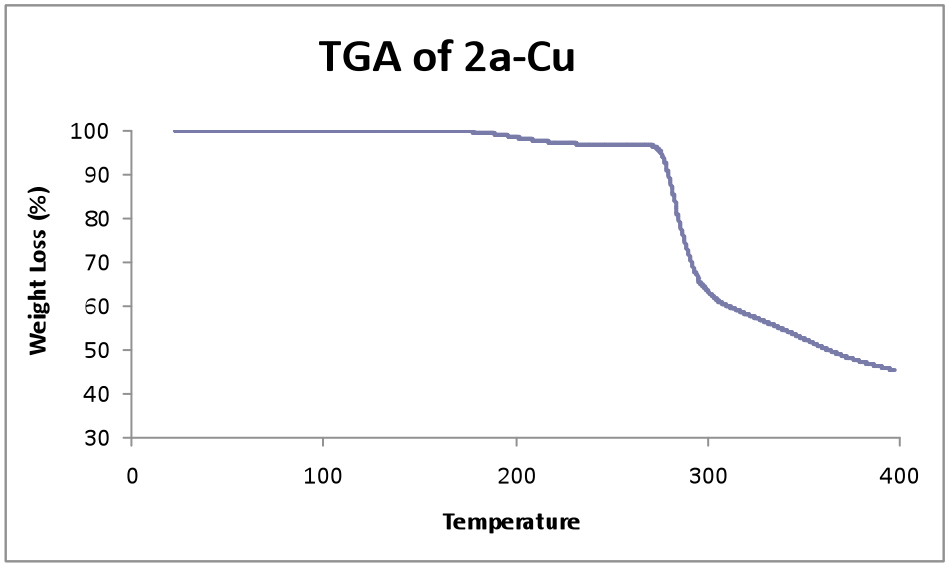

Figure 45. TGA of **2a-Cu** crystal. A small weight loss can be seen occuring at around 190 °C of about 2-3% with decomposition occuring at around 300 °C.

The DSC of **2a-Cu** shows a small endotherm that begins around 200 °C which correlates with the water from the framework with a subsequent massive endotherm that starts at 250 °C till 300 °C.

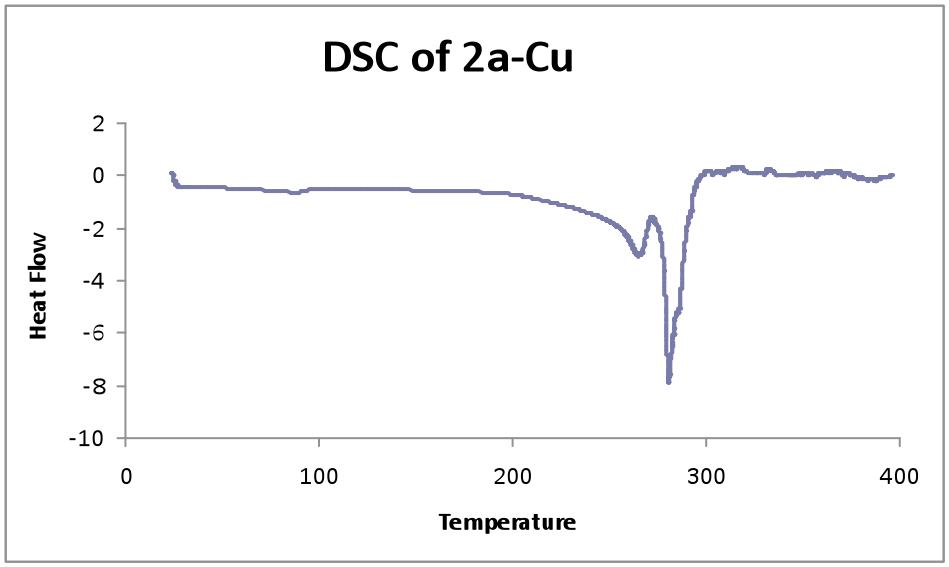

Figure 46. DSC of **2a-Cu** crystal. A endotherm can be seen starting at about 190 °C and ending at 300 °C.

The second framework that was synthesized from the benzimidazole benzoic acid ligand was a 2-D framework with copper which displays two significant weight loss curves. The first one begins at room temperature until 70 °C giving a 18% overall weight loss. The line plateaus and finally decreases down to 50% due to decomposition. It was seen that the crystals do not maintain crystallinity when examined by microscope. Crystals that were left out of solution were examined and opaqueness and massive cracking of the crystal occurred.

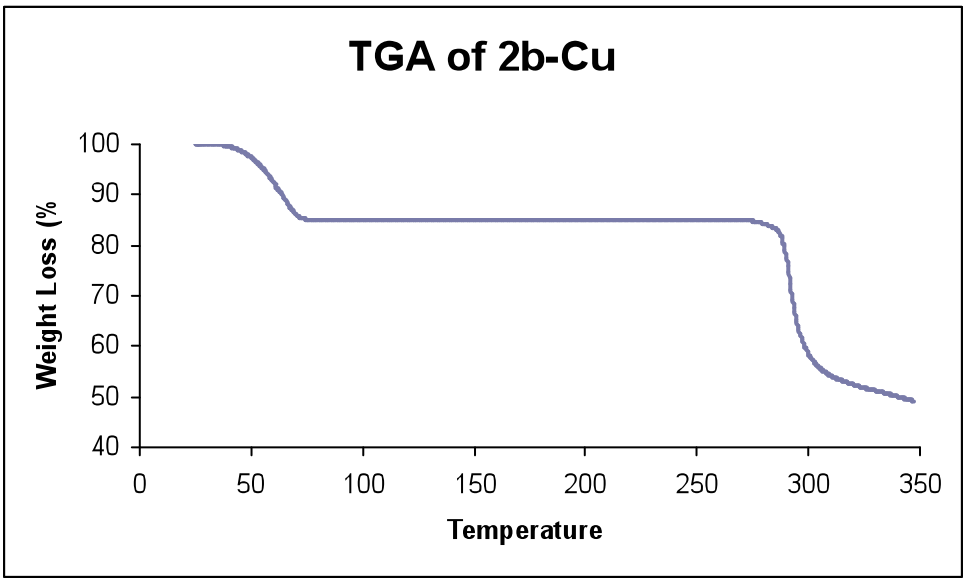

Figure 47. TGA plot of **2b-Cu** crystal. Weight loss of 18% suggests loss two ethanol molecules and one water molecule between room temperature and 80° C.

The DSC of **2b-Cu** shown below displays two major endotherms the first one beginning at around 60 °C and ending at around 150 °C and the second occurring at 270 °C till

about 300 °C. The first endotherm can be attributed to loss of guest solvent molecules from the framework. Crystals that were removed from the TGA that were heated to 100 °C no longer displayed crystallinity and resembled a powder. This leads to the conclusion that it's possible that the first endotherm can be attributed to decomposition as well as loss of solvent molecules from within the framework. The second endotherm can be attributed to further decomposition of the framework.

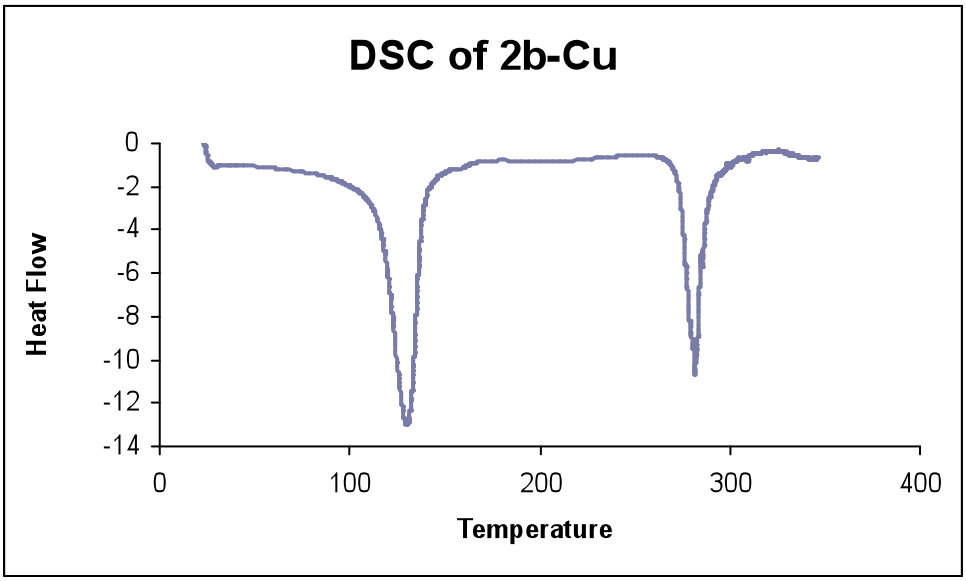

Figure 48. DSC plot of **2b-Cu** crystal. First peak corresponds to weight loss of two ethanol and one water molecule. Second peak corresponds to decomposition of the complex.

The next framework **2-Cd** displays a weight loss that begins at room temperature and continues to 100 °C. The overall loss is 16% however it can be seen that the top of the graph line doesn't begin exactly at 100%. The reason for this is that the TGA experiment equilibrated the crystals at 25 °C and didn't begin data collection until equilibration was set, however the crystals were weighed before equilibration was established leading to the discrepancy seen in the graph.

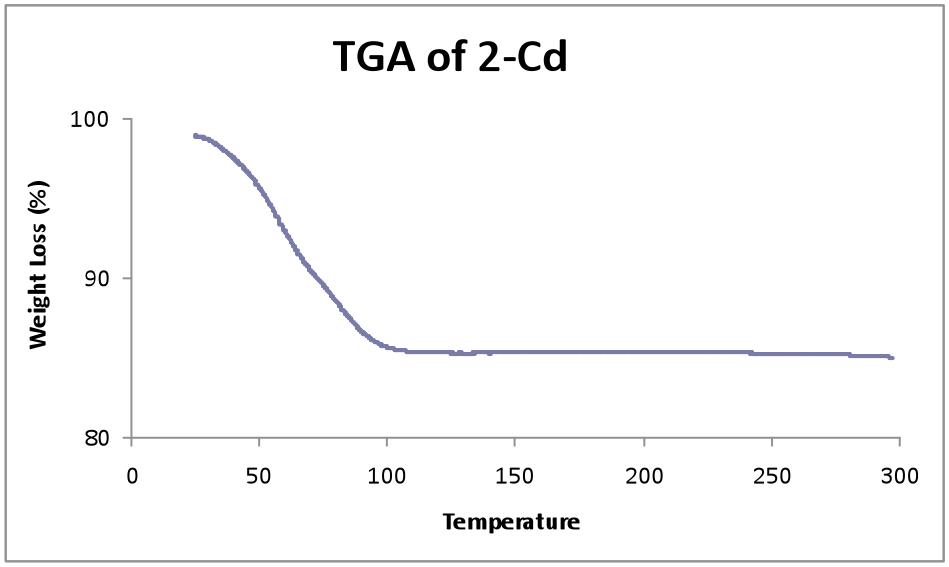

Figure 49. TGA plot of **2-Cd** crystal. Rapid weight loss is seen at room temperature of about 16%.

The DSC plot shows a large broad endotherm that begins at room temperature and continues on until 220 °C. Loss of solvent from the framework could trigger a collapse of the crystal since there are two endotherms so closely related to each other.

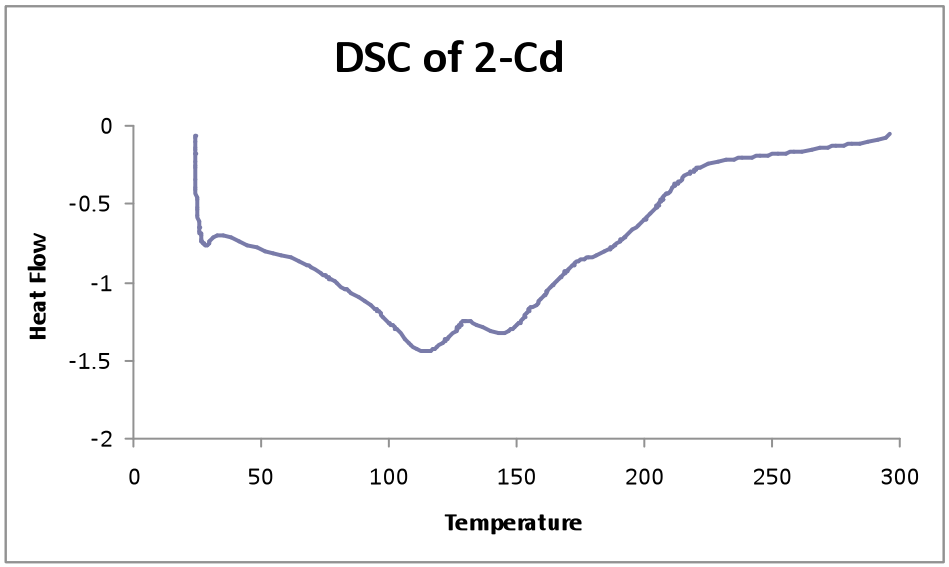

Figure 50. DSC plot of **2-Cd** crystal. A large endotherm is seen beginning at room temperature and extending out to 300 °C.

The crystals of **3-Cu** were examined for porous behavior using TGA and exhibited a weight loss of 30% for the initial weight loss. There is a second weight loss a little past 250 °C which is attributed to decomposition of the framework. The major amount of weight loss is seen at the beginning of the graph and most likely doesn't require heating for removal.

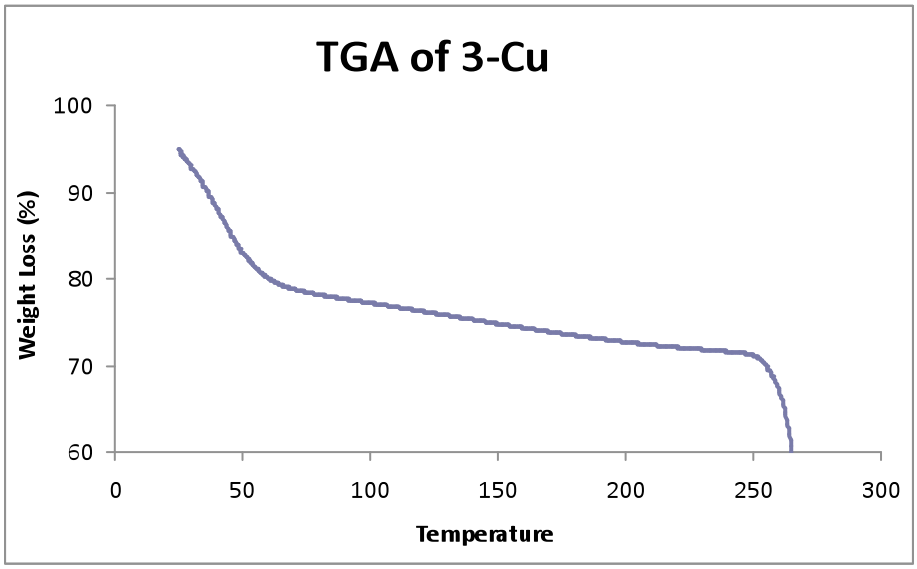

Figure 51. TGA plot of **3-Cu** crystal shows a weight loss of 30%.

The DSC for the framework displays a large triple endotherm at 65 °C that ends at 110 °C. A second small endotherm is seen past 250 °C. It is possible that there is a different endotherm for solvent bound to the framework versus solvent just sitting in the channels with no binding.

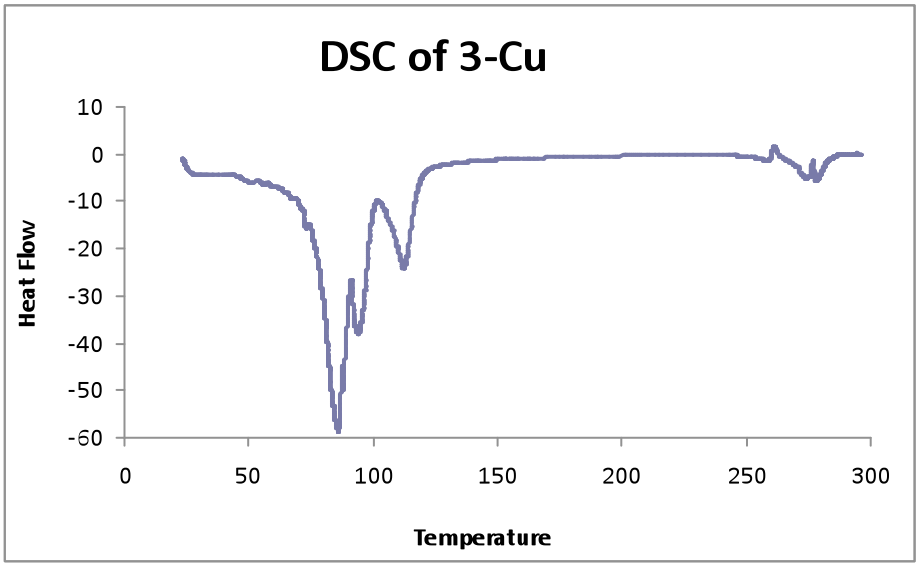

Figure 52. DSC plot of **3-Cu** crystal shows an endotherm at around 75° C and two endotherms following the initial one.

The bar graph below shows the weight loss of all the MOFs to display the different weight loss percents. It is clear that **3-Cu** displays the largest weight loss overall out of all the MOFs at 30%. The MOF that displays the second highest weight loss is **1-Cu** followed by **2b-Cu**. There appears to be no correlation between the ligand type and the overall weight loss. The three largest weight losses are seen by copper MOFs and the two smallest, except for the non-porous **2a-Cu**, are both exhibited by cadmium MOFs.

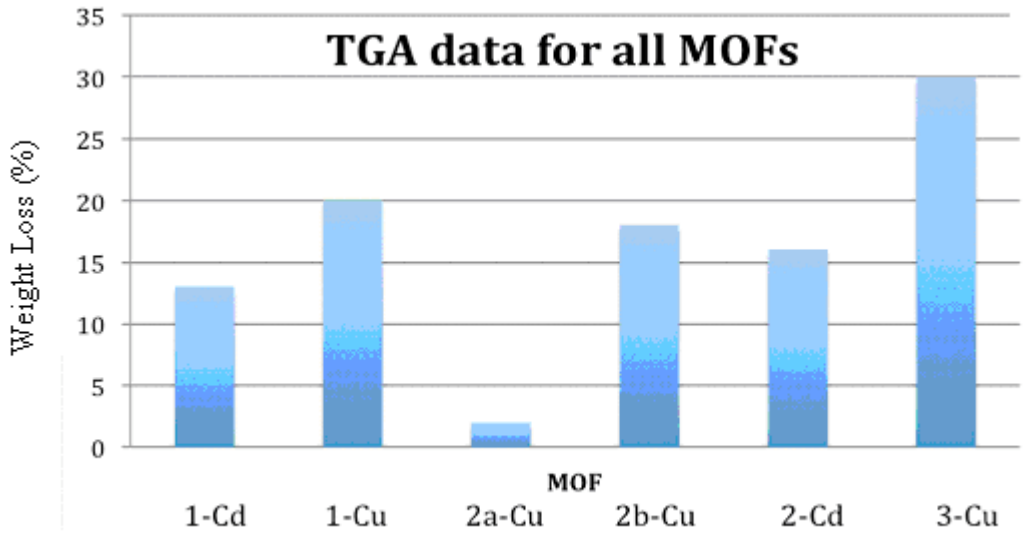

Figure 53. TGA data for all MOFs

5.6 Reversibility of guest loss

In order to determine if guest molecules that were lost from the crystal could be reintroduced back into the framework experiments were devised. Crystals were evacuated using high vacuum instead of heat to lessen the stress that was felt by the crystal. The two main solvents that were focused on for guest reuptake were ethanol and water. In the case of **3-Cu** uptake of rhodamine b was examined. Due to the large porous nature of the crystal it was chosen as the most viable candidate in allowing large guest molecules to enter the crystal. It is noted that for all of the MOFs there is a reduction in the loading of the guest molecules. A reason this could be happening is due to the fact that the reloading occurs using diffusion of guest molecules from the surface into the crystal. There would be a decrease in the rate of diffusion when the channels near the surface of the crystal become filled with guest molecules. This hindered diffusion could prevent a complete loading of crystals with the guest molecules as seen with the MOFs shown below.

In the case of the first crystal, after evacuation of the crystals of **1-Cd** using high vacuum, they were resolvated using a combination of ethanol and water in a chamber with a low house vaccum applied to it. When the TGA collected is examined, it is apparent that the initial weight loss has increased from the 1% seen from the evacuated crystals to about 3%.

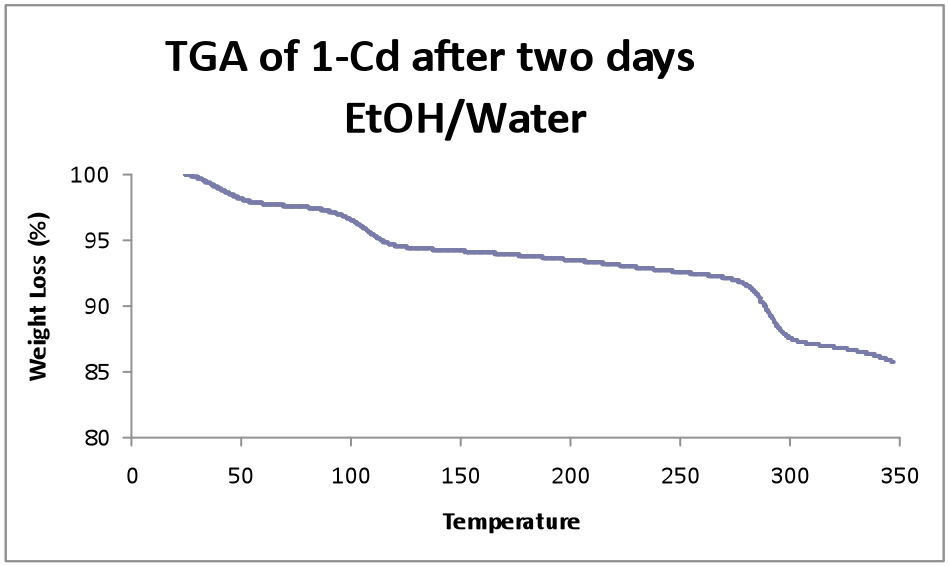

Figure 54. TGA plot of **1-Cd** crystal. The crystals were evacuated using a high pressure vaccum for two days and placed into a ethanol and water chamber under low pressure vaccum for two days.

In order to determine how much guest loss occurs just at room temperature the crystals were placed into the TGA and the temperature was held for 2 hours. The weight loss percent was plotted versus time and can be seen below for **1-Cd**. It can be seen that there is a sharp loss of weight that starts at the point the crystals are placed within the TGA chamber. The sharp decrease in weight slowly starts to level off at around 20 minutes but still continues to lose weight the whole 2 hours the crystals are weighed. During the two hours the crystals are kept in the TGA the overall weight loss is around 16%. Due to the

steep weight loss at the beginning of the experiment it can be assumed that the overall weight loss is in fact higher than what is seen in the graph due to the time delay of removal from growth solution to placement into the chamber. This makes it difficult to determine the exact total weight loss of the frameworks.

Crystals of **1-Cu** were evacatued then placed within a sealed chamber with ethanol. A low pressure house vaccum was pulled on the chamber to ensure a sealed environment and left for a week. The crystals were heated to 200 °C and it can be seen that the crystals lost 6% of the overall weight from just ethanol.

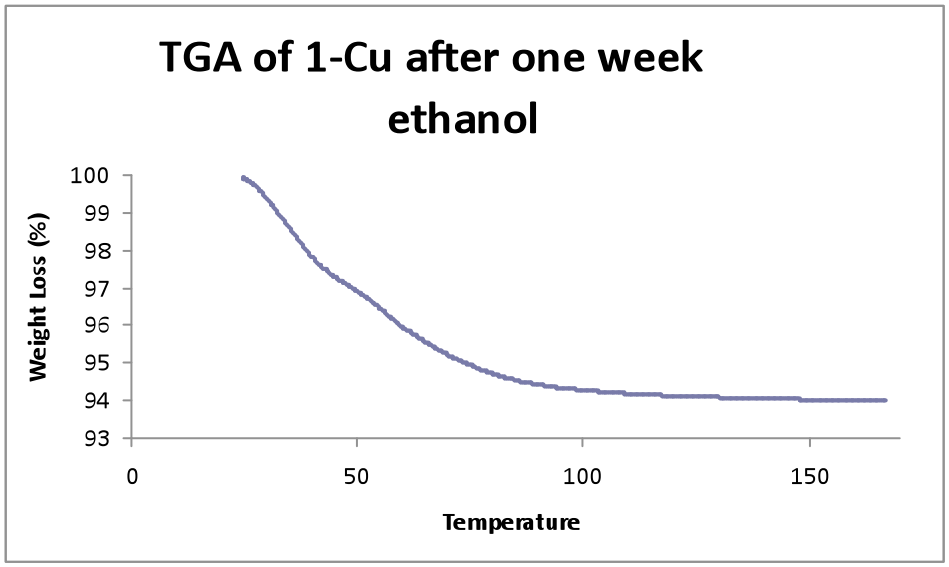

Figure 55. TGA of **1-Cu** crystal that was evacuated then placed into a chamber with ethanol for a week. Starting from room temperature a 6% weight loss is exhibited.

Crystals of **1-Cu** were evacatued then placed within a sealed chamber with water. A low pressure house vaccum was pulled on the chamber to ensure a sealed environment and left for a week. The crystals were heated to 200 °C and it can be seen that the crystals lost 10% of the overall weight from just water. It appears that the crystals exposed to just

water held onto the guest solvent molecule slightly stronger than the ethanol exposed crystals when examining the TGA graph. The water exposed crystals curve appears more concave than the ethanol exposed crystals leading to this conclusion.

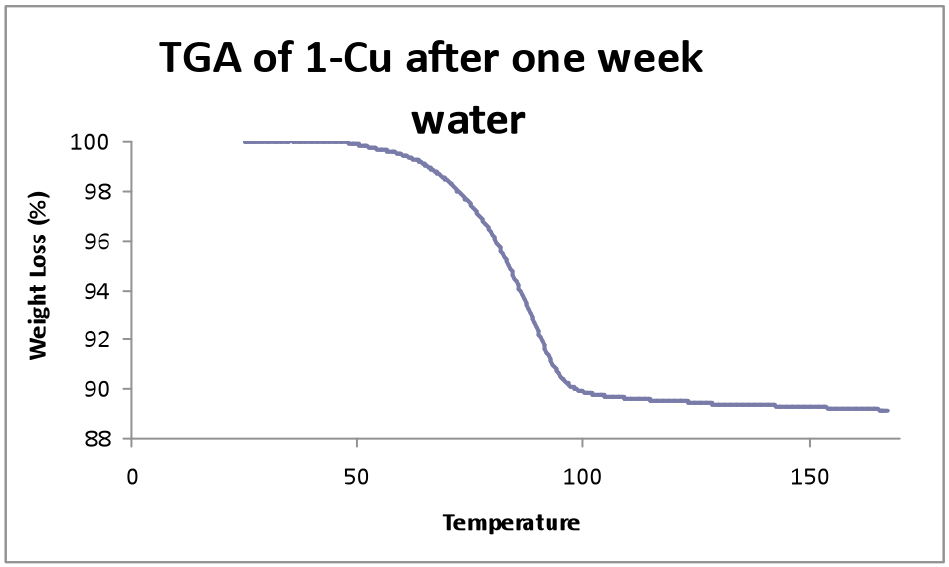

Figure 56. TGA of **1-Cu** crystal that was evacuated then placed into a chamber with water for a week. Starting from room temperature a 10% weight loss is exhibited.

A resolvation experiment of both ethanol and water in equal amounts was done on **1-Cu** to determine if the resolvation of the two different guest solvent molecules was possibly selective. The TGA experiment was run on crystals placed within a chamber with ethanol and water in a 1:1 ratio. The chamber was sealed from outside atmospheric influences using a low pressure house vaccum. From the TGA it is seen that the crystals lose around 17% of their overall mass.

The overall mass loss equals the sum of the weight loss from the crystals of straight water resolvation and straight ethanol resolvation. This leads to the possible conclusion that the preferred binding sites or areas of solvent storage is selective for the two differnet types of solvent. If this was a size selective solvent storage framework then the amount of water resolvation crystals should show a higher percentage of weight loss than what is seen exhibited.

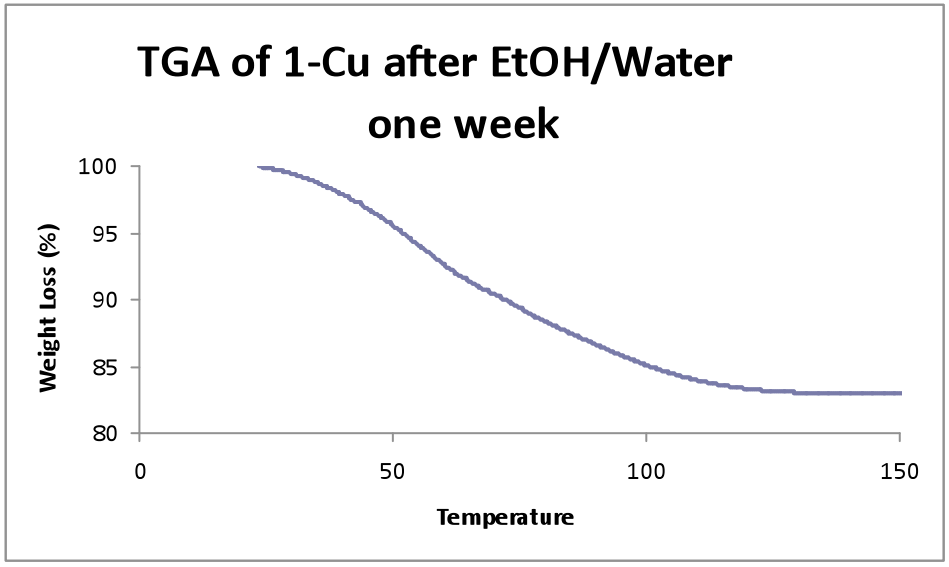

Figure 57. TGA of **1-Cu** crystal that was evacuated then placed into a chamber with water and ethanol for a week. Starting from room temperature a 17% weight loss is exhibited.

In order to determine if the frameworks lose guest solvent molecules at room temperature a TGA experiment was conducted where the crystals were kept at room temperature in the instrument for eighteen minutes. Within those eighteen minutes it was seen that the framework did indeed lose guest solvent moleules from within the framework. In just 18

minutes the frameworks show a loss of 5%. The framework upon heating loses 17% of it's mass so about one-third of the mass loss is from room temperature evaporation from the framework.

The crystals of **2-Cd** were resolvated in a chamber with ethanol and water sealed under house vaccum after having been evacuated using high vaccum. After resolvation the crystals lose 15% of their mass. Since the crystals lost 5% of their mass after vaccum removal it can be inferred that the crystals gained 10% of their original mass back from resolvation.

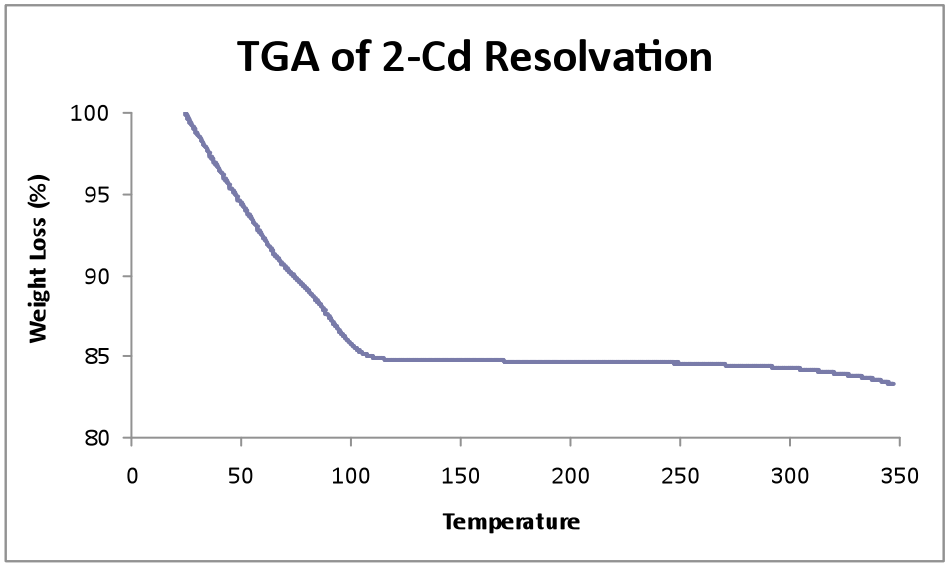

Figure 58. TGA of **2-Cd** crystal that were placed in a chamber with ethanol and water. Resolvation occurred in 2 days with an overall weight loss of 15%.

Crystals of **3-Cu** were resolvated using the same conditions as used for the previous experiment. The crystals were exposed to atmospheric ethanol and water for one week and an overall reuptake of 13% was seen for the crystal. This amount is not close to the amount of guest molecule seen exiting the crystal from the original TGA. A reason that

the crystal was only able to reabsorb a little less than half of its mass is due to the fact that the framework has such large pores that any atmospheric vapor molecules of the solvent would not be tightly bound to the framework and would leave the framework rapidly. It was seen from the original TGA that the largest percent of weight loss occurred at room temperature and very rapidly. The correlation is that the large weight loss would occur from loosely bound guest molecules that leave so rapidly they would not be measured by the TGA instrument, simply due to the fact that it takes too long to transfer the crystals and begin recording the data.

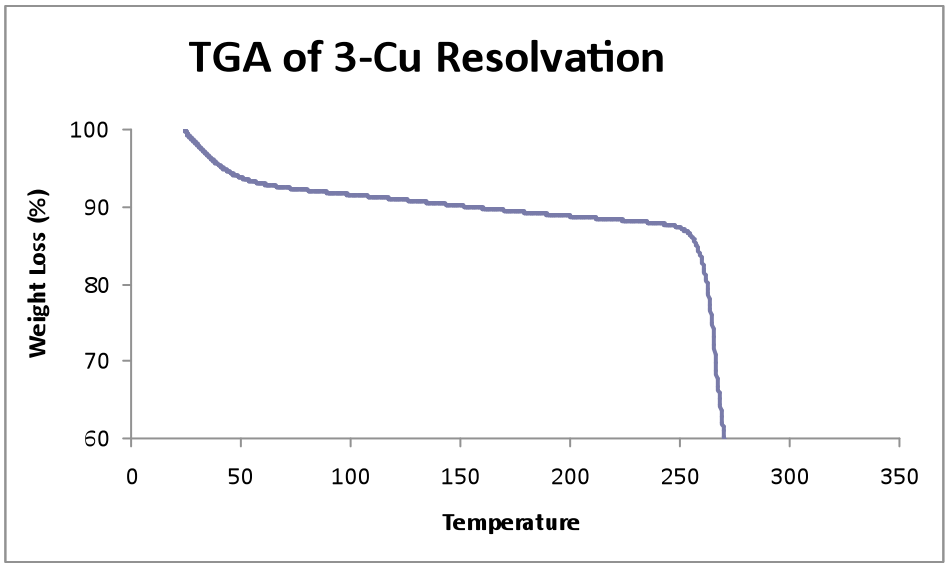

Figure 59. TGA plot of **3-Cu** crystals that were placed in a chamber with ethanol and water. Resolvation occurred in 1 week with an overall weight loss of 12%.

In the case of **3-Cu**, the channels of the crystal are large enough to fit a fairly large molecule inside. The guest molecule chosen is rhodamine b which is a large dye molecule that is readily quantified using UV-VIS spectroscopy. Utilizing a standard graph made from a set of known rhodamine b concentrations the amount of rhodamine b

that was found in the crystals by percent weight was determined. Two different sets of crystals were used. The first set of crystals were crystals of **3-Cu** that had been taken straight from solution with only the surface adsorbed solvent molecules being removed by drying. The other set of crystals were crystals that had been evacuated using a high vacuum pump. The reasoning behind the two sets of crystals was to see if removing guest molecules from inside of the crystal would affect the dye molecule entering the crystal. It was found that the crystal **3-Cu** was able to take up 4.9% of its own mass in the dye rhodamine b. The crystals that had been evacuated before exposure to rhodamine b were able to take up 5.3% of their own mass in the dye. The difference between the two dye uptakes is so small that it is possible that there is no difference between evacuated crystals and non-evacuated crystals. This could mean that the dye has a preferential need to go inside of the pores, regardless of whether or not there are already guest molecules present in the crystal. This type of preferential need to go inside of the framework is promising.

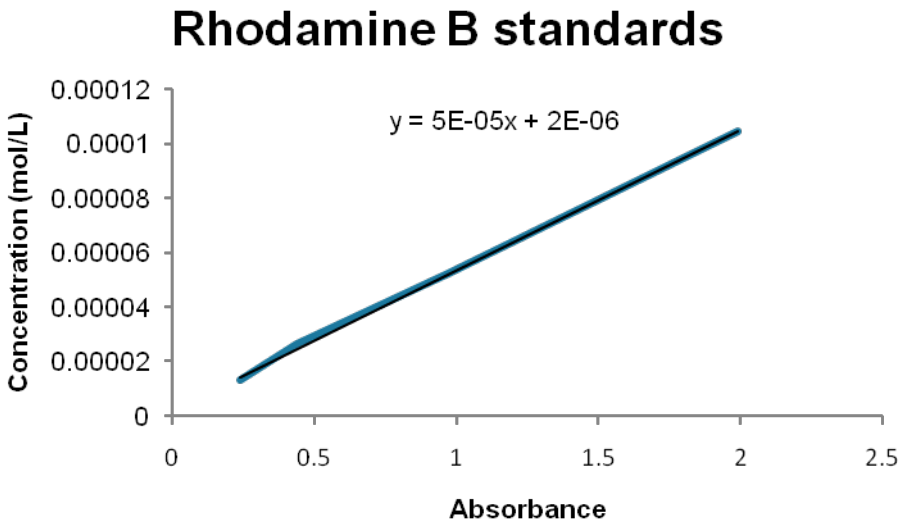

Figure 60. Graph of rhodamine b standards

5.7 Stability of MOFs and crystalline solids

In order to determine how much of the guest molecules in the resolvation experiment were truly reabsorbed by the crystal it became necessary to see if the evacuated crystals still retained any of their original guest molecules after evacuation. The reversibly porous MOFs were examined to see if the guest molecules could be removed from the crystal completely. It is known from the previously shown TGAs that guest molecules can leave simply by sitting at room temperature and can also leave upon heating or application of a strong vacuum. In order to determine how much guest molecules are lost at room temperature, TGA was used as tool to find the amount of non-bound or loosely bound guest molecules present within the crystal. It is known that for MOFs **1-Cd**, **1-Cu**, **2-Cd**, and **3-Cu** reversible porous behavior is seen. The evacuated crystals were used for the resolvation experiments, so it is clear that the crystals retain their porosity upon evacuation.

The crystals of **1-Cd** were evacuated using high vaccum for two days. A TGA was taken of the evacuated crystals. It can be seen from Figure X that the initial weight loss that was seen from the crystals that were taken straight from the growth solution is significantly diminished. The crystals appear to lose about less than 1% of their overall weight and maintain the weight until 100°C with the rest of the TGA looking similar to the TGA of **1-Cd** crystals straight from solution.

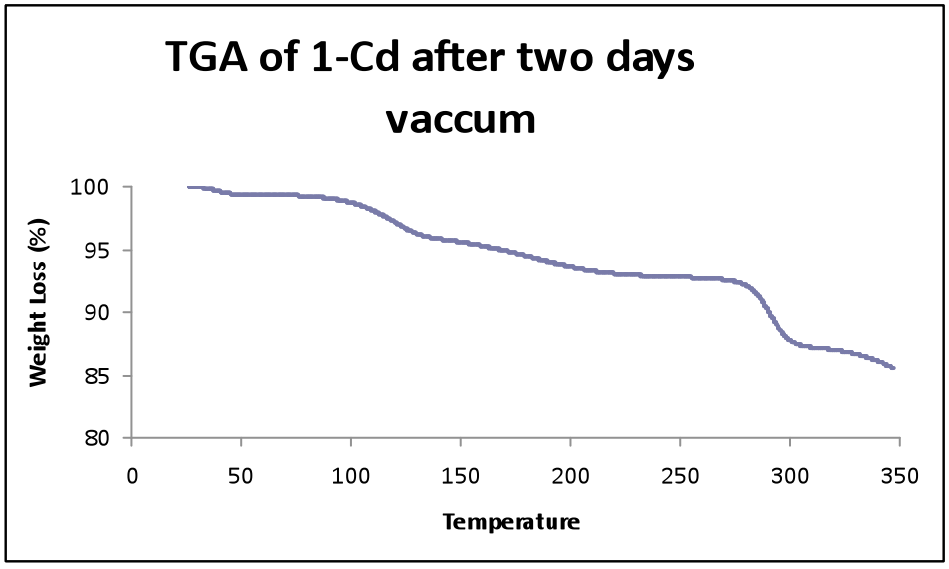

Figure 61. TGA plot of **1-Cd** crystal. The crystals were placed under high pressure vaccum for two days.

When crystals of **1-Cd** were examined using TGA for two hours at a constant temperature of 25 °C it is clearly seen that there is a steep initial weight loss of around 8-9%. The slope begins to level out and the rate of guest loss is decreased signficantly. Due to the high rate of weight loss at the beginning of the graph, the time taken from removal of solution to placement inside the instrument with data collection, there could be a large percent of mass loss that was not properly recorded because of the lag time.

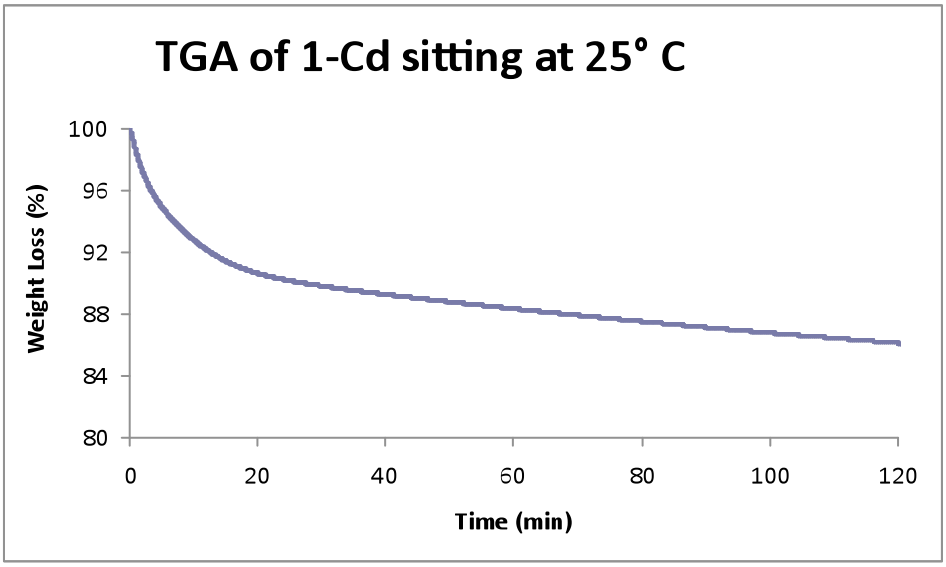

Figure 62. TGA plot of **1-Cd** crystal. The crystals were held at room temperature for 2 hours.

Crystals of **1-Cu** were kept at 25 °C for 18 minutes. During that time it can be seen from the graph that the crystals lose weight at a steady rate and that the beginning loss is not a sharp steep slope like the one seen for **1-Cd** previously. The crystal loses 5% of its mass in 18 minutes at room temperature.

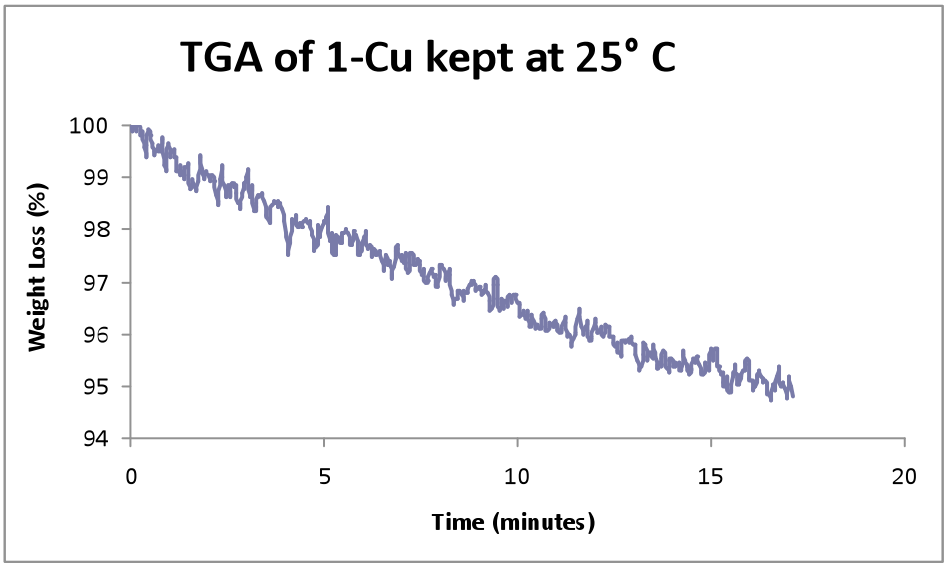

Figure 63. TGA of **1-Cu** crystal kept at room temperature for 18 minutes. An overall weight loss of 5 % can be seen for the crystal.

The crystals of **2-Cd** were evacuated by high vaccum for one and a half hours to see if evacuation by high vaccum was both possible and effective in removing guest molecules form the crystal. It can be seen from the graph that the crystals seem to retain 5% of their mass that would otherwise be lost during heating as seen in the TGA. This leads to the conclusion that at least 5% of the guest molecules are tightly bound within the framework and that the high vacuum was effective in removing the more loosely bound guest molecules.

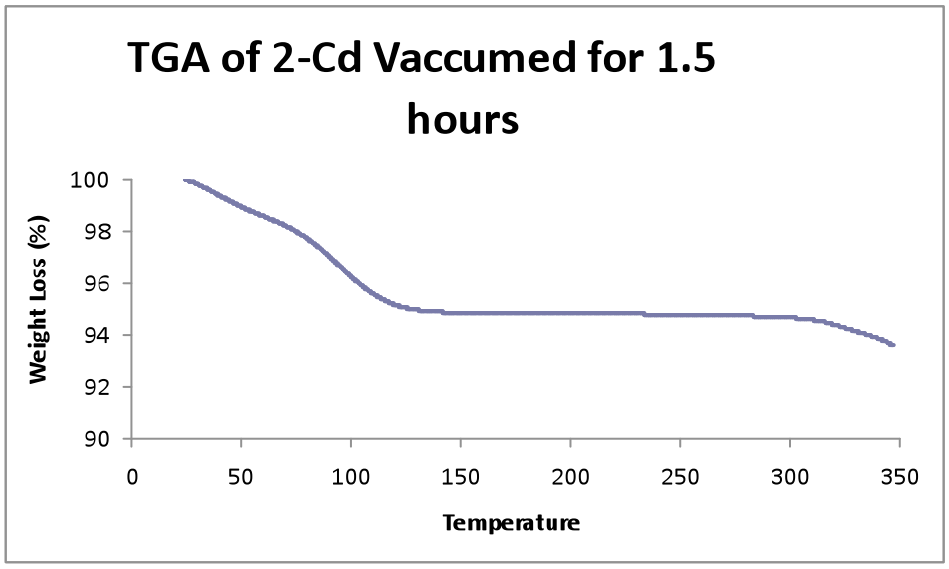

Figure 64. TGA of **2-Cd** crystal evacuated under high pressure vaccum for 1.5 hours. TGA shows a weight loss of 5 %.

Crystals of **2-Cd** were examined to see how much weight is lost from sitting at room temperature. Upon examination after two hours the crystals lose 12% of their mass. The initial weight loss at the beginning of the graph is very steep and then begins to slow down. The slope is distinctly steeper than the slope of the guest molecules that were removed from the evacuated crystals after heating. At the end of 120 minutes the line has not plateaued but is close to plateauing.

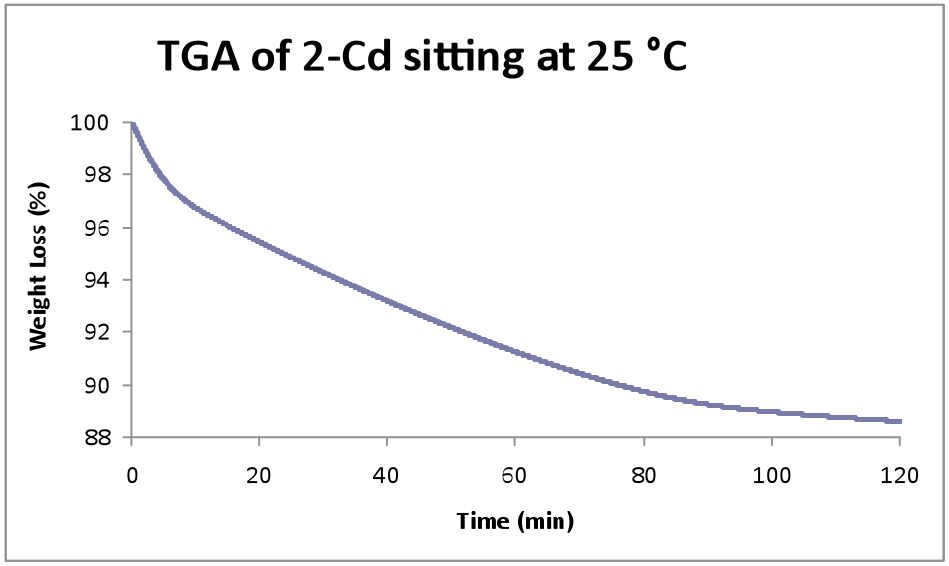

Figure 65. TGA of **2-Cd** crystal kept at room temperature for 120 minutes. An overall weight loss of 11 % can be seen for the crystal.

Crystals of **3-Cu** that were evacuated using high vacuum were examined by TGA to see how much solvent was still held within the framework. It is assumed that guest solvent molecules that were still held within the framework after exposure to high vacuum are held more tightly than the guest molecules that were removed. It can be seen that the framework still retains about 5% of its mass after evacuation for 24 hours.

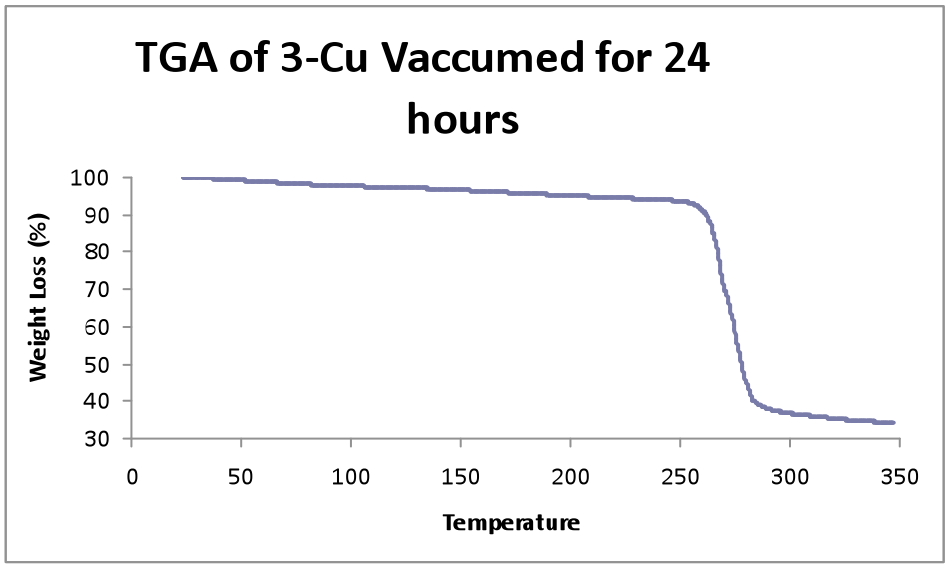

Figure 66. TGA of **3-Cu** crystal evacuated under high pressure vaccum for 24 hours. TGA shows a weight loss of 5 %.

To determine how much solvent is lost from the framework at room temperature the crystals were held at room temperature for two hours and it is apparent that the crystals lose a large amount of its mass at room temperature and it happens rapidly. The overall weight loss of the crystals is 30% of the overall weight. The rate of weight loss at the beginning of the graph gives evidence that the weight loss is higher than 30% due to lag time between removal from solvent and beginning of the TGA experiment.

Due to the fact that all the crystals appear to lose mass at room temperature it is safe to assume that the weight loss that is seen exhibited by the crystals is in fact lower than the actual weight loss displayed by the crystal. From the point of removal from the growth

solution the crystals are losing mass and continue to do so without a mass recording until the TGA begins. It is safe to say that the MOFs lose around 6-7% of their mass that is not recorded by the TGA due to the lagtime between removal from solvent and recording of the weight loss by the TGA instrument.

Most of the weight loss that is seen exhibited by the frameworks are clearly lost just sitting at room temperature. This means that the guest molecules are not that tightly bound in the crystal to begin with. The fact that most of the guest molecules are not tightly bound within the crystal makes it more surprising that the crystals are able to resolvate such a high amount per weight percent. The driving force of the guest molecules entering the crystals must be high in order to resolvate the crystal such a high amount. If there was no driving force in the crystals pulling the guest molecules in then the amount of mass loss upon heating with TGA would be minimal.

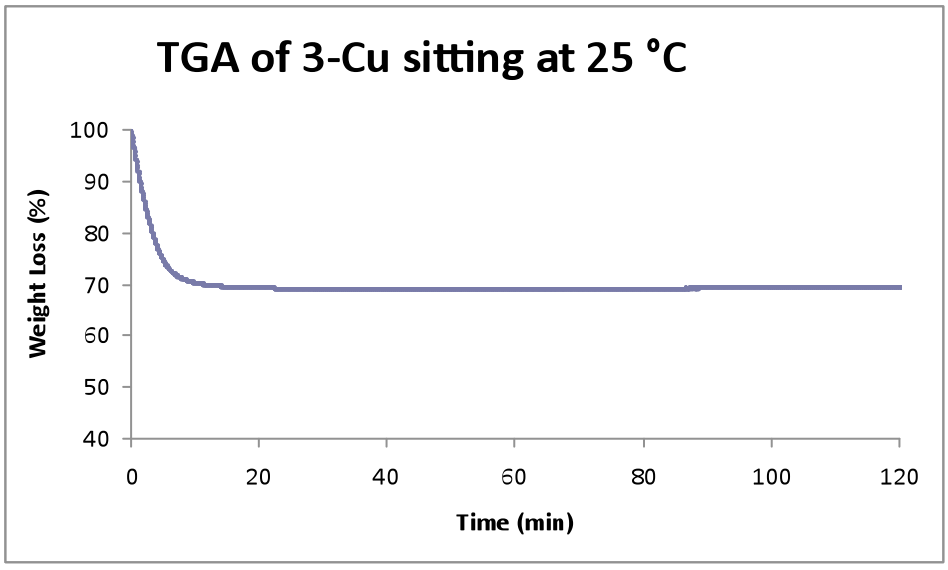

Figure 67. TGA of **3-Cu** crystal kept at room temperature for 120 minutes.

Another way to determine if the crystal maintains its structure is using powder x-ray diffraction. By comparing the powder x-ray patterns before and after heating and after resolvation, it is possible to see if the patterns match. A matching pattern indicates that the crystal lattice is the same. If the peaks seem to shift from side to side or increase or decrease in height, this could be indicative of breathing of the lattice. The powder x-ray in black is the pattern for crystals taken straight from solution. The red powder x-ray is the pattern for the evacuated crystals. The blue powder x-ray is for the crystals that have been resolvated. Shown last is the powder overlay for each of the MOFs to make it easier to see any similarities or differences between the three powder x-rays. It was seen that MOFs **1-Cd**, **1-Cu**, **2-Cd**, and **3-Cu** were able to resolvate after evacuation. This means that the crystals are still crystalline and the pores or channels are still open for guest molecules to enter the crystal. Although the crystals all display peaks, meaning they still are crystalline in nature, the peaks of the three overlay powder patterns do not match up for any of the crystals except for the nonporous **2a-Cu**. The rest of the crystals, except for **2b-Cu**, were seen to be reversibly porous so it is assumed that the disappearance of peaks is due to breathing of the lattice or a rearrangement of the structure. Collapse of the lattice is improbable due to the reuptake of guest molecules seen previously. The powder x-rays for all the MOFs can b seen below in figures 68-91.

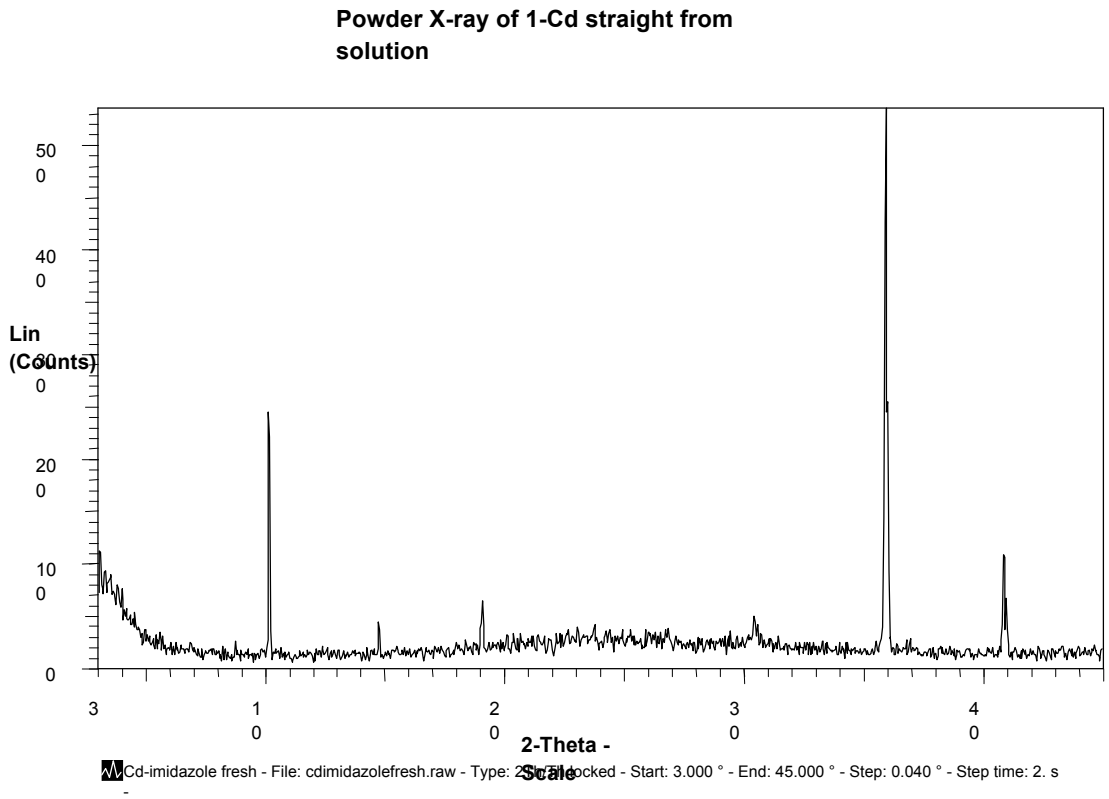

Figure 68. Powder X-ray of **1-Cd** crystals taken straight out of solution.

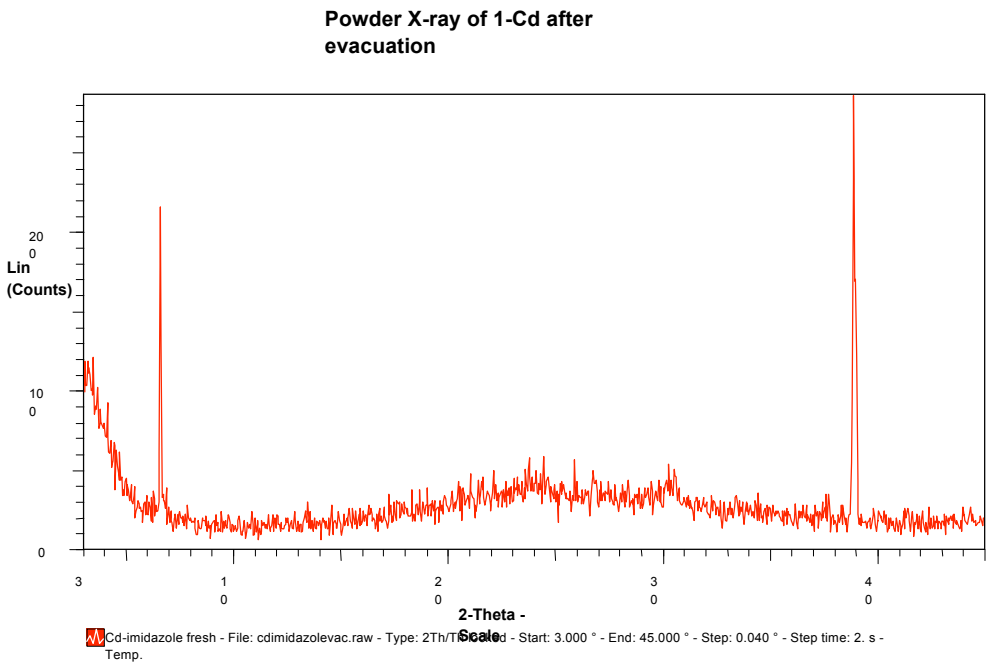

Figure 69. Powder X-ray of **1-Cd** crystals that were evacuated using high vacuum for 24 hours.

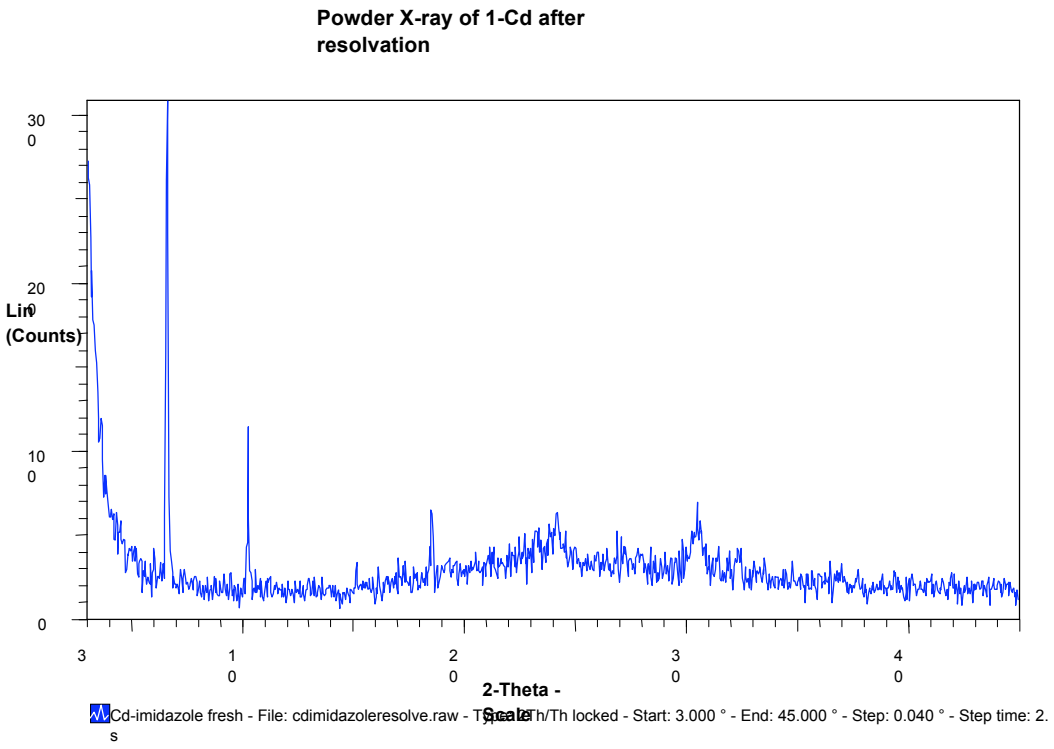

Figure 70. Powder X-ray of **1-Cd** after being resolvated using exposure to ethanol and water for 2 days.

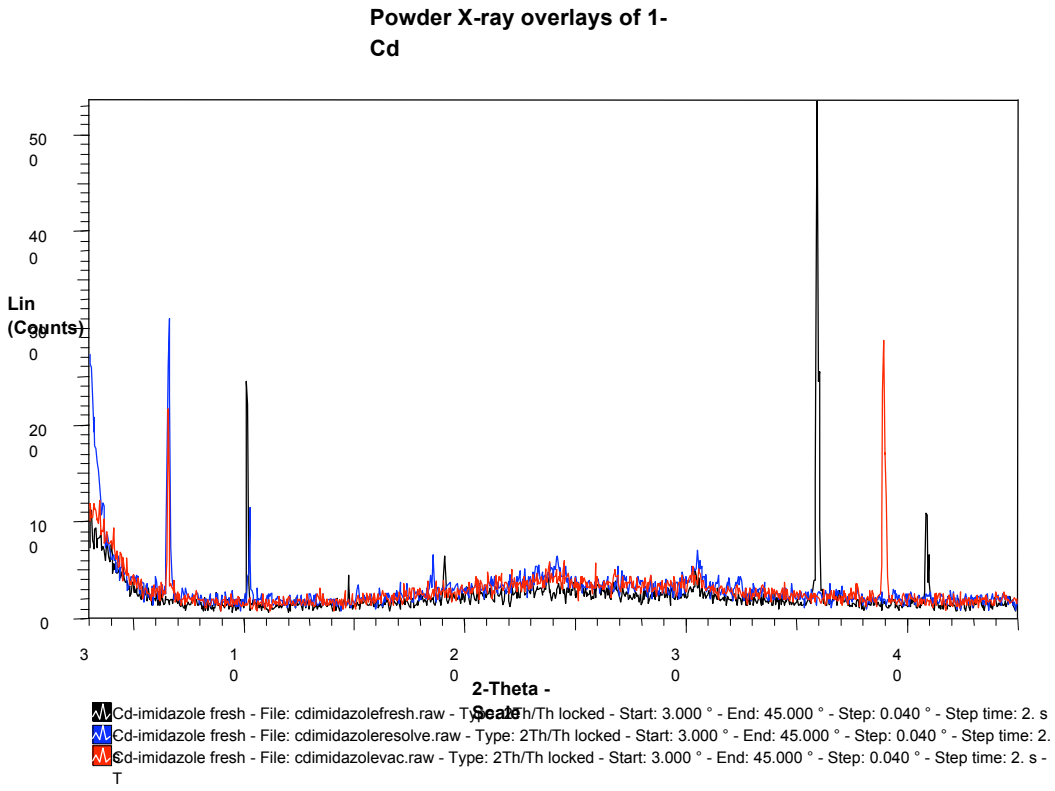

Figure 71. Powder X-ray overlays of **1-Cd**.

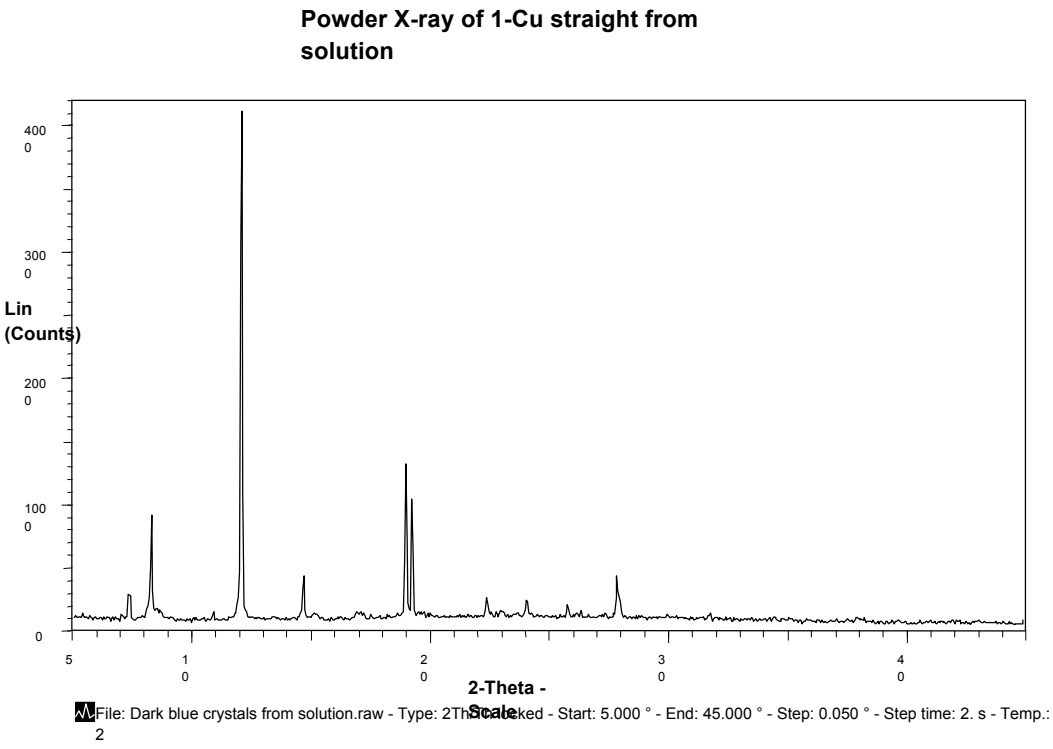

Figure 72. Powder X-ray of **1-Cu** crystals taken straight from solution.

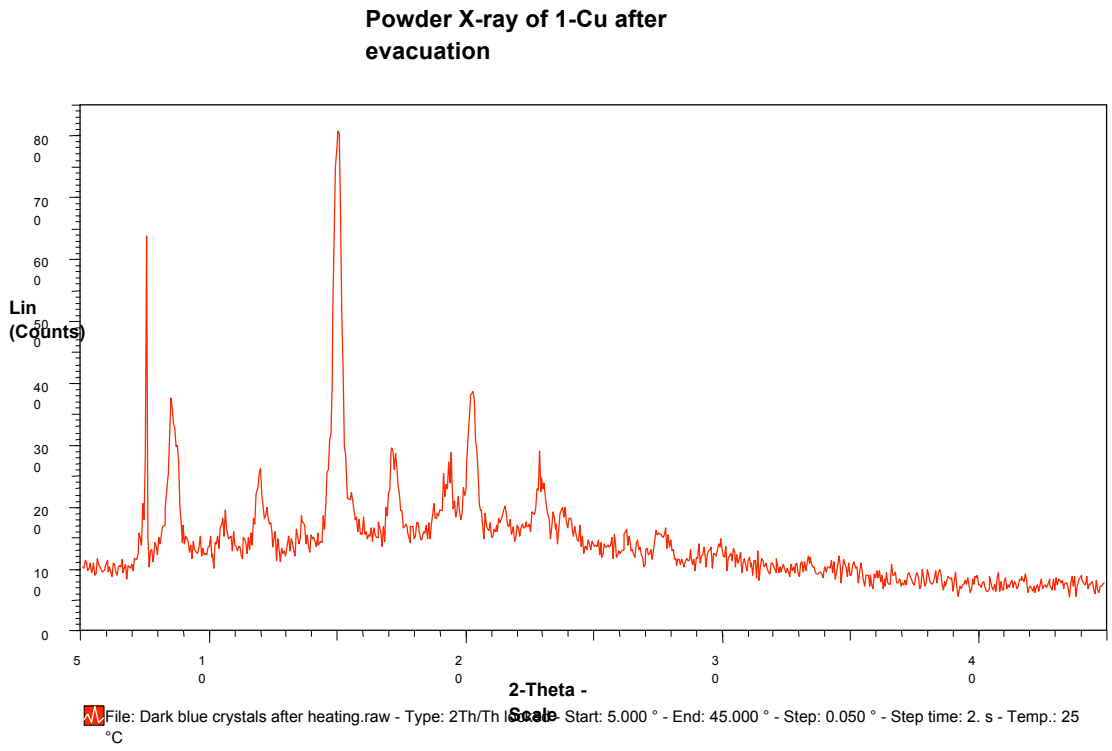

Figure 73. Powder X-ray pattern of **1-Cu** after evacuation using high vacuum for 24 hours.

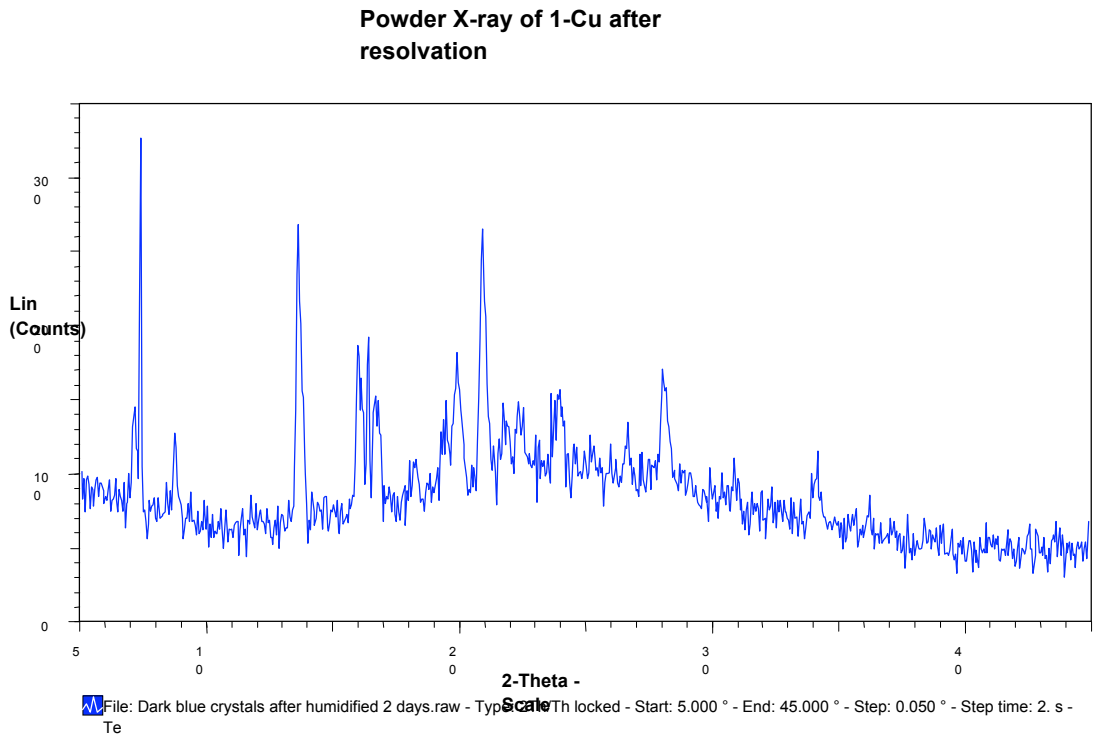

Figure 74. Powder X-ray of **1-Cu** after two day exposure to atmospheric ethanol and water.

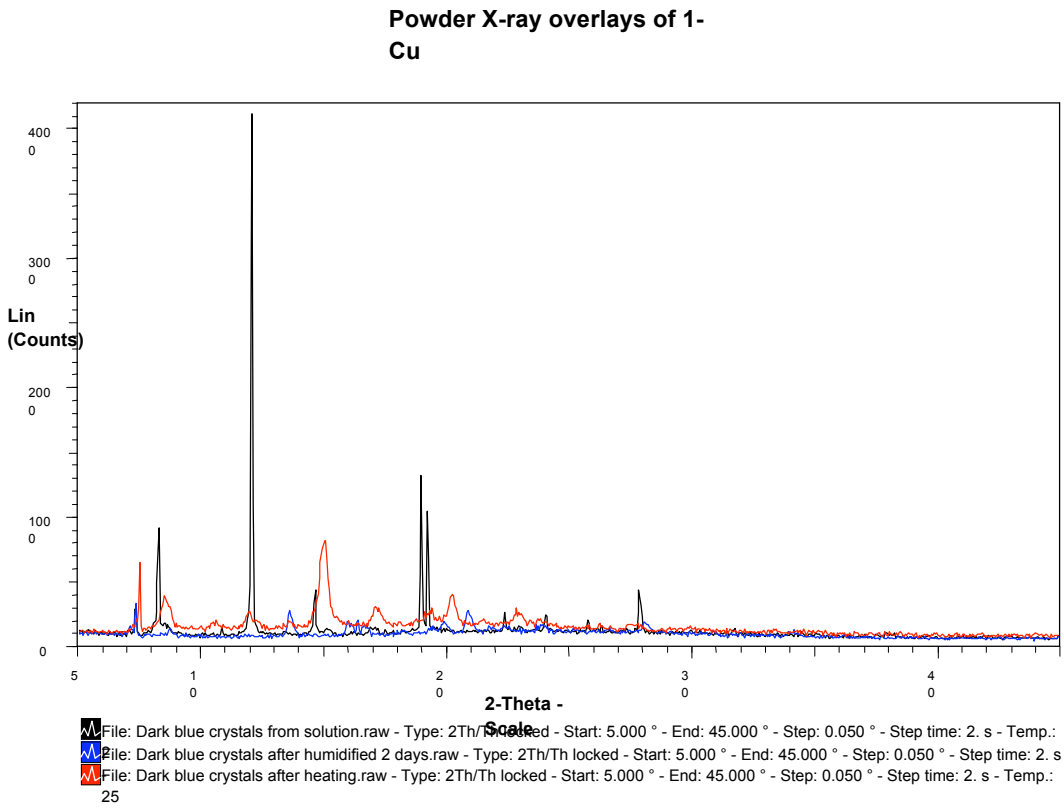

Figure 75. Powder X-ray overlays of **1-Cu**.

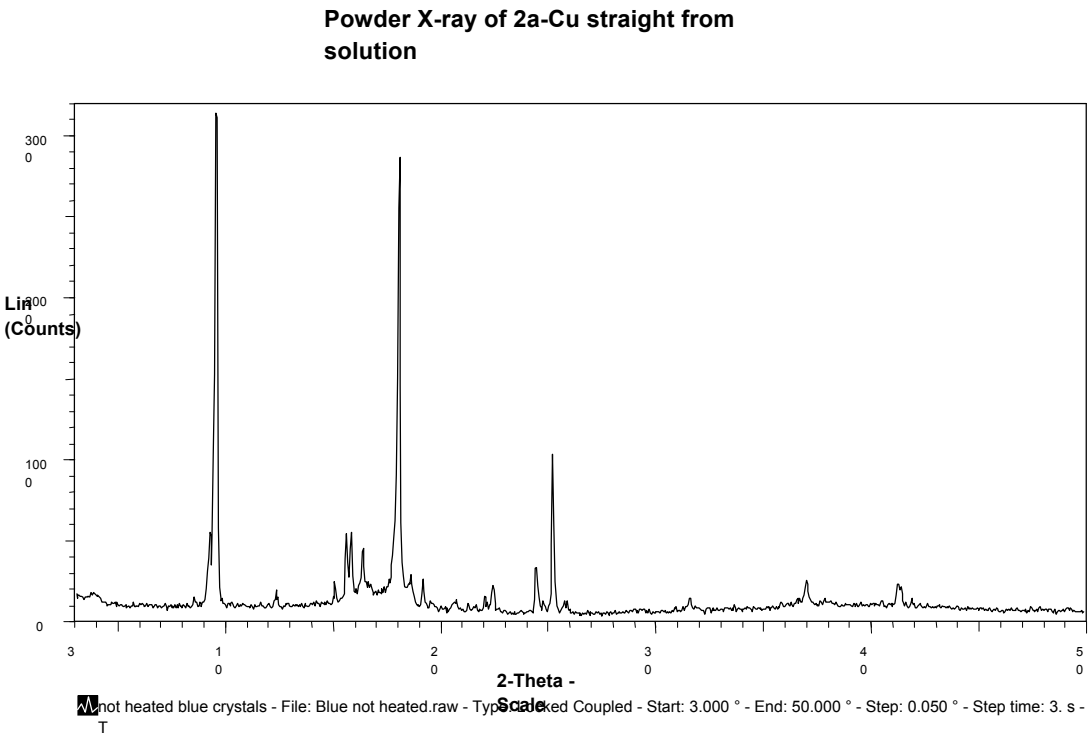

Figure 76. Powder X-ray of **2a-Cu**

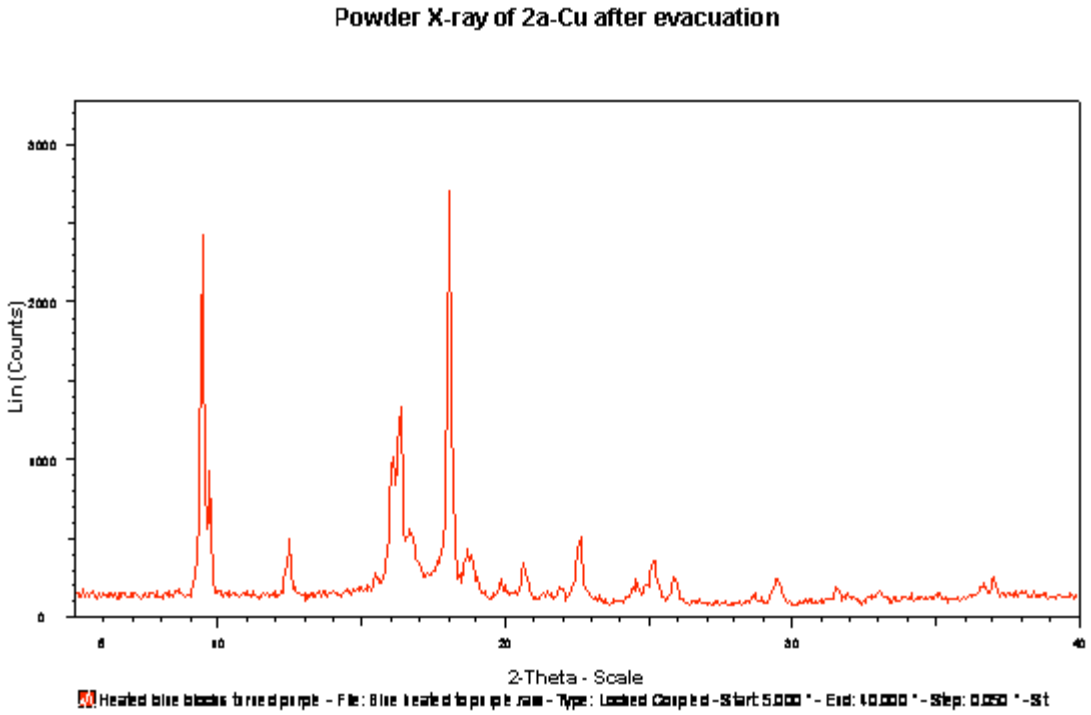

Figure 77. Powder X-ray of **2a-Cu** after evacuation using high vacuum.

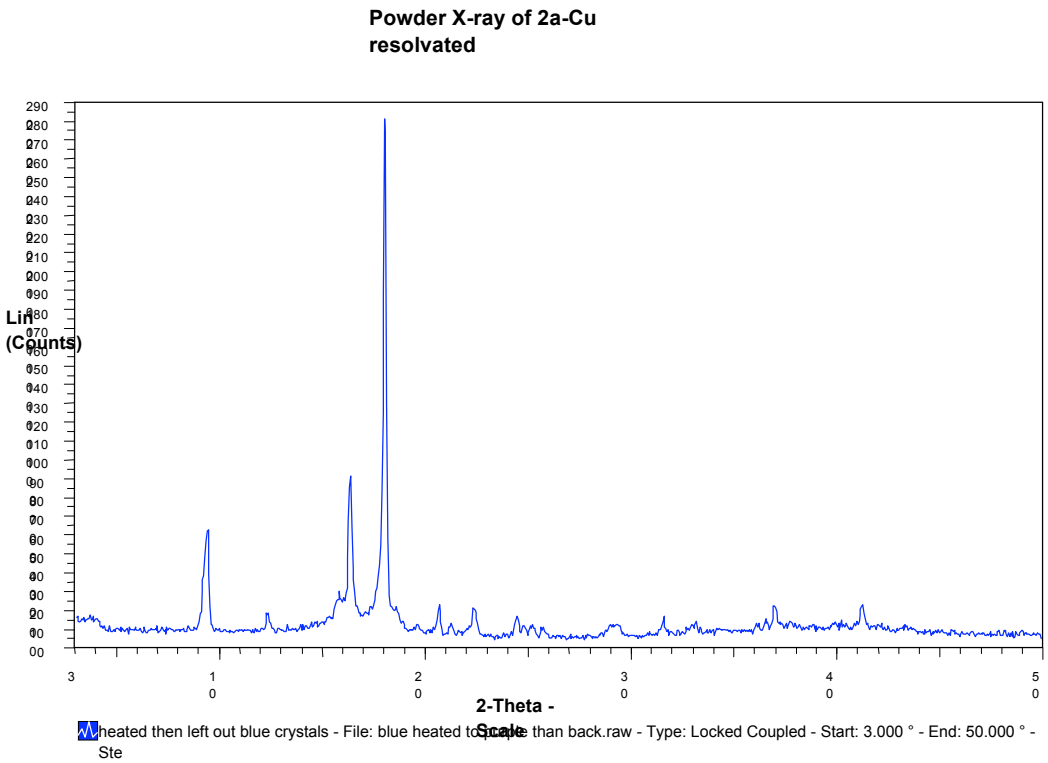

Figure 78. Powder X-ray of **2a-Cu** resolvated using atmospheric ethanol and water.

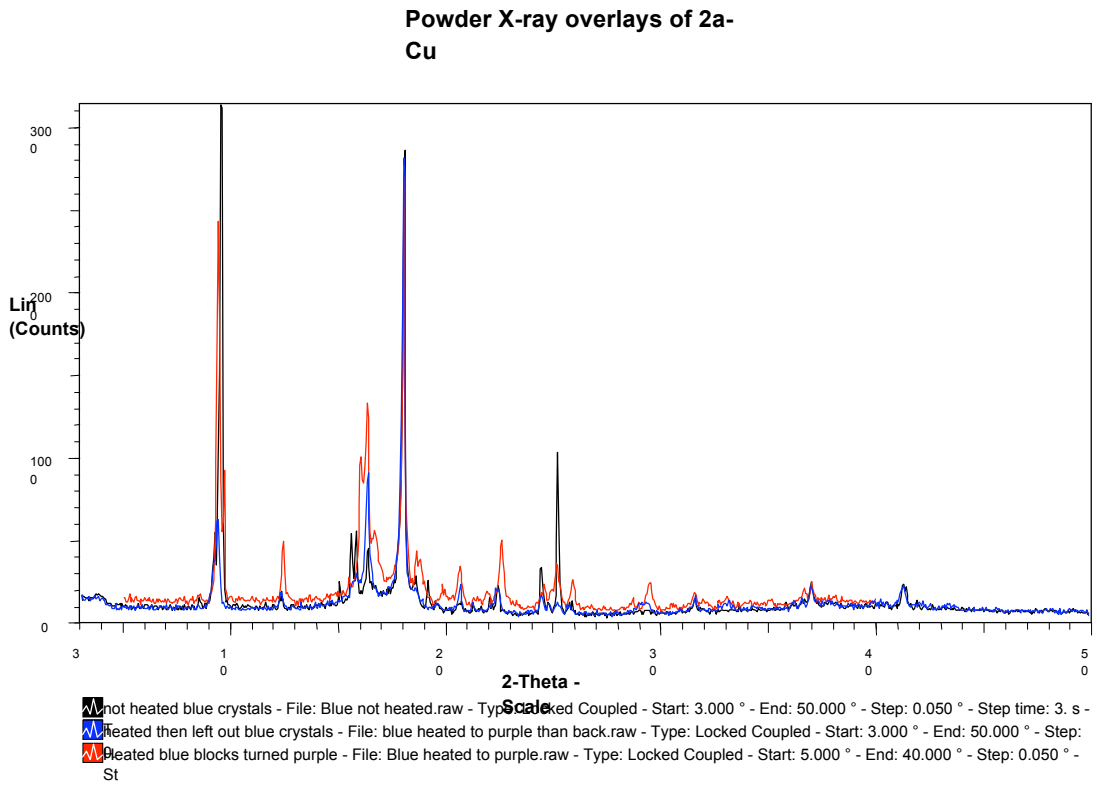

Figure 79. Powder X-ray overlay for **2a-Cu**.

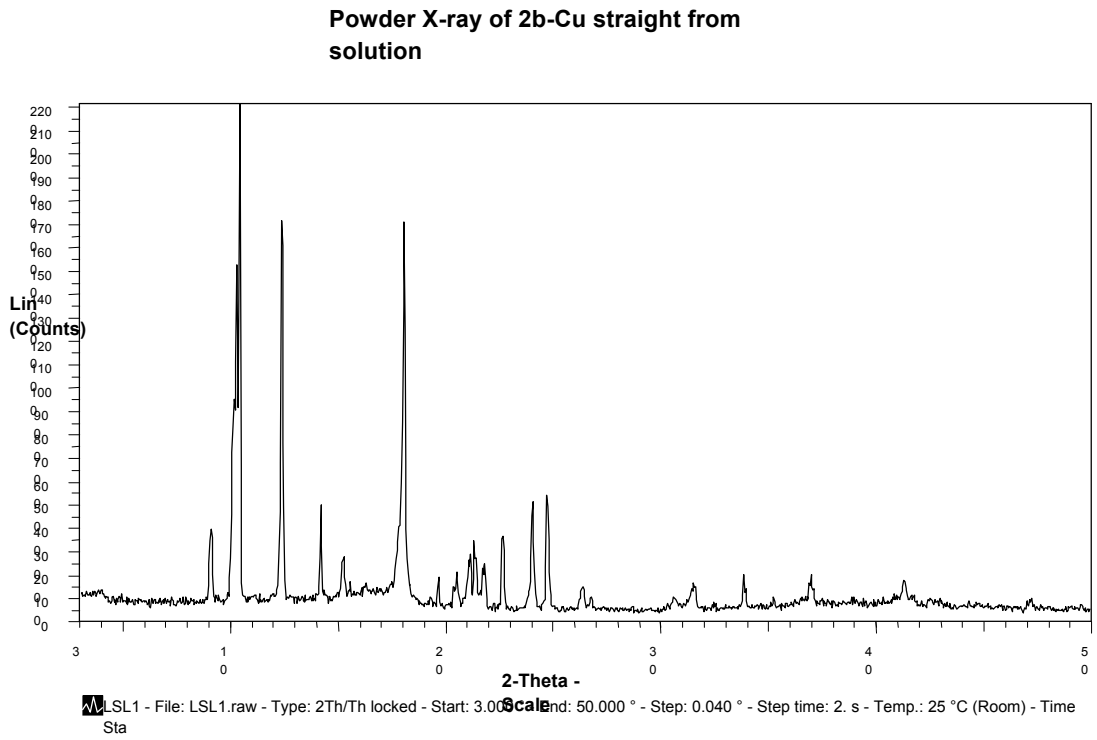

Figure 80. Powder X-ray of **2b-Cu** crystals taken straight from solution.

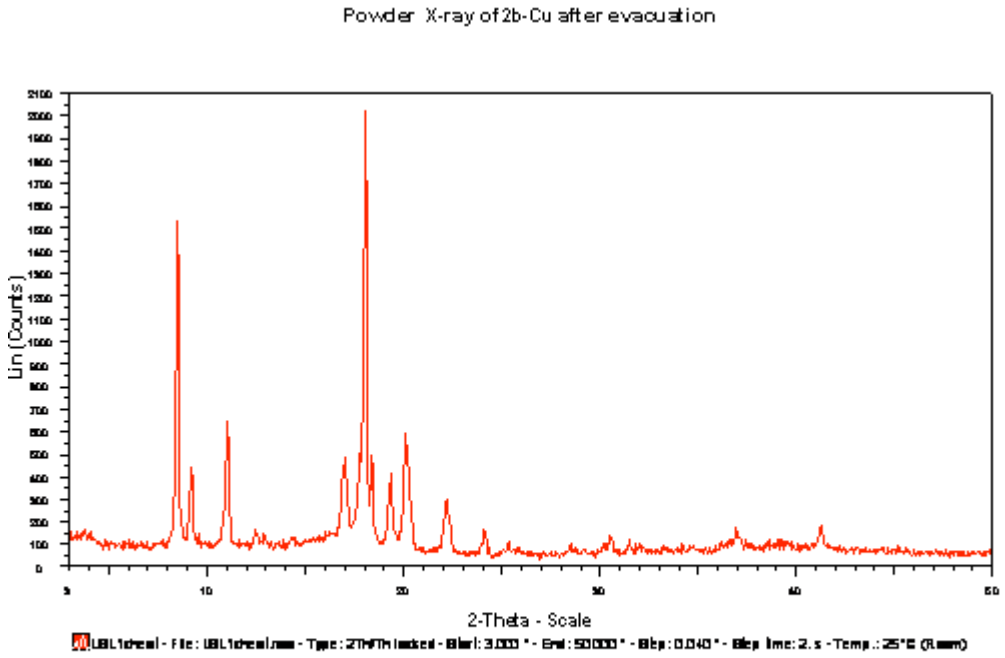

Figure 81. Powder X-ray of **2b-Cu** after evacuation using high vacuum. Evacuation occurred over 24 hours.

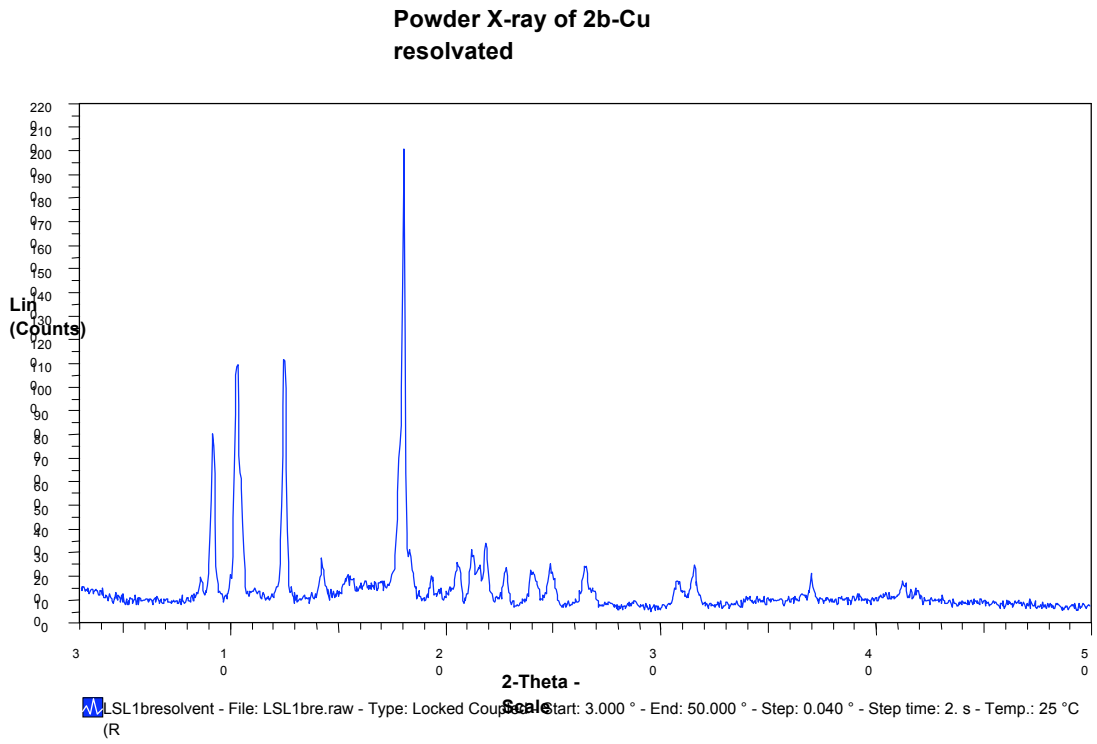

Figure 82. Powder X-ray of **2b-Cu** after exposure to atmospheric ethanol and water for 2 days.

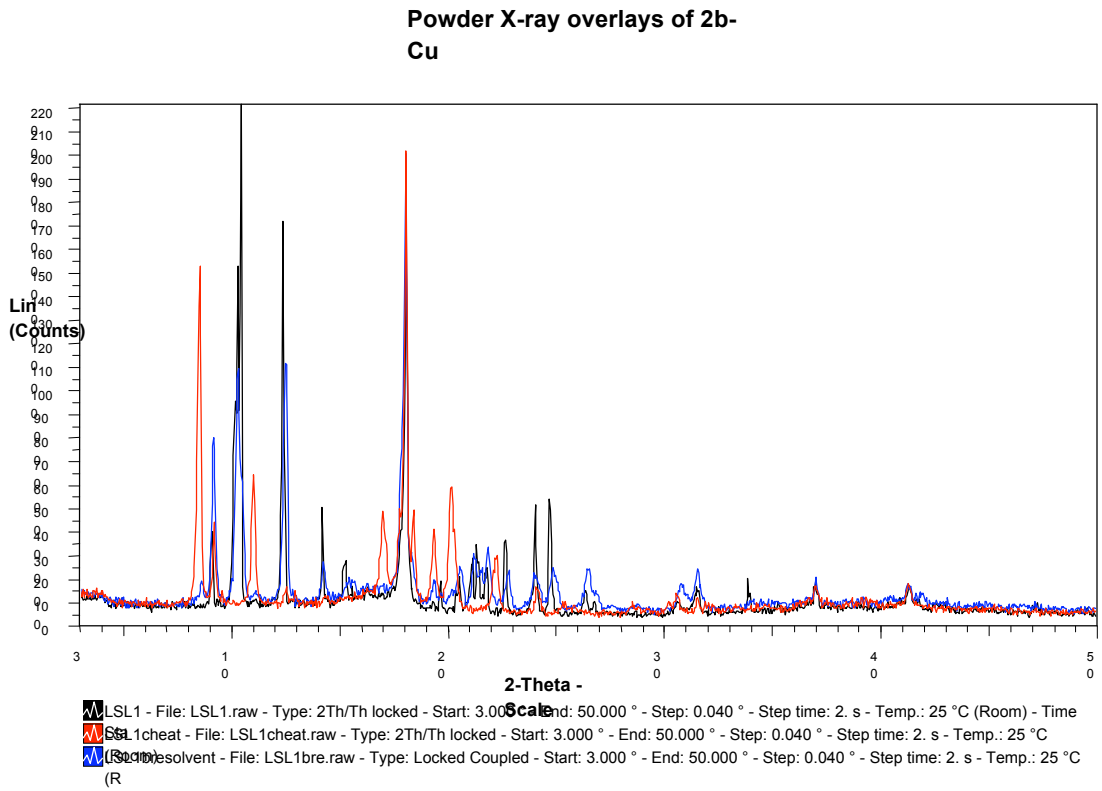

Figure 83. Powder X-ray overlays of **2b-Cu**.

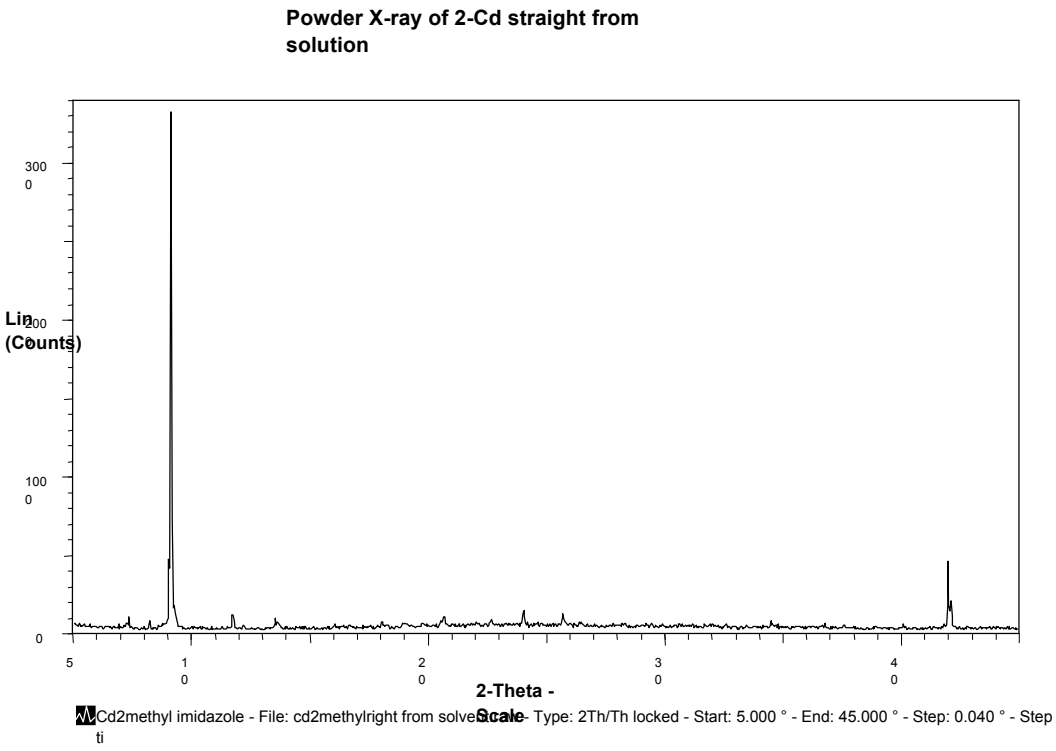

Figure 84. Powder X-ray of **2-Cd** crystals taken straight from solution.

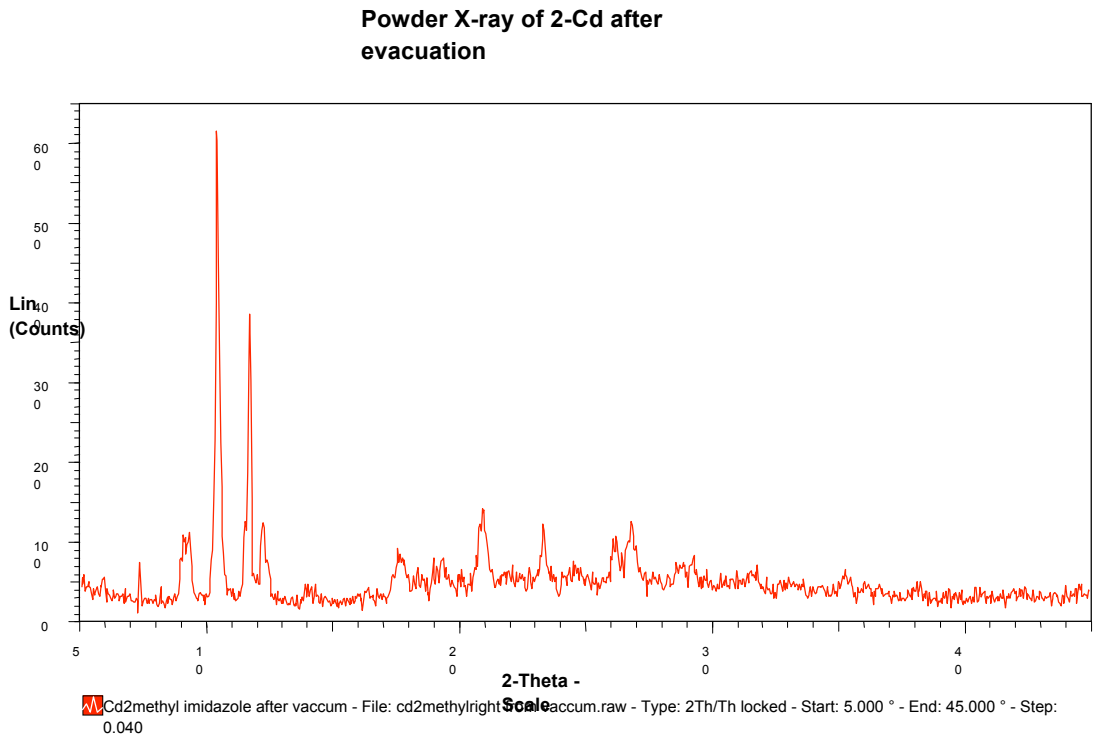

Figure 85. Powder X-ray of **2-Cd** crystals after high vacuum evacuation for 24 hours.

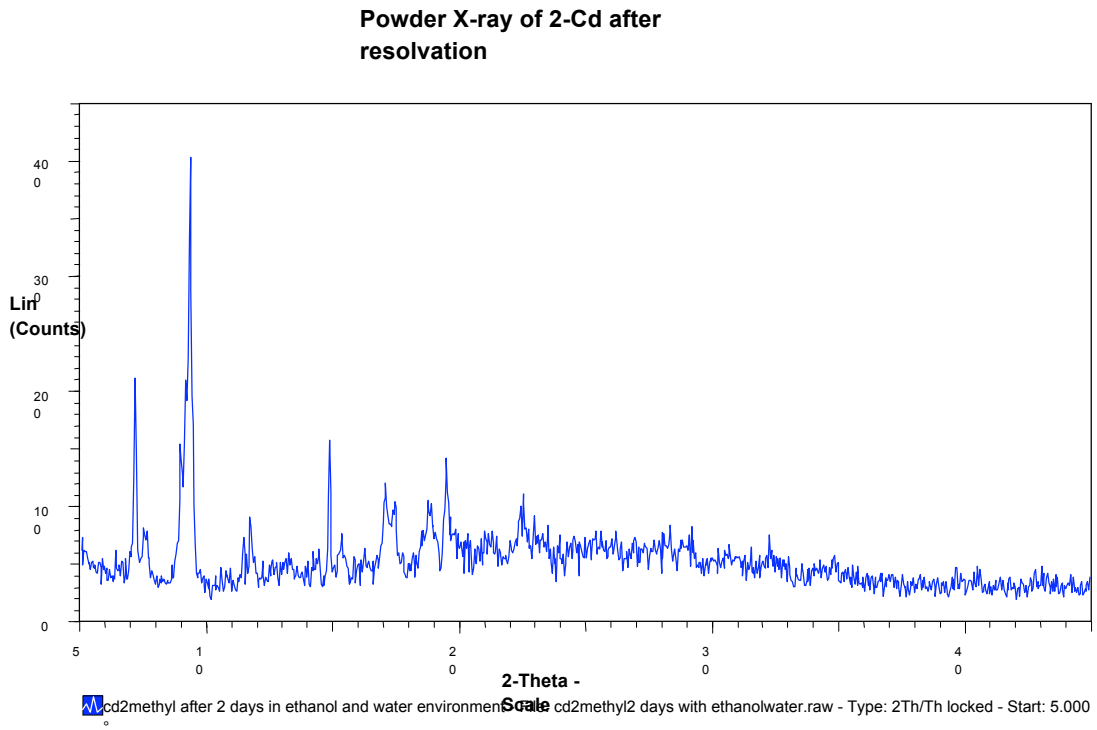

Figure 86. Powder X-ray of **2-Cd** after resolvation for 2 days with atmospheric ethanol and water.

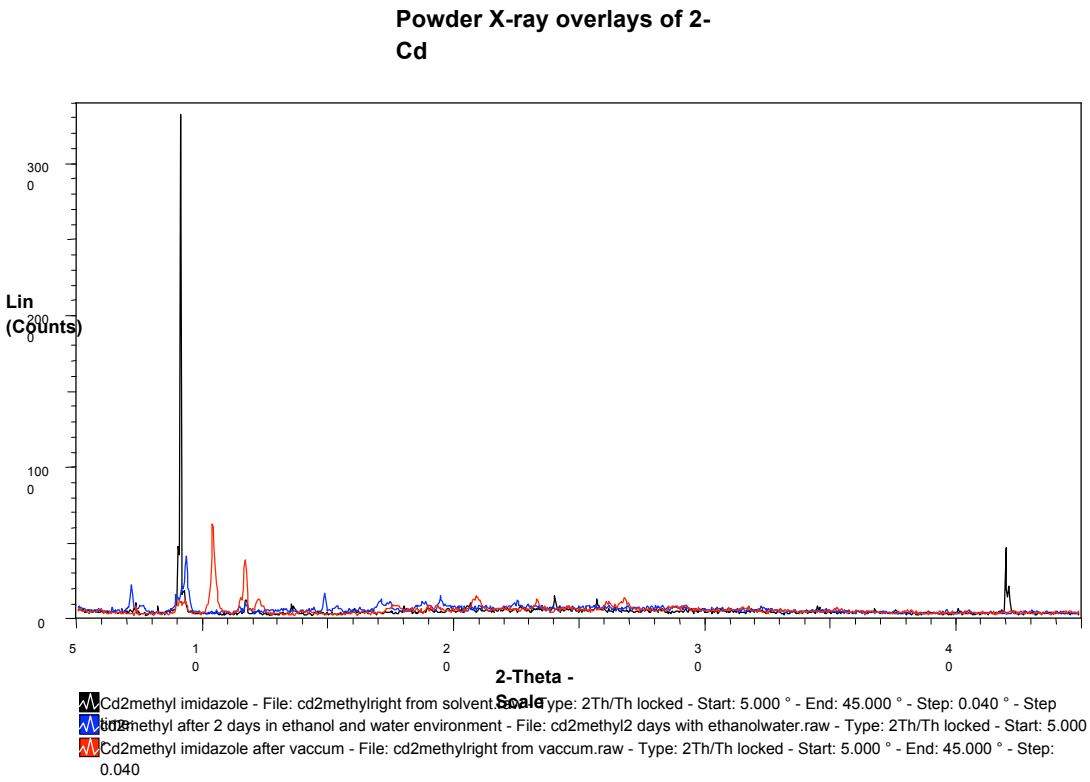

Figure 87. Powder X-ray overlay of **2-Cd**.

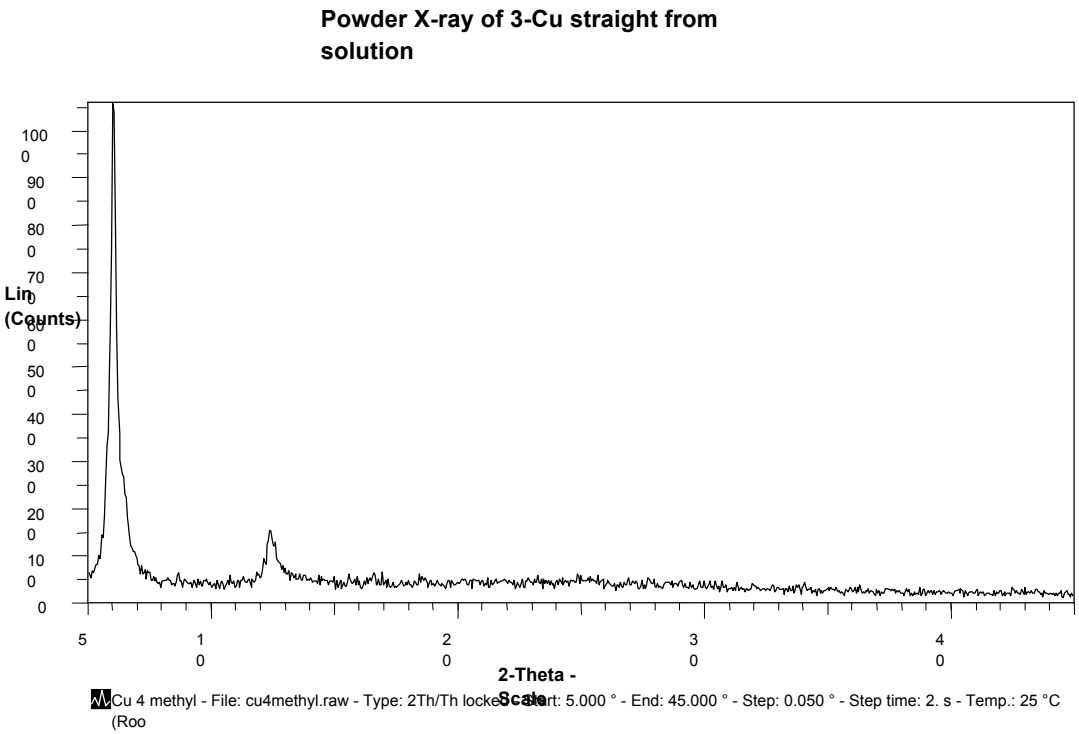

Figure 88. Powder X-ray of **3-Cu** crystals straight from solution.

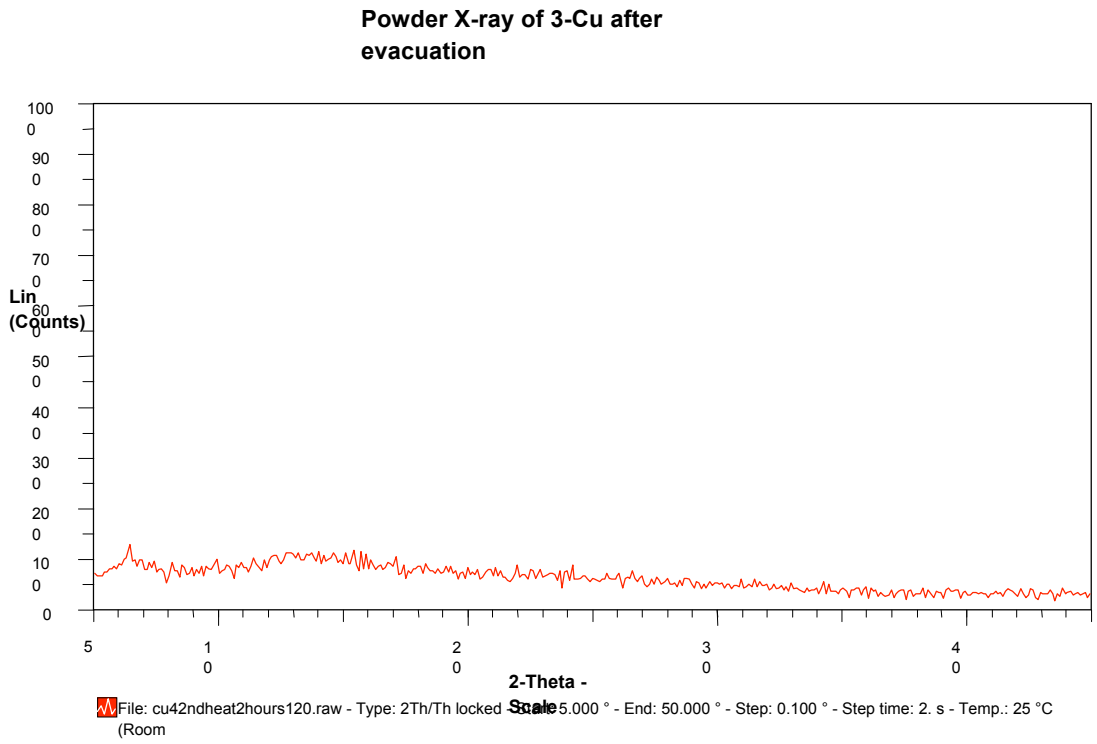

Figure 89. Powder X-ray of **3-Cu** after evacuation using high vacuum for 24 hours.

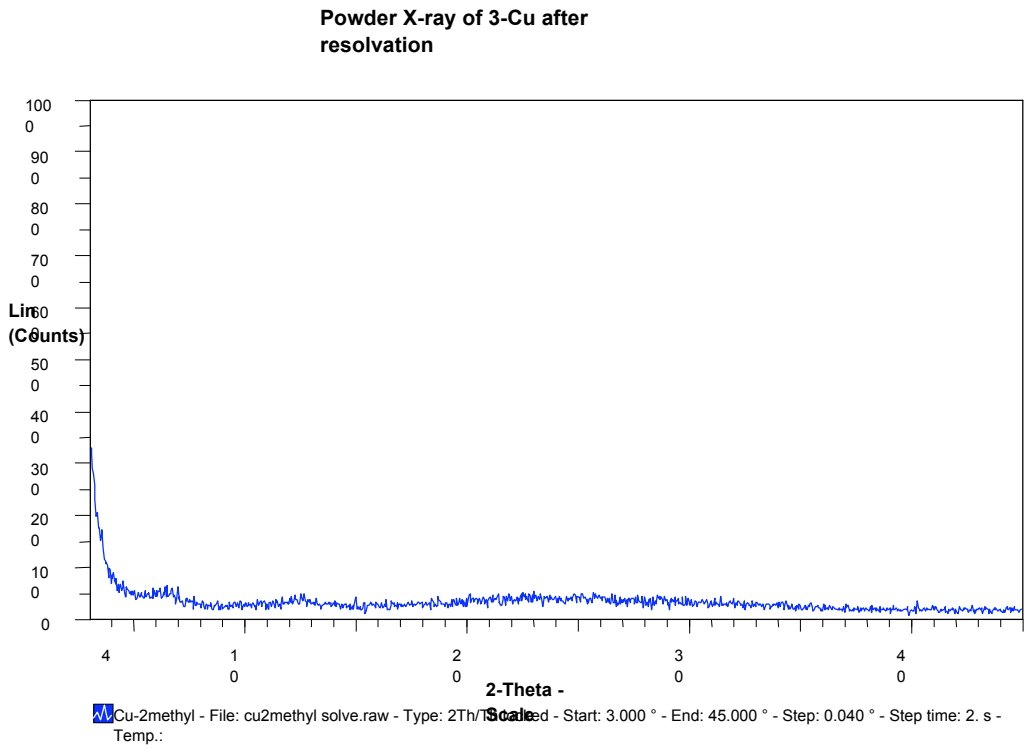

Figure 90. Powder X-ray of **3-Cu** after resolvation with atmospheric ethanol and water for 2 days.

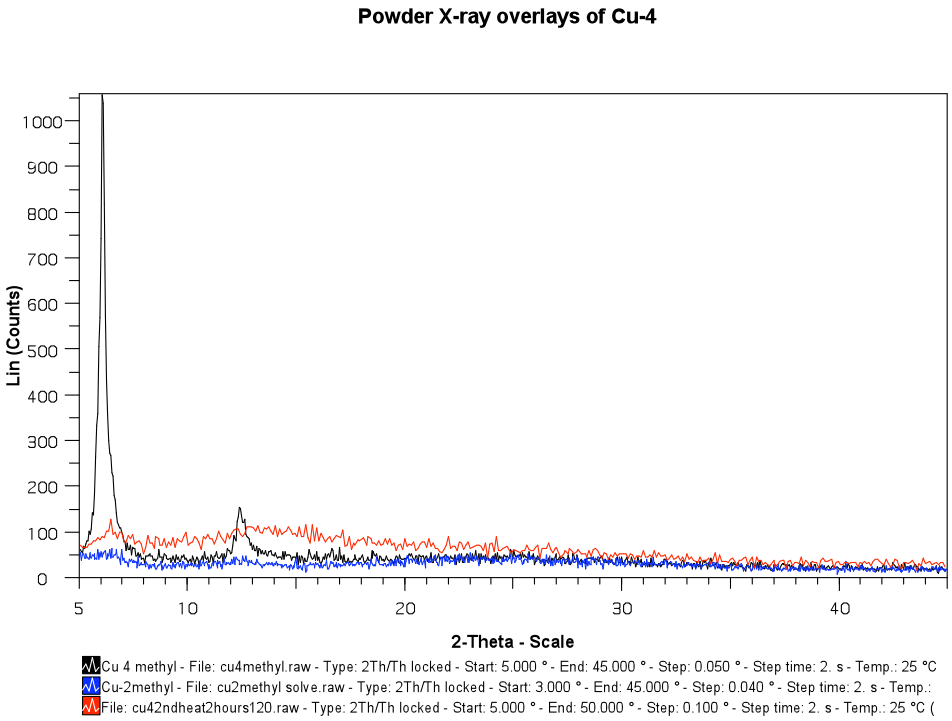

Figure 91. Powder overlay of **3-Cu** crystals.

Conclusion.

We have successfully synthesized six new frameworks using an imidazole and carboxylate binding functional groups. The frameworks exhibited 1-D, 2-D, and 3-D arrangements with the two different transition metals copper and cadmium. All six MOF crystal structures were solved using single x-ray diffraction. Out of the six MOFs, five were seen to exhibit large porous behavior **1-Cd**, **1-Cu**, **2-Cd**, **2b-Cu** and **3-Cu**. From the five porous MOFs, four displayed stability and reversibility of guest molecules. It was shown that **1-Cd**, **1-Cu**, **2-Cd**, and **3-Cu** display reversibly porous behavior upon atmospheric conditions in the presence of ethanol and water. Although the powder patterns did not match before evacuation and after resolvation the fact that the crystals were able to reabsorb guest molecules leads to the conclusion that the shifts and disappearance/appearances of peaks in the powder pattern is attributed to breathing or stretching of the lattice. It was also seen that a large dye molecule, rhodamine b, was successfully introduced into **3-Cu** crystals with an overall uptake of 5.3% of its own mass. Crystals were exposed to atmospheric ethanol and water and allowed to resolvated. TGA of the reversibly porous MOFs showed reuptake of the guest molecules. There was no instance of complete reloading of the lost guest molecules seen in the crystals. This is due to the need of a driving force to get guest molecules back into the crystal lattice it is not surprising that the crystal was unable to achieve full reloading considering that the driving force will be diminished the more the crystal is filled with guest molecules. The porous materials represent a new class of materials that can be modified to meet the specifications of the porous materials as necessary.

REFERNCES

(1) http://artculturelanguagesfashion.blogspot.com/2008/01/i-love-spongebob-squarepants.html

(2) http://www.searchanddiscovery.com/documents/cantrell/images/figure_06.htm

(3) Chin, D. N.; Zerkowski, J. A.; MacDonald, J. C.; Whitesides, G. M. In *Organised Molecular Assemblies in the Solid State*; Whitesell, J. K., Ed.; John Wiley and Sons: New York, 1999; pp 185-253.

(4) Coe, S.; Kane, J. J.; Nguyen, T. L.; Toledo, L. M.; Wininger, E.; Fowler, F. W.; Lauher, J. W. "Molecular Symmetry and the Design of Molecular Solids: The Oxalamide Functionality as a Persistent Hydrogen-Bonding Unit", *J. Am. Chem. Soc.* **1997**, *119*, 86-93.

(5) Ducharme, Y.; Wuest, J. D. "Use of Hydrogen Bonds to Control Molecular Aggregation. Extensive, Self-Complementary Arrays of Donors and Acceptors", *J. Org. Chem.* **1988**, *53*, 5787-5789.

(6) Foxman, B. M.; Guarrera, D. J.; Taylor, L. D.; VanEngen, D.; Warner, J. C. "Environmentally Benign Synthesis Using Crystal Engineering: Steric Accomodation in Non-Covalent Derivatives of Hydroquinones", *Cryst. Eng.* **1998**, *1*, 109-118.

(7) Geib, S. J.; Vicent, C.; Fan, E.; Hamilton, A. D. "A Self-Assembling Hydrogen-Bonded Helix", *Angew. Chem. Int. Ed. Engl.* **1993**, *32*, 119-121.

(8) Harris, K. D. M.; Stainton, N. M.; Callan, A. M.; Howie, R. A. "Crystal Engineering of Hydrogen-Bonded Cocrystals Between Cyanuric Acid and 'Diamide' Molecules", *J. Mater. Chem.* **1993**, *3*, 947-952.

(9) Hollingsworth, M. D.; Santarsiero, B. D.; Oumar-Mahamat, H.; Nichols, C. J. "New Series of 1:1 Layered Complexes of α,ω-Dinitriles and Urea", *Chem. Mater.* **1991**, *3*, 23-25.

(10) Kane, J. J.; Liao, R.-F.; Lauher, J. W.; Fowler, F. W. "Preparation of Layered Diacetylenes as a Demonstration of Strategies of Supramolecular Synthesis", *J. Am. Chem. Soc.* **1995**, *117*, 12003-12004.

(11) Karle, I. L.; Ranganathan, D.; Haridas, V. "A Persistent Preference for Layer Motifs in Self-Assemblies of Five Squarates and Hydrogen Squarates by Hydrogen Bonding [X-H...O; X = N, O, or Cl]: A Crystallographic Study of Five Organic Salts", *J. Am. Chem. Soc.* **1996**, *118*, 7128-7133.

(12) Karle, I. L.; Rangathanan, D.; Haridas, V. "Molecular Recognition: The Demonstration of 1,3-Bis[(pyrid-2-ylamino)carbonyl]adamantane as an Exceptionally Versatile Assembler of One-Dimensional Motifs", *J. Am. Chem. Soc.* **1997**, *119*, 2777-2783.

(13) Lehn, J.-M.; Mascal, M.; DeCian, A.; Fischer, J. "Molecular Recognition Directed Self-Assembly of Ordered Supramolecular Strands by Cocrystallization of

Complementary Molecular Components", *J. Chem. Soc., Chem. Commun.* **1990**, 479-481.

(14) MacDonald, J. C.; Whitesides, G. M. "Solid-State Structures of Hydrogen-Bonded Tapes Based on Cyclic Secondary Diamides", *Chem. Rev.* **1994**, *94*, 2383-2420.

(15) MacDonald, J. C.; Dorrestein, P. C.; Pilley, M. M.; Foote, M. M.; Lundburg, J. L. "Design of Layered Crystalline Materials Using Coordination Chemistry and Hydrogen Bonds", *J. Am. Chem. Soc.* **2000**, *accepted for publication*.

(16) Mascal, M.; Fallon, P. S.; Batsanov, A. S.; Heywood, B. R.; Champ, S.; Colclough, M. "The Ion-pair Reinforced, Hydrogen-bonding Molecular Ribbon", *J. Chem. Soc., Chem. Commun.* **1995**, 805-806.

(17) Palacin, S.; Chin, D. N.; Simanek, E. E.; MacDonald, J. C.; Whitesides, G. M.; McBride, M. T.; Palmore, G. T. R. "Hydrogen-Bonded Tapes Based on Symmetrically Substituted Diketopiperazines: A Robust Structural Motif for the Engineering of Molecular Solids", *J. Am. Chem. Soc.* **1997**, *119*, 11807-11816.

(18) Palmore, G. T. R.; Luo, T.-J. M.; Martin, T. L.; McBride-Wieser, M. T.; Voong, N. T.; Land, T. A.; DeYoreo, J. J. "Using the AFM to Study the Assembly of Molecular Solids", *ACA Trans.* **1998**, *33*, 45-57.

(19) Palmore, G. T. R.; Luo, T.-J. M.; McBride-Weiser, M. T.; Picciotto, E. A.; Reynoso-Paz, C. M. "Engineering Crystalline Architecture with Diketopiperazines: An Investigation of the Strength of Hydrogen-Bonded Tapes Based on the Cyclic Dipeptide of (S)-Aspartic Acid", *Chem. Mater.* **1999**, *11*, 3315-3328.

(20) Palmore, G. T. R.; MacDonald, J. C. In *The Amide Linkage: Structural Significance in Chemistry, Biochemistry and Materials Science*; Greenberg, A., Breneman, C. M., Liebman, J. F., Eds.; John Wiley and Sons: New York, 2000; pp 291-336.

(21) Pedireddi, V. R.; Chatterjee, S.; Ranganathan, A.; Rao, C. N. R. "Noncovalent Synthesis of Layered and Channel Structures Involving Sulfur Mediated Hydrogen Bonds", *J. Am. Chem. Soc.* **1997**, *119*, 10867-10868.

(22) Schwiebert, K. E.; Chin, D. N.; MacDonald, J. C.; Whitesides, G. M. "Engineering the Solid State with 2-Benzimidazolones", *J. Am. Chem. Soc.* **1996**, *118*, 4018-4029.

(23) Simanek, E. E.; Tsoi, A.; Wang, C. C. C.; Whitesides, G. M.; McBride, M. T.; Palmore, G. T. R. "Benzimidazolene-2-thiones: A New Class of Molecules for the Engineering of Molecular Tapes in the Organic Solid State", *Chem. Mat.* **1997**, *9*, 1954-1961.

(24) Holman, K. T.; Pivovar, A. M.; Ward, M. D. "Engineering Crystal Symmetry and Polar Order in Molecular Host Frameworks", *Science* **2001**, *294*, 1907-1911.

(25) Xue, F.; Mak, T. C. W. "Hydrogen-bonded anionic layer structures constructed from 4,4'-bipheyldicarboxylate and water molecules, and also with urea as an additional component", *J. Phys. Org. Chem.* **2000**, *13*, 405-414.

(26) Moulton, B.; Zaworotko, M. J. "From Molecules to Crystal Engineering: Supramolecular Isomerism and Polymorphism in Network Solids", *Chem. Rev.* **2001**, *101*, 1629-1658.

(27) Moulton, B.; Rather, E. B.; Zaworotko, M. J. "Interpenetration of covalent and noncovalent networks in the crystal structures of $\{[M(4,4'\text{-bipyridine})_2(NO_3)_2]\bullet 2p\text{-nitroaniline}\}_2$ where M=Co, 1, Ni, 2, Zn, 3", *Cryst. Eng.* **2001**, *4*, 309-317.

(28) Biradha, K.; Seward, C.; Zaworotko, M. J. "Helical Coordination Polymers with Large Chiral Cavities", *Angew. Chem. Int. Ed. Engl.* **1999**, *38*, 492-494.

(29) Biradha, K.; Dennis, D.; MacKinnon, V. A.; Sharma, C. V. K.; Zaworotko, M. J. "Supramolecular Synthesis of Organic Laminates with Affinity for Aromatic Guests: A New Class of Clay Mimics", *J. Am. Chem. Soc.* **1998**, *120*, 11894-11903.

(30) Moulton, B.; Lu, J.; Zaworotko, M. J. "Periodic Tiling of Pentagons: The First Example of a Two-Dimensional $(5,^3_4)$-net", *J. Am. Chem. Soc.* **2001**, *123*, 9224-9225.

(31) Ayyappan, P.; Evans, O. R.; Lin, W. "A Novel Coordination Polymer Containing Both Interdigitated 1D Chains and Interpenetrated 2D Grids", *Inorg. Chem.* **2002**, *41*, 3328-3330.

(32) Chapman, M. E.; Ayyappan, P.; Foxman, B. M.; Yee, G. T.; Lin, W. "Synthesis, X-ray Structures, and Magnetic Properties of Copper(II) Pyridinecarboxylate Coordination Networks", *Cryst. Growth Design* **2001**, *1*, 159-163.

(33) Evans, O. R.; Lin, W. "Synthesis of Zinc Oxalate Coordination Polymers via Unprecedented Oxidative Coupling of Methanol to Oxalic Acid", *Cryst. Growth Design* **2001**, *1*, 9-11.

(34) Lin, W.; Chapman, M. E.; Wang, Z.; Yee, G. T. "Three-Dimensional Manganese(II) Coordination Polymers Based on *m*-Pyridinecarboxylates: Synthesis, X-ray Structures, and Magnetic Properties", *Inorg. Chem.* **2000**, *39*, 4169-4173.

(35) Wang, Z.; Xiong, R.-G.; Foxman, B. M.; Wilson, S. R.; Lin, W. "Two- and Three-Dimensional Cadmium Coordination Polymers Based on *N*,*N*-(2-Pyridyl)-(4-pyridylmethyl)amine", *Inorg. Chem.* **1999**, *38*, 1523-1528.

(36) Lin, W.; Wang, Z.; Ma, L. "A Novel Octupolar Metal-Organic NLO Material Based on a Chiral 2D Coordination Network", *J. Am. Chem. Soc.* **1999**, *121*, 11249-11250.

(37) Lin, W.; Evans, O. R.; Xiong, R.-G.; Wang, Z. "Supramolecular Engineering of Chiral and Acentric 2D Networks, Synthesis, Structures, and Second-Order Nonlinear Optical Properties of Bis(nicotinato)zinc and Bis{3-[2-(4-pyridyl)ethenyl]benzoato}cadmium", *J. Am. Chem. Soc.* **1998**, *120*, 13272-13273.

(38) Plaut, D. J.; Holman, K. T.; Pivovar, A. M.; Ward, M. D. "Building molecular frameworks with tailored pore structures", *J. Phys. Org. Chem.* **2002**, *13*, 858-869.

(39) Russel, V. A.; Evans, C. C.; Li, W.; Ward, M. D. "Nanoporous Molecular Sandwiches: Pillared Two-Dimensional Hydrogen-Bonded Networks with Adjustable Porosity", *Science* **1997**, *276*, 575-579.

(40) Suslick, K. S.; Rakow, N. A.; Kosal, M. E.; Chou, J.-H. "The materials chemistry of porphyrins and metalloporphyrins", *J. Porphyrins and Phthalocyanines* **2000**, *4*, 407-413.

(41) Seo, J. S.; Whang, D.; Lee, H.; Jun, S. I.; Oh, J.; Jeon, Y. J.; Kim, K. "A homochiral metal-organic porous material for enantioselective separation and catalysis", *Nature* **2000**, *404*, 982-986.

(42) Gudbjartson, H.; Biradha, K.; Poirier, K. M.; Zaworotko, M. J. "Novel Nanoporous Coordination Polymer Sustained by Self-Assembly of T-Shaped Moieties", *J. Am. Chem. Soc.* **1999**, *121*, 2599-2600.

(43) Rosi, N. L.; Eddaoudi, M.; Kim, J.; O'Keeffe, M.; Yaghi, O. M. "Infinite Secondary Building Units and Forbidden Catenation in Metal-Organic Frameworks", *Angew. Chem. Int. Ed. Engl.* **2002**, *41*, 284-287.

(44) Kim, J.; Chen, B.; Reineke, T. M.; Li, H.; Eddaoudi, M.; Moler, D. B.; O'Keeffe, M.; Yaghi, O. M. "Assembly of Metal-Organic Frameworks from Large Organic and Inorganic Secondary Building Units: New Examples and Simplifying Principles for Complex Structures", *J. Am. Chem. Soc.* **2001**, *123*, 8239-8247.

(45) Li, H.; Laine, A.; O'Keeffe, M.; Yaghi, O. M. "Supertetrhedral Sulfide Crystals with Giant Cavities and Channels", *Science* **1999**, *283*, 1145-1147.

(46) Barton, T. J.; Bull, L. M.; Klemperer, W. G.; Loy, D. A.; McEnaney, B.; Misono, M.; Monson, P. A.; Pez, G.; Scherer, G. W.; Vartuli, J. C.; Yaghi, O. M. "Tailored Porous Materials", *Chem. Mater.* **1999**, *11*, 2633-2656.

(47) Yaghi, O. M.; Li, H.; Davis, C.; Richardson, D.; Groy, T. L. "Synthetic Strategies, Structure Patterns and Emerging Properties in the Chemistry of Modular Porous Solids", *Acc. Chem. Res.* **1998**, *31*, 474-484.

(48) Cui, Y.; Ngo, H. L.; Lin, W. "New Rigid Angular Dicarboxylic Acid for the Construction of Nanoscopic Supramolecules: From a Molecular Rectangle to a 1-D Coordination Polymer", *Inorg. Chem.* **1033**, *41*, 1033-1035.

(49) Evans, O. R.; Ngo, H. L.; Lin, W. "Chiral Porous Solids Based on Lamellar Lanthanide Phosphonates", *J. Am. Chem. Soc.* **2001**, *123*, 10395-10396.

(50) Ayyappan, P.; Evans, O. R.; Lin, W. "Three-Dimensional Open Frameworks Based on Cobalt(II) and Nickel(II) *m*-Pyridinecarboxylates", *Inorg. Chem.* **2001**, *40*, 4627-4632.

(51) Evans, O. R.; Lin, W. "Pillared 3D Metal-Organic Frameworks with Rectangular Channels. Synthesis and Characterization of Coordination Polymers Bases on Tricadmium Carboxylates", *Inorg. Chem.* **2000**, *39*, 2189-2198.

(52) Evans, O. R.; Wang, Z.; Xiong, R.-G.; Foxman, B. M.; Lin, W. "Nanoporous, Interpenetrated Metal-Organic Diamondoid Networks", *Inorg. Chem.* **1999**, *38*, 2969-2973.

(53) Evans, O. R.; Lin, W. "Crystal Engineering of NLO Materials Based on Metal-Organic Coordination Networks", *Acc. Chem. Res.* **2002**, *35*, 511-522.

(54) Yaghi, O.; O'Keeffe, M.; Ockwig, N.; Chae, H.; Eddaoudi, M.; Kim, J. "Reticular synthesis and the design of new materials", *Nature*. **2003**, *423*, 705-714.

(55) Yu, M.; Xie, L.; Liu, S.; Wang, C.; Cheng, H.; Ren, Y.; Su, Z. " Photoluminescent metal-organic framework with hex topology constructed from infinite rod-shaped secondary building unites and single *e,e-trans*-1,4-cycolhexanedicarboxylic dianion", *Inorganica Chimica Acta*. **2007**, *9*, 3108-3112.

(56) Eddaoudi, M.; Kim, J.; Rosi, N.; Vodak, D.; Wachter, J.; O'Keeffe, M.; Yaghi, O. M. "Systematic Design of Pore Size and Functionality in Isoreticular MOFs and Their Application in Methane Storage", *Science* **2002**, *295*, 469-472.

(57) Eddaoudi, M.; Kim, J.; O'Keeffe, M.; Yaghi, O. M. "$Cu_2[o\text{-}Br\text{-}C_6H_3(CO_2)_2]_2(H_2O)_2\bullet(DMF)_8(H_2O_2)_2$: A Framework Deliberately Designed To Have the NbO Structure Type", *J. Am. Chem. Soc*. **2002**, *124*, 376-377.

(58) Chen, B.; Eddaoudi, M.; Hyde, S. T.; O'Keeffe, M.; Yaghi, O. M. "Interwoven Metal-Organic Framework on a Periodic Minimal Surface with Extra-Large Pores", *Science* **2001**, *291*, 10211023.

(59) Li, H.; Eddaoudi, M.; O'Keeffe, M.; Yaghi, O. M. "Design and synthesis of an exceptionally stable and highly porous metal-organic framework", *Nature* **1999**, *402*, 276-279.

(60) Lu, J.; Mondal, A.; Moulton, B.; Zaworotko, M. J. "Polygons and Faceted Polyhedra and Nanoporous Networks", *Angew. Chem. Int. Ed. Engl*. **2001**, *40*, 2133-2116.

(61) Bourne, S. A.; Lu, J.; Mondal, A.; Moulton, B.; Zaworotko, M. J. "Self-Assembly of Nanometer-Scale Secondary Building Units into an Undulating Two-Dimensional Network with Two Types of Hydrophobic Cavity", *Angew. Chem. Int. Ed. Engl*. **2001**, *40*, 2111-2113.

(62) MacDonald, J.C.; Dorrestein, P.C.; Pilley, M.M.; Foote, M.M.; Lundburg, J.L. "Design of Layered Crystalline Materials Using Coordination Chemistry and Hydrogen Bonds", *J. Am. Chem. Soc*. **2000**, *47*, 11692-11702. a

(63) MacDonald, J.C.; Dorrestein, P.C. "Design of Robust Molecular Layers Using Ionic Hydrogen Bonds and Metal-Ligand Interactions", *ACA Trans*. **1998**, *33*, 121-131.

(64) Davis, M.E.; Lobo, R.F. *Chem. Mater*. **1992**, *4*, 756-768.

(65) Chapman, M.; Ayyappan, P.; Foxman, B.; Yee, G.; Lin, W. *Crystal Growth & Design*. **2001**, *2*, 159-163.

(66) T.K. Morgan, et al, *J. Med. Chem*., **1990**, *33*, 1091